



HAL
open science

Phenomenological analysis of charged lepton flavour changes

Albert Saporta

► **To cite this version:**

Albert Saporta. Phenomenological analysis of charged lepton flavour changes. Physics [physics]. Université de Lyon, 2019. English. NNT : 2019LYSE1110 . tel-02319188

HAL Id: tel-02319188

<https://theses.hal.science/tel-02319188>

Submitted on 17 Oct 2019

HAL is a multi-disciplinary open access archive for the deposit and dissemination of scientific research documents, whether they are published or not. The documents may come from teaching and research institutions in France or abroad, or from public or private research centers.

L'archive ouverte pluridisciplinaire **HAL**, est destinée au dépôt et à la diffusion de documents scientifiques de niveau recherche, publiés ou non, émanant des établissements d'enseignement et de recherche français ou étrangers, des laboratoires publics ou privés.

N°d'ordre NNT : xxx



THESE de DOCTORAT DE L'UNIVERSITE DE LYON

opérée au sein de
l'Université Claude Bernard Lyon 1

Ecole Doctorale ED52
Physique et astrophysique de Lyon

Spécialité de doctorat : Physique théorique
Discipline : Physique des particules

Soutenue publiquement le 17/07/2019, par :
Albert Saporta

Phenomenological analysis of charged lepton flavour changes

Devant le jury composé de :

GASCON Jules, Professeur, IPNL

Président

TEIXEIRA Ana, Chargée de Recherche, LPC

Rapporteuse

SMITH Christopher, Chargé de Recherche, LPSC

Rapporteur

KNEUR Jean-Loïc, Directeur de Recherche, L2C

Examineur

DAVIDSON Sacha, Directrice de Recherche, LUPM

Directrice de thèse

CACCIAPAGLIA Giacomo, Chargé de Recherche, IPNL

Co-directeur de thèse

ABSTRACT

In this doctoral thesis, we investigate charged lepton flavour violating processes in effective field theory, in which possible new physics effects can be parametrized by higher dimensional gauge invariant operators built from Standard Model fields. The discovery of neutrino oscillations is a clear evidence that lepton flavour violation can occur and that neutrinos are massive. In the Standard Model extended with massive neutrinos, charged lepton flavour violating processes are strongly suppressed, and the discovery of such processes would be a clear signal of physics beyond the Standard Model.

After a general introduction on the Standard Model of particle physics and beyond, this manuscript contains two introductory chapters.

The first one introduce the theoretical and experimental context for the searches of charged lepton flavour violating processes, and their huge potential to constrain new physics model. We make a review of many processes and the current experiments, then we discuss the prospects for the upcoming experiments.

The second chapter describe the formalism of the effective field theory approach. We discuss the principles of renormalization and loop integrals calculations with dimensional regularization. We also discuss the renormalization group equations that describe the running and the mixing of the coefficients with the energy scale. Finally, we discuss two different approaches in effective field theories.

After introducing the experimental context and the effective field theory formalism, we study the $\mu \rightarrow e$ conversion on nuclei in a top-down approach and charged lepton flavour violating two and three body decays of pseudoscalar mesons in a bottom-up approach. We first list all the operators and their associated coefficients that contribute to the processes. In our work, we mostly focus on dimension six operators. We compute the branching ratios for each processes as a function of the operator coefficients at the experimental scale, and use the experimental upper limit to constrain the coefficients.

We also use the renormalization group equations to compute the running and the mixing of the coefficients with energy scale in both top-down and bottom-up approaches.

The results discussed in this thesis are based on two publications [1, 2].

RÉSUMÉ

Dans cette thèse de doctorat, nous étudions les processus de violation de la saveur des leptons chargés dans le cadre de la théorie des champs effective, dans laquelle les effets de nouvelle physique peuvent être paramétrés par des opérateurs invariants de jauge et de dimension plus élevées, construits avec les champs du modèle standard. La découverte de l'oscillation des neutrinos est une preuve claire que la violation de la saveur leptonique peut se produire et que les neutrinos ont une masse. Dans le modèle standard avec des neutrinos massifs, les processus de violation de la saveur des leptons chargés sont fortement supprimés, et la découverte de tels processus serait un signal clair de physique au-delà du modèle standard.

Après une introduction générale sur le modèle standard de la physique des particules et au-delà, ce manuscrit contient deux chapitres d'introduction.

Le premier chapitre présente le contexte théorique et expérimental pour les recherches de processus de violation de la saveur des leptons chargés, et leur potentiel pour contraindre les modèles de nouvelle physique. Nous faisons une revue de nombreux processus et des expériences actuelles, puis nous discutons des perspectives pour les expériences à venir.

Le deuxième chapitre décrit le formalisme de l'approche de la théorie des champs effective. Nous discutons des principes de la renormalisation et du calcul des boucles avec la régularisation dimensionnelle. Nous discutons également des équations du groupe de renormalisation qui décrivent l'évolution et le mélange des coefficients avec l'échelle d'énergie. Enfin, nous abordons deux approches différentes dans la théorie des champs effective.

Après avoir introduit le contexte expérimental et le formalisme de la théorie des champs effective, nous étudions la conversion d'un muon en électron dans les noyaux dans une approche top-down, et la violation de la saveur des leptons chargés dans les désintégrations à deux et trois corps de mésons pseudo-scalaires dans une approche bottom-up.

Nous listons d'abord les opérateurs et les coefficients associés qui contribuent aux processus. Dans notre travail, nous nous concentrerons principalement sur les opérateurs de dimension six. Nous calculons les rapports de branchement pour chaque processus en fonction des coefficients des opérateurs à l'échelle expérimentale et utilisons les bornes expérimentales pour contraindre les coefficients.

Nous utilisons également les équations du groupe de renormalisation pour calculer l'évolution et le mélange des coefficients avec l'échelle d'énergie dans les approches top-down et bottom-up.

Les résultats présentés dans cette thèse sont basés sur deux publications [1, 2].

ACKNOWLEDGEMENTS

First, I would like to thank my thesis advisor Sacha Davidson, for her endless support during the three years of my PhD, especially in the difficult moments I have been through. We met in unusual circumstances, and despite the fact that I had not a strong background in quantum field theory, you gave me the chance to work with you on physics beyond the standard model.

I also would like to thank my co advisor Giacomo Cacciapaglia, for the help when I was stuck on calculations, for the very interesting discussions on BSM physics and for the Cosmic rays project.

I also would like to thank Ana Teixeira and Christopher Smith for accepting to be reviewers of my thesis, and Jules Gascon and Jean-Loic Kneur for accepting to be examiners of my thesis.

I want to thank all the PhD students for the great moments we had at work and outside!! Thanks for the great lunches and coffee breaks, for the useful and useless debates about math, physics, life and other absurd topics ;) and for the great support in the difficult moments of the thesis. The list is very long and I will not give the names but you know who you are.

Finally, I want to thank all my friends who were present in every moments and gave me the confidence I needed to become who I am today. Thank you for your faith, your support and your love. You know who you are.

TABLE OF CONTENTS

	Page
List of Tables	xiii
List of Figures	xv
1 Introduction	1
2 The standard model of particle physics and beyond	3
2.1 Physics Beyond the Standard Model	3
2.1.1 Evidence of New Physics	3
2.1.2 BSM models	9
3 Charged Lepton Flavour Violation	13
3.1 Charged Lepton Flavour Violation in the SM extended with massive neutrinos . .	14
3.2 Experimental status of CLFV processes	16
3.2.1 Muon channel	16
3.2.2 Tau channel	20
3.2.3 Meson channel	22
3.3 Future directions	23
4 Effective Field Theory	25
4.1 Effective Lagrangian	25
4.1.1 Contact interactions	26
4.2 Renormalization	27
4.2.1 Dimensional regularization	28
4.2.2 Renormalization	30
4.3 Running of the QED and QCD coupling constants	32
4.3.1 Running of the QED coupling constant	32
4.3.2 Running of the QCD coupling constant	33
4.4 Running of the Wilson coefficients	33
4.4.1 Renormalization Group evolution of the Wilson coefficients	35
4.4.2 Why do we need EFT?	35

TABLE OF CONTENTS

4.5	Matching	37
4.6	Bottom-up vs top-down approach	38
4.6.1	Top-down EFT	38
4.6.2	Bottom-up EFT	38
5	Spin-dependent $\mu \rightarrow e$ conversion on light nuclei	41
5.1	Introduction	42
5.2	Operators	43
5.3	Estimating the SD and SI rate in light nuclei	46
5.3.1	Estimating the SD and SI rate in Aluminium	47
5.3.2	Spin-dependent conversion in other light nuclei	54
5.4	Parametric expansions and uncertainties	55
5.5	Implications of including the SD rate	58
5.5.1	Leptoquarks	58
5.5.2	Bounds on arbitrary coefficients of four operators	62
5.5.3	Reconstructing nucleon coefficients	64
5.6	Summary	68
6	Constraints on $2l2q$ operators from $\mu \leftrightarrow e$ flavour-changing meson decays	71
6.1	Introduction	71
6.2	A basis of $\mu - e$ interactions at low energy	73
6.3	Leptonic and semileptonic pseudoscalar meson decays	74
6.3.1	Leptonic decay branching ratio	75
6.3.2	Semileptonic decay branching ratio	75
6.4	Covariance matrix	77
6.4.1	Bounds on the coefficients	78
6.5	Renormalization Group Equations (RGEs)	78
6.5.1	Anomalous dimensions for meson decays	79
6.5.2	RGEs of operator coefficients	81
6.5.3	Evolution of the bounds	81
6.5.4	Single operator approximation	84
6.5.5	Updating the bounds	84
6.6	Conclusion	85
7	Conclusions and prospects	87
A	$G_O^{N,q}$	91
B	The tensor contribution to the SD and SI rates	93

C	RG Evolution	95
D	Constants	99
E	Kinematics and form factors for semileptonic decays	101
F	RGEs	103
G	Covariance matrix	105
H	Covariance matrices at Λ_{exp} and Λ_W	107
	Bibliography	111

LIST OF TABLES

TABLE	Page
3.1 Historical progress for the upper limit on $\mathcal{B}(\mu^+ \rightarrow e^+ \gamma)$. * (expected)	17
3.2 Historical progress for the upper limit on $\mathcal{B}(\mu^+ \rightarrow e^+ e^+ e^-)$	17
3.3 Historical progress for the upper limit on $\mathcal{B}(\mu^- N \rightarrow e^- N)$	18
3.4 Historical progress for the upper limit on $\mathcal{B}(\mu^- N \rightarrow e^+ N)$	19
3.5 Example of current upper limits on selected CLFV leptonic and radiative decays in the tau channel	21
3.6 Example of current upper limits on selected CLFV semileptonic decays in the tau channel, involving pseudoscalar and vector mesons	21
3.7 Example of future expected upper limit on CLFV processes in the tau channel from the Belle II experiment	22
3.8 Example of upper limits on some CLFV processes in the meson channel. Top left pannel : two body decay of vector meson. Top right panel : two body decay of pseudoscalar meson. Bottom panel : three body decay of pseudoscalar meson.	23
5.1 Lepton flavour-changing operators induced in the leptoquark scenarios of equations (5.39 -5.41). The coefficients are given at the leptoquark mass scale M , in the basis of section 5.2.	59
6.1 Experimental bounds on leptonic and semileptonic decays.	78
6.2 Constraints on the dimensionless four-fermion coefficients $c_{P,X}^{l_1 l_2 q_i q_j}$ and $c_{S,X}^{l_1 l_2 q_i q_j}$ at the experimental (Λ_{exp} for K and D mesons decay and Λ_{m_b} for B meson decays) and weak (Λ_W) scale after the RGEs evolution. The last two columns are the sensitivities, or Single Operator (SO) at a time bounds, see subsection 6.5.4. All bounds apply under permutation of the lepton and/or quark indices.	82
6.3 Constraints on the dimensionless four-fermion coefficients $c_{A,X}^{l_1 l_2 q_i q_j}$ and $c_{V,X}^{l_1 l_2 q_i q_j}$ at the experimental (Λ_{exp} for K and D mesons decay and Λ_{m_b} for B meson decays) and weak (Λ_W) scale after the RGEs evolution. The last two columns are the sensitivities, or Single Operator (SO) at a time bounds, see subsection 6.5.4. All bounds apply under permutation of the lepton and/or quark indices.	82

6.4 Constraints on the dimensionless four-fermion coefficients $\epsilon_{T_X}^{l_1 l_2 q_i q_j}$ at the experimental (Λ_{exp} for K and D mesons decay and Λ_{m_b} for B meson decays) and weak (Λ_W) scale after the RGEs evolution. The last two columns are the sensitivities, or Single Operator (SO) at a time bounds, see subsection 6.5.4. All bounds apply under permutation of the lepton and/or quark indices. 83

LIST OF FIGURES

FIGURE	Page
2.1 Rotation curve of a spiral Galaxy (from Mon. Not. Roy. Astron. Soc., 249:523). For ordinary baryonic matter, the circular velocity is expected to decrease far away from the galactic center (dashed line). However, the measurements show that the velocity stays flat at large distances, which favors the hypothesis of the presence of invisible matter.	6
3.1 Example of one-loop diagram for the decay $\mu \rightarrow e\gamma$ in the SM extended with massive neutrinos.	15
4.1 Decay of the muon. Left : decay via a W boson. Right : decay described by a four fermion contact interaction.	27
4.2 Evolution of the strong coupling α_s with the energy scale \mathcal{Q} (from Phys. Rev., D98(3):030001, 2018).	34
5.1 Diagrams contributing to $\mu \rightarrow e$ conversion in the presence of axial and pseudoscalar CLFV operators (represented by the grey blob)	46
5.2 This plot illustrates the prospects for distinguishing SI operators involving up quarks, from those involving down quarks, and vector operators from scalars. The continuous green [dashed red] line is the ratio, given in eqn (5.45) [eqn (5.46)], of $\mu \rightarrow e$ conversion rates induced by $\mathcal{O}_{V,X}^{uu}$ and $\mathcal{O}_{V,X}^{dd}$ [$\mathcal{O}_{S,X}^{uu}$ and $\mathcal{O}_{S,X}^{dd}$], assuming equal coefficients. The stars on the green line are an analytic approximation. The dotted blue line is the ratio, given in eqn (5.47), of $\mu \rightarrow e$ conversion rates induced by $\mathcal{O}_{V,X}^{uu}$ and $\mathcal{O}_{S,X}^{uu}$, with coefficients selected to give the same rate on Niobium ($Z=41$).	61
5.3 A representation of the discriminating power of a target (labelled by Z), with respect to Aluminium. On the vertical axis is the invariant measure, given in eqn (5.55), of the misalignment in coefficient space of the target with respect to Aluminium.	66
5.4 An operator-dependent measure of the discriminating power of a targets (labelled by Z). On the vertical axis is the measure given in of eqn (5.56), of the relative sensitivity(normalised to Aluminium) of a target to the operators $O = \tilde{C}_{S,X}^{pp}$ (continuous black), $O = \tilde{C}_{S,X}^{nn}$ (dotted green), $\tilde{C}_{V,X}^{pp}$ (dashed red) and $O = \tilde{C}_{V,X}^{nn}$ (dot-dashed blue).	67

6.1	Examples of one-loop gauge vertex corrections to 4-fermion operators. The wave-function renormalization diagrams are missing.	80
C.1	Examples of one-loop gauge vertex corrections to 4-fermion operators. The first two diagrams are the penguins. The last six diagrams contribute to operator mixing and running, but can only change the Lorentz or gauge structure of the operators, not the flavour structure. Missing are the wave-function renormalisation diagrams; for $V \pm A$ Lorentz structure in the grey blob, this cancels diagrams 3 and 4.	96

INTRODUCTION

The Standard Model (SM) [3–5] of elementary particle physics describes the properties of the fundamental constituents of matter and their possible interactions via the electroweak and the strong interactions. The SM describes accurately most of the observed physical phenomena, and is one of the most successful theory, as many predictions have been verified by a very large number of measurements.

The discovery of the Higgs boson [6, 7] in 2012 by the ATLAS and CMS collaborations at the Large Hadron Collider (LHC) is one of the greatest success of the SM. The experimental data collected show that the Higgs boson properties are in excellent agreement with the SM predictions, and many experiments are pursuing the study of the Higgs properties.

However, even with the tremendous success of the SM, there are many clear signs that it is not a complete theory and in fact cannot be a theory of everything because it fails to explain many experimental observations.

For example, the SM does not include gravitational interactions, cannot provide candidates for dark matter or explain the observed baryon asymmetry of the Universe. These unsolved issues, along with the hierarchy problem or the strong CP problem are a clear signal that there is physics Beyond the Standard Model (BSM). In the last years, the birth of BSM physics has lead to the development of many theoretical models, predicting the existence of new particles and interactions, and new structures, as an extension to the SM. The quest for new physics has also lead to the creation of many experiments, performing searches of signatures that could be either the manifestation of a new particle or a new process among known particles. Precision measurements are also a great place to look for new physics effects, that could manifest themselves through very small deviations of processes involving SM particles.

Another striking example is the discovery of neutrino oscillations that established non zero neutrino masses and mixing angles. As the neutrinos are taken massless in the SM, new physics is required to explain the oscillation data or any processes involving Lepton Flavour Violation (LFV). Another possibility to search for new physics signatures is to look for Charged Lepton Flavour Violation (CLFV) processes [8, 9], that changes the flavour of charged leptons. The discovery of such processes, forbidden in the SM, or strongly suppressed in the SM extended with massive neutrinos, would be a clear signal of BSM physics. Many experiments are searching for CLFV processes, for example $\mu \leftrightarrow e$ flavour changes can be probed in the decays $\mu \rightarrow e\gamma$ [10] and $\mu \rightarrow 3e$ [11, 12], in $\mu \rightarrow e$ conversion on nuclei [13–15] or in various meson decays such as $K \rightarrow \bar{\mu}e$ [16–19]. Also, the sensitivity to CLFV processes will improve by several orders of magnitude in the coming years, as many experiments are under construction. These huge improvements in the experimental sensitivity in the next years are the reason for our interest in CLFV processes and their huge potential to constrain BSM models.

In this thesis, we focus on CLFV processes involving muons and electrons. The results discussed in chapters 5 and 6 of this manuscript are based on two publications [1, 2]. The outline of the PhD is organized as follows :

- In chapter 2, we first review many signs of BSM physics and then give a short list of BSM scenarios.
- In chapter 3, we make a review of the CLFV processes and their potential to constrain BSM models.
- In chapter 4, we discuss Effective Field Theory, the mathematical framework used to perform calculations and to constrain BSM models.
- In chapter 5, we discuss the CLFV process called $\mu \rightarrow e$ conversion on nuclei in a top-down Effective Field Theory.
- In chapter 6 we discuss CLFV pseudoscalar meson decays in a bottom-up Effective Field Theory.
- Finally, we conclude in chapter 7.

THE STANDARD MODEL OF PARTICLE PHYSICS AND BEYOND

The Standard Model (SM) of particle physics is a renormalizable Quantum Field Theory that describes the properties of elementary particles and their possible interactions via the electroweak and the strong interactions. The SM is one of the most successful theory nowadays, as it has been tested from the eV scale (atomic structure) to the TeV scale. The SM predictions are in excellent agreement with the experimental data in most of the cases, especially the electroweak precision tests. Despite the tremendous success of the SM, there are clear signs that this is not a complete theory, as there are still several issues that cannot be explained with the SM. This has led to the birth of physics Beyond the Standard Model (BSM), that aims at extending the SM to address the unsolved issues.

2.1 Physics Beyond the Standard Model

In this chapter, we give in a first part an overview of signs of New Physics (NP). In a second part, we give a short list of theoretical extensions to the SM.

2.1.1 Evidence of New Physics

In this section, we give some examples of unsolved issues that are a clear sign of BSM physics.

2.1.1.1 Gravitational interactions

One of the most striking issue that shows the SM cannot be a theory of everything is the fact it describes only three of the four fundamental interactions between elementary particles. Indeed, gravitational interactions are not included in the SM as until today, it is still not clear to find how gravity could be quantized and added as an extension to the SM.

2.1.1.2 Hierarchy problem

An interesting issue is the fact that the fermion masses span a very large range, from MeV to 174 GeV, and the SM cannot provide any explanation for the large hierarchy of fermion masses. Another well known issue is the hierarchy problem. Here, the question is why the electroweak interactions are much stronger than the gravitational interactions at the microscopic level. Another formulation of the hierarchy problem is to ask why the Higgs boson is much lighter than the Planck mass (or the grand unification energy). Indeed, one would expect that the large quantum contributions to the square of the Higgs boson mass would make the mass huge, comparable to the scale at which new physics appears, as the Higgs potential is highly sensitive to new physics that couples to the Higgs field. If we consider the existence of new heavy fermions, the self energy diagrams involving the Higgs boson and the additional particles give large contributions to the square of the Higgs mass, proportional to the ultraviolet cut-off used to regularize the divergences of the loops. The cut-off is of the order of the new physics scale, at which the new heavy fermions appear. A major issue is the fact that if the new physics scale is the Planck scale, the mass of the Higgs boson should be much larger than the measured value. Another way to compute the loop integrals would be the use of dimensional regularization, in order to ignore the cut-off, but even in this case, the Higgs mass still receives contributions proportional to the squared mass of the additional particles that couples to the Higgs field. That is the hierarchy problem : if there are additional particles at high energy, it is not clear how to explain why the Higgs mass is so small.

2.1.1.3 The baryon asymmetry

A very puzzling issue is the fact that the Universe is mostly made of matter. As ordinary matter is baryonic, this excess of matter over anti-matter implies a baryon asymmetry, that can be defined as :

$$(2.1) \quad Y_B = \frac{n_B - \bar{n}_B}{s} \neq 0$$

where n_B and \bar{n}_B are the number densities of baryons and anti-baryons, s is the entropy. As the value of Y_B is $\sim 10^{-10}$, baryon number must be violated. Independent measurements of the baryon density have been made with the estimation of the Big Bang Nucleosynthesis (BBN) [20–22] relic densities and from the measurements of the temperature fluctuation spectrum of the Cosmic Microwave Background (CMB). The baryon asymmetry has been measured very precisely by the WMAP and Planck collaborations [23–25].

In the past few decades, particle-physics experiments have shown that the laws of nature do not apply equally to matter and antimatter. A famous hypothesis to explain the imbalance of matter and antimatter in the observed universe is the so called baryogenesis [26–29], a process that took place during the early universe that produced baryonic asymmetry. In 1967, Andrei

Sakharov proposed a set of three conditions that must be satisfied in order to have a baryogenesis [30] :

- Baryon number B violation.
- C and CP violation, so that matter and antimatter have a different behavior
- Interactions out of thermal equilibrium, as particles and antiparticles have the same abundance in equilibrium

However, in the SM, CP violation (included in the CKM matrix) and the out of equilibrium dynamics at the electroweak phase transition are not strong enough to explain the observed asymmetry. This means that BSM physics is required to produce baryogenesis.

2.1.1.4 Dark matter

Numerous observations suggest that most of the mass in the Universe is made of some dark matter of unknown composition. This dark matter is not sensitive to the electromagnetic and strong interactions and interact very weakly with ordinary matter. Evidences for dark matter are provided at different scales. A first hint for dark matter came at galactic scales from the observation that various luminous objects such as stars, gas clouds, globular clusters, and especially entire galaxies, move faster than predicted by the Newtonian theory of gravitation. A very important result is the measurements of the velocities of stars in the Milky Way by J.H. Oort in 1932 [31]. Indeed, some stars were found to move with velocities larger than the escape velocity of the gravitational potential of luminous matter. This was one of the first indication for the existence of a new type of invisible matter in the Milky Way.

In 1933, F. Zwicky studied the velocity distribution of several galaxies in the Coma galaxy cluster [32]. He obtained an approximate value of the mass of the cluster using the Virial theorem and compared it to the mass distribution (obtained with the observation of the luminosity of nebulae in the cluster). He found a discrepancy between the mass of luminous matter and the mass calculated via the Newtonian law of gravity. This discrepancy suggested the existence of some non-luminous matter in the cluster, and was another evidence for the existence of dark matter.

Another very important evidence for the existence of dark matter is the measurement of rotation curves of spiral galaxies, that is to say the measurement of the circular velocities of stars and gas as a function of their distance from the galactic centre. Vera Rubin studied the rotation curves in 1970 [33, 34]. Most of the resulting rotation curves have a flat behavior at large distances, outside the edge of the visible disk. This was not expected and showed that the visible matter was only a fraction of the gravitational matter, as only additional invisible matter could explain the observed rotation curves. An example is given in fig. 2.1 (from [35]).

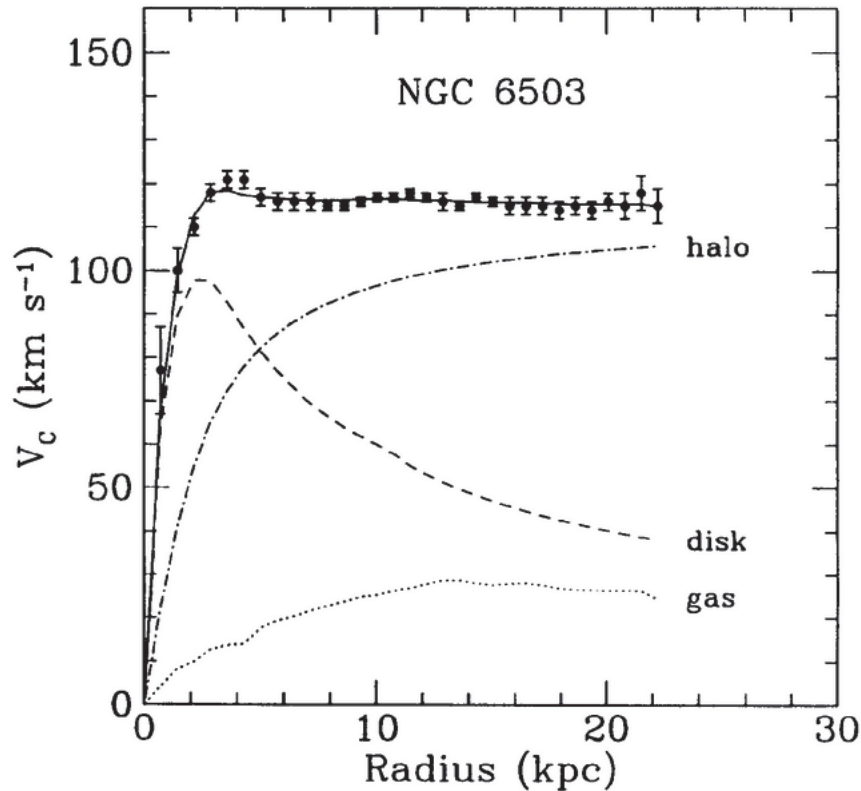


Figure 2.1: Rotation curve of a spiral Galaxy (from *Mon. Not. Roy. Astron. Soc.*, 249:523). For ordinary baryonic matter, the circular velocity is expected to decrease far away from the galactic center (dashed line). However, the measurements show that the velocity stays flat at large distances, which favors the hypothesis of the presence of invisible matter.

At the cosmological scale, various measurements, such as the anisotropy of the CMB, combined with data from Baryon Acoustic Oscillations and Type Ia Supernovae, give a value of the dark matter density. The PLANCK collaboration obtain the following value [24] :

$$(2.2) \quad \Omega_c h^2 = 0.1188 \pm 0.0010$$

The PLANCK collaboration also obtained the following baryon density $\Omega_b h^2 = 0.02230 \pm 0.00014$ [24]. It is clear that the baryon density is not large enough to account for all the dark matter in the Universe. This means that the candidates for dark matter are non-baryonic. The nature of dark matter is still unknown, but the observations lead to a specific profile for non-baryonic dark matter candidates :

- They must have a lifetime near the age of the Universe, otherwise they would have decayed by now

- They must be very weakly interacting with ordinary matter, and cannot have electromagnetic or strong interactions
- They must have the right relic abundance
- They must be cold (non relativistic) during structure formation, as the hot dark matter scenario is almost completely excluded by CMB precision measurements

There are no candidates with such properties in the SM, which means that BSM physics is required to provide non-baryonic cold dark matter. There are many dark matter candidates, such as neutrinos or axions. However, the most famous candidate is the weakly interacting massive particle (WIMP) and is proposed in many extensions of the SM. A large number of experiments are currently searching for WIMPs or other dark matter candidates.

2.1.1.5 Neutrino oscillations

In the SM, there are three flavours of left handed neutrinos (ν_e, ν_μ and ν_τ), that are massless and only sensitive to the weak interaction. They do not mix which means that there are no flavour changes in the SM. However, many evidences of neutrino oscillations come from experiments measuring fluxes of neutrinos produced in the Sun, in the atmosphere, in accelerators and in nuclear reactors. The discovery of neutrino oscillations [36, 37] established non zero neutrino masses and mixing angles [38], and was a striking example of processes involving flavour changes in the lepton sector. A way to introduce lepton flavour changes in the SM is to add a neutrino mass term which can be done via a neutrino mass matrix that is not diagonalized in the charged lepton mass basis. This matrix would give rise to flavour changes and neutrino oscillations (see subsection 3.1). Indeed, the probability for an oscillation between two flavours can be written [38] :

$$(2.3) \quad P(\nu_l \rightarrow \nu_{l'}) = \sum_j |U_{l'j}|^2 |U_{lj}|^2 + 2 \sum_{j>k} |U_{l'j} U_{lj}^* U_{lk} U_{l'k}^*| \cos\left(\frac{\Delta m_{jk}^2 L}{2p} - \phi_{ll';jk}\right)$$

$$(2.4) \quad P(\bar{\nu}_l \rightarrow \bar{\nu}_{l'}) = \sum_j |U_{l'j}|^2 |U_{lj}|^2 + 2 \sum_{j>k} |U_{l'j} U_{lj}^* U_{lk} U_{l'k}^*| \cos\left(\frac{\Delta m_{jk}^2 L}{2p} + \phi_{ll';jk}\right)$$

where $l, l' \in e, \mu, \tau$, $\phi_{ll';jk} = \arg(U_{l'j} U_{lj}^* U_{lk} U_{l'k}^*)$, L is the neutrino oscillation length associated with $\Delta m_{jk}^2 = m_j^2 - m_k^2$, $p = \frac{p_j + p_k}{2}$ ($p_{j,k}$ and $m_{j,k}$ are the neutrino momentum and mass). U is the PMNS neutrino mixing matrix [39–42] which can be written :

$$U = \begin{pmatrix} c_{12}c_{13} & s_{12}c_{13} & s_{13}e^{-i\delta} \\ -s_{12}c_{23} - c_{12}s_{23}s_{13}e^{i\delta} & c_{12}c_{23} - s_{12}s_{23}s_{13}e^{i\delta} & s_{23}c_{13} \\ s_{12}s_{23} - c_{12}c_{23}s_{13}e^{i\delta} & -c_{12}s_{23} - s_{12}c_{23}s_{13}e^{i\delta} & c_{23}c_{13} \end{pmatrix} \\
 \times \begin{pmatrix} 1 & 0 & 0 \\ 0 & e^{i\alpha_2/2} & 0 \\ 0 & 0 & e^{i\alpha_3/2} \end{pmatrix}$$

(2.5)

where $c_{ij} = \cos\theta_{ij}$, $s_{ij} = \sin\theta_{ij}$, $\theta_{ij} = [0, \frac{\pi}{2}]$ the mixing angle, $\delta = [0, 2\pi]$ is the Dirac CP violation phase and α_2 and α_3 are two Majorana CP violation phases [43–46].

In the case the neutrinos are Dirac particles, the parameters are the three mixing angles and the phase δ . If the neutrinos are Majorana particles, that is to say their own antiparticle, then the phases α_2 and α_3 must be added to the lepton mixing matrix.

Thus, with the three angles $\theta_{12}, \theta_{13}, \theta_{23}$, the masses m_1, m_2, m_3 and, depending on the nature of neutrinos, one or three CP violation phases, this makes seven or nine additional parameters in the SM extended with massive neutrinos.

The Dirac phase δ can be studied in neutrino oscillations, as it implies a difference between anti neutrinos and neutrinos oscillation probabilities. Some experiments, sensitive to lepton number violation, like the HEIDELBERG-MOSCOW neutrinoless double beta decays [47] experiment could measure the α_2 and α_3 Majorana phases. Notice that only differences of neutrino masses can be probed in neutrino oscillation experiments. The KATRIN experiment [48] is working on determining the absolute mass scale of neutrinos.

The discovery of flavour changes between neutral leptons is a strong motivation to search for processes involving charged lepton flavour changes. In chapter three, we will discuss processes that involve flavour violation in the charged lepton sector.

2.1.1.6 B physics

Many anomalies have been observed in semileptonic B-decays, that exhibit deviations from the SM predictions in the following ratios :

$$R(K^{(*)}) = BR[B \rightarrow K^{(*)}\mu^+\mu^-] / BR[B \rightarrow K^{(*)}e^+e^-] \\
 R(D^{(*)}) = BR[B \rightarrow D^{(*)}\tau\nu] / BR[B \rightarrow D^{(*)}l\nu] \\
 R(J/\psi) = BR[B_c^+ \rightarrow J/\psi\tau^+\nu] / BR[B_c^+ \rightarrow J/\psi\mu^+\nu]$$

(2.6)

In $R(K)$ and $R(K^*)$, the deviations from the SM are at the $2, 6\sigma$ and $2, 2 - 2, 4\sigma$ level [49, 50], and in $R(D)$ and $R(D^*)$, the deviations from the SM expectation are at the 4σ level [51]. Notice that a deviation of about 2σ was measured in $R(J/\psi)$ [52]. The anomalies observed in $R(K)$ [49], $R(K^{(*)})$ [50] and in $R(D^{(*)})$ [53–55] also suggest lepton flavour universality violation (LFUV) [51, 56–61]. Thus, semileptonic B-decays and the observed anomalies provide powerful probes for testing the SM and for searching for the effects of BSM physics.

2.1.2 BSM models

In this section we make a short review of some BSM models that have been proposed in order to solve the issues mentioned above.

2.1.2.1 Supersymmetry

Supersymmetry or SUSY was developed from various studies [62–65] and is a theory that introduce a new symmetry between fermions and bosons. SUSY predicts that for every bosonic (fermionic) degree of freedom, there is a corresponding fermionic (bosonic) degree of freedom. However, SUSY implicates the existence of undiscovered particles, called the superpartners of the particles already known. These superpartners should have a much larger mass than their partners, otherwise they would have already been detected.

Also, the proton could decay much faster compared to the actual observed lifetime of the proton ($> 10^{29}$ years), into a pion and a positron via a quark superpartner called squark. To solve this issue, a new concept called R-parity was proposed. By introducing R-parity, that can be written [66] :

$$(2.7) \quad P_R = (-1)^{3(B-L)+2s}$$

where s is the spin, B the baryon number, and L the lepton number. $P_R = 1$ for the particles and $P_R = -1$ for the superpartners. When R-parity is conserved, the proton becomes stable, and the predicted lifetime is in agreement with current data.

Another very appealing aspect of R-parity conservation, is that it naturally provides a good dark matter candidate, as in this case, the lightest supersymmetric particle is stable (and has to be neutral of electric and color charge and interacts weakly with baryonic matter).

SUSY also provides a solution to the hierarchy problem, as the new bosonic and fermionic degrees of freedom contributions to the Higgs mass cancel exactly if their couplings and masses are related to each other.

2.1.2.2 Right handed neutrinos

As we saw in subsection 2.1.1.5, neutrino oscillations proved that neutrinos are massive. Giving to the neutrinos a Yukawa coupling to the Higgs field generates neutrino masses after the

electroweak symmetry breaking. A way to generate the neutrino masses is to add right handed neutrinos to the SM. However, as the neutrino masses are extremely small, the corresponding Yukawa couplings must be unnaturally small. A famous example in which this problem is solved is the seesaw mechanism [67–70], as a large Majorana mass term is given to the right handed neutrino, which would push the masses of the active neutrinos down and provide a simple explanation for the small neutrino masses.

Right handed neutrinos can also address many other unsolved issues, as light right-handed neutrinos could also be dark matter candidates. There are also leptogenesis models in which the baryon asymmetry of the Universe is produced from a lepton asymmetry, as in the case of heavy right-handed neutrinos, a new source of CP violating couplings is provided. The phenomenology of right handed neutrinos is reviewed in deeper details in [71].

2.1.2.3 Extra dimensions

It is also possible to add additional dimensions the four dimensional space-time. As an example, adding compact extra dimensions that only affect physics at high energy scales, it is possible to define the Planck mass on the extra dimensional space, which would be much smaller than the Planck mass observed in the regular four dimensional space. This could address the hierarchy problem. Also, one can consider the case of universal extra dimensions [72], in which all SM particles propagate. For example, the fifth dimensional Kaluza-Klein [73, 74] model provides, in the form of stable Kaluza-Klein partners, good dark matter candidates, as they are stable and may have the desired relic density [75–77].

2.1.2.4 Leptoquark models

Leptoquarks (LQs) [78] are hypothetical particles (of scalar or vector nature) that carry both a baryon number (B) and a lepton number (L), and that can turn quarks into leptons and vice versa. They appear in many extensions of the SM, such as the Pati and Salam SU(4) model [79–81], Grand Unified Theories [82–91], technicolour theories [92–96], as well as in various composite models [97–103].

LQs are proposed in many new physics scenarios. For example, LQs provide a solution to the deviations from the SM predictions observed in the ratios of semi-leptonic B decays $R(K^*)$ and $R(D^*)$ [104, 105]. LQ states can also contribute to rare charged lepton processes. There are many examples of these processes, that provide constraints on LQ interactions, such as charged lepton flavour violating decays of the form $l \rightarrow l'\gamma$ or $l \rightarrow l'l'l''$, $\mu - e$ conversion in nuclei, as well as meson decays or anomalous magnetic moments. For example, scalar leptoquarks may contribute to the muon anomalous magnetic moment [106, 107]. Implications of LQs models for charged lepton flavour violation observables are discussed in [108–111].

A review of LQs models along with the issue they address and with the current status of LQs searches at collider is given in [112].

CHARGED LEPTON FLAVOUR VIOLATION

As we saw in subsection 2.1.1.5, the discovery and the confirmation of neutrino oscillations [36, 37] established non zero neutrino masses and mixing angles [38] and was a clear observation of processes involving flavour violation in the lepton sector. However, the SM cannot explain neutrino oscillations or flavour violation in the lepton sector, as the neutrinos are taken massless and there is no mixing between lepton families. It is thus clear that BSM physics is required to address these issues, and must be in agreement with the current constraints on lepton flavour violating processes. The discovery of neutrino oscillations is also a strong motivation to look for flavour violation in the charged lepton sector, the so called Charged Lepton Flavour Violation (CLFV) processes [8, 9]. In fact, once neutrino masses are introduced in the SM, they contribute to CLFV processes via loop diagrams. However, the CLFV rates are GIM suppressed by a factor $\propto (m_\nu/M_W)^4 \sim 10^{-48}$ [113], leading to unobservably small branching ratios in current experiments, of the order $\sim 10^{-54}$. In the case of Majorana neutrinos, for example in models of seesaw type, the GIM suppression may not occur anymore, but the CLFV branching ratios could still be unobservably small. Thus, the discovery of a CLFV process would be a clear signal of BSM physics, and many extensions to the SM predict large CLFV effects. Many experiments are currently searching for CLFV processes, and many are currently under construction and plan to improve their sensitivity to flavour violation by several orders of magnitude. These exceptional improvements in the experimental sensitivity are the reason for our interest in specific CLFV processes and their huge potential for constraining and discriminating BSM models.

In this chapter, we review the theory of lepton flavour violation in the SM extended with massive neutrinos and discuss the current and future experimental status of various CLFV processes.

3.1 Charged Lepton Flavour Violation in the SM extended with massive neutrinos

In the minimal SM with massless neutrinos, we do not expect flavour violation in the lepton sector. The fermion masses and the mixing among different generations arise from the Yukawa couplings of the fermion fields with the Higgs field. The Lagrangian for the SM leptons can be written

$$(3.1) \quad \mathcal{L} = i \underbrace{\left(\bar{l}^i \mathcal{D} l^i + \bar{e}_R^j \mathcal{D} e_R^j \right)}_{\text{Kinetic terms}} - \underbrace{\mathbf{Y}_{ij} \bar{l}^i e_R^j H}_{\text{Yukawa coupling}} + h.c$$

where $l^i \in \begin{pmatrix} \nu_e \\ e \end{pmatrix}_L, \begin{pmatrix} \nu_\mu \\ \mu \end{pmatrix}_L, \begin{pmatrix} \nu_\tau \\ \tau \end{pmatrix}_L$ and $e_R^j \in e_R, \mu_R, \tau_R$. H is the Higgs field, $\mathcal{D} = D_\mu \gamma^\mu$ is the covariant derivative and \mathbf{Y}_{ij} is a 3×3 Yukawa coupling matrix for the charged leptons. The SM fermions are grouped into generations and differ by a quantum number called flavour. In the lepton sector, a lepton flavour can be assigned to each generation : $L_e = 1$ (-1) for e^- , ν_e (e^+ , $\bar{\nu}_e$), $L_\mu = 1$ (-1) for μ^- , ν_μ (μ^+ , $\bar{\nu}_\mu$) and $L_\tau = 1$ (-1) for τ^- , ν_τ (τ^+ , $\bar{\nu}_\tau$). Substituting the vacuum expectation value (VEV) for the Higgs field in the Yukawa part of eqn. 3.1 gives the charged lepton mass terms that can be written :

$$(3.2) \quad \mathcal{L}_{mass} = -M_{ij} \bar{l}_L^i e_R^j, \quad M_{ij} = \frac{v}{\sqrt{2}} \mathbf{Y}_{ij}$$

where M_{ij} is the charged lepton mass matrix, which can be a general complex 3×3 matrix and v is the VEV. Such matrices can be diagonalized by two unitary transformations, one for left-handed leptons and one for right-handed leptons that have the same charge. Indeed, the charged lepton mass matrix of eqn 3.2 is diagonalized by the unitary transformations on l^i and e_R^j . This means that in the mass diagonalized basis, the charged weak current interactions for leptons are diagonal and can be written :

$$(3.3) \quad \mathcal{L}_{W\bar{\nu}e} = \frac{g}{\sqrt{2}} \left(\bar{\nu}_{iL} \gamma^\mu e_{iL} W_\mu^+ + \bar{e}_{iL} \gamma^\mu \nu_{iL} W_\mu^- \right)$$

where g is the SU(2) coupling constant and W_μ a SU(2) gauge boson. Thus, if neutrinos are taken massless, lepton flavour is conserved and neutrino oscillations or CLFV processes can not be explained in the SM.

However, as we saw in subsection 2.1.1.5, the observation of neutrino oscillations indicate that neutrinos have a mass and that there are mixing angles. In the SM extended with massive neutrinos, these masses, that can be introduced via a neutrino mass matrix, can contribute to

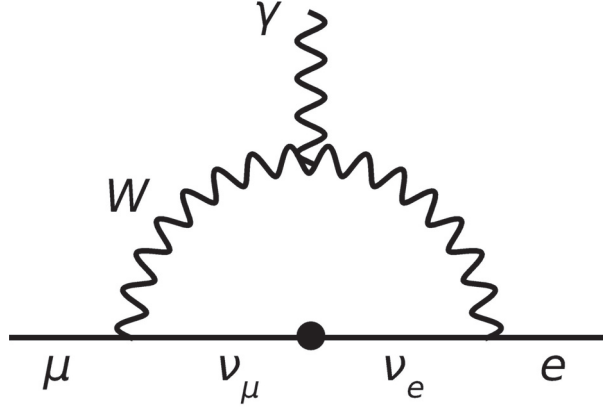


Figure 3.1: Example of one-loop diagram for the decay $\mu \rightarrow e\gamma$ in the SM extended with massive neutrinos.

CLFV processes at the loop level. In fig 3.1, we give an example of a one-loop diagram that would contribute to the CLFV muon decay $\mu \rightarrow e\gamma$.

However, due to the GIM mechanism, the rates of the CLFV processes are strongly suppressed as the neutrinos masses are much smaller than the W boson mass. Let us consider the branching ratio of the radiative CLFV muon decay $\mu \rightarrow e\gamma$ that can be written [113, 114] :

$$(3.4) \quad BR(\mu \rightarrow e\gamma) = \frac{3\alpha}{32\pi} \underbrace{\left| \sum_{i=1}^3 U_{ei}^* U_{\mu i} \frac{m_{\nu i}^2}{M_W^2} \right|^2}_{\text{GIM suppression factor}} \sim (2.5 - 3.9) \times 10^{-55}$$

where U is the PMNS matrix defined in eqn. 2.5 and α the fine structure constant.

Similar calculation of branching ratios of processes involving taus as well as other processes such as $l_1 \rightarrow l_2 l_3 \bar{l}_4$ lead to extremely small results. This means that in the SM extended with neutrino masses, CLFV rates are way too small to be observed in current or future experiments.

However, in the case of Majorana neutrinos, the GIM suppression in CLFV rates may not occur anymore. A simple example is provided by the seesaw mechanism (see 2.1.2.2), in which the SM is extended by adding right-handed neutrinos with Majorana mass terms M_R . The spontaneous breaking of the electroweak symmetry induces Dirac mass terms, as well as mixing among left-handed and right-handed neutrinos. Once the neutrino mass matrix is diagonalized, the resulting eigenstates are Majorana fields. Moreover, the PMNS matrix of eqn. 2.5 does not coincide anymore with the matrix U' that appears in the charged current. The matrix U' is not unitary and can be written in terms of M_R and the neutrino Yukawa couplings \mathbf{Y}_ν [115, 116] :

$$(3.5) \quad U' = \left(1 - \frac{v^2}{2} \mathbf{Y}_\nu^\dagger M_R^{-2} \mathbf{Y}_\nu\right) U$$

In this case, the matrix U appears in diagrams of the form of figure 3.1 and there is no GIM suppression. In fact, in model of seesaw type, the suppression factor $\frac{m_{\nu i}^2}{M_W^2}$ is replaced by a factor $\propto \frac{m_{\nu i}}{M_R}$, which means that the CLFV rates may still be suppressed. For example, for $m_\nu = 1eV$ and $M_R = 10^{10}GeV$, CLFV branching ratios are at the level $\sim 10^{-40}$ or less. This issue is reviewed in [8, 9].

The discovery of a CLFV process would thus be a clear and striking signal of BSM physics. In fact, many BSM models predict measurable CLFV rates and many experiments are currently searching for CLFV processes.

3.2 Experimental status of CLFV processes

In this section, we list various CLFV processes, in the muon, tau and meson channels and discuss the experimental status.

3.2.1 Muon channel

We list four of the major CLFV processes in the muon channel (the Muonium to anti-muonium conversion is detailed in [8]).

3.2.1.1 $\mu^+ \rightarrow e^+ \gamma$ decay

The experimental signature of the $\mu^+ \rightarrow e^+ \gamma$ decay at rest is a positron and a photon in coincidence, moving back-to-back and with their energies equal to half of the muon mass. It is interesting to notice that negative muon cannot be used, since it would be captured by a nucleus when stopped in a material. More detail on the detector resolution and on the sensitivity limitation from the backgrounds of various experiments can be found in [8, 9, 117].

The search for $\mu^+ \rightarrow e^+ \gamma$ have been actively promoted by intense muon beams available at the meson factories. Experiments have been working on improving the detection resolution of the positron energy, the photon energy, the timing between the positron and photon, and the angle between the positron and photon. These improvements, combined with intense muon beams, have lead to huge improvements of the sensitivity to the $\mu^+ \rightarrow e^+ \gamma$ decay. As this decay has not been observed yet, experiments can set an upper limit or the branching ratio, that can be written

$$(3.6) \quad \mathcal{B}(\mu^+ \rightarrow e^+ \gamma) = \frac{\Gamma(\mu^+ \rightarrow e^+ \gamma)}{\Gamma(\mu^+ \rightarrow e^+ \nu \bar{\nu})}$$

In table 3.1, we give a list of upper limits on $\mathcal{B}(\mu^+ \rightarrow e^+ \gamma)$ obtained in the past experiments. It is amazing to see how much the experimental sensitivity has improved over the years.

The MEG collaboration [123] at PSI have reach a sensitivity at a 10^{-13} level, and completed data taking in 2013. Important upgrades are planned in order to increase the sensitivity of the

Experiment (year)	Upper limit
TRIUMF (1977)	$3,6 \times 10^{-9}$ [118]
SIN (1980)	1×10^{-9} [119]
E328 (1982)	$1,7 \times 10^{-10}$ [120]
Crystal Box (1988)	$4,9 \times 10^{-11}$ [121]
MEGA (1999)	$1,2 \times 10^{-11}$ [122]
MEG (2013)	$4,2 \times 10^{-13}$ [123]
MEG II (2016)	5×10^{-14} * [124]

 Table 3.1: Historical progress for the upper limit on $\mathcal{B}(\mu^+ \rightarrow e^+ \gamma)$. * (expected)

experiment by an order of magnitude. These changes to the experiment, known as MEG II, are detailed in [125].

3.2.1.2 $\mu^+ \rightarrow e^+ e^+ e^-$

The signature of the $\mu^+ \rightarrow e^+ e^+ e^-$ decay consists of two positrons and one electron coming from a common vertex and with a total energy equal to the muon mass. However, the energy distribution of each daughter particle depends on the dynamics of the underlying unknown physics. This issue has been reviewed in [8]. Momentum conservation imply that the momentum of the three particles have to lie in a plane. The maximum energy that can be carried away by a positron / electron is half of the muon mass energy.

Collaboration/Lab (year)	Upper limit
Dubna (1976)	1.9×10^{-9} [126]
LAMPF/Crystal Box (1984)	1.3×10^{-10} [127]
SIN/SINDRUM (1984)	1.6×10^{-10} [128]
SIN/SINDRUM (1985)	2.4×10^{-12} [11]
LAMPF/Crystal Box (1988)	3.5×10^{-11} [121]
SIN/SINDRUM (1988)	1.0×10^{-12} [129]
JINR (1991)	3.6×10^{-11} [130]

 Table 3.2: Historical progress for the upper limit on $\mathcal{B}(\mu^+ \rightarrow e^+ e^+ e^-)$

As for the $\mu^+ \rightarrow e^+ \gamma$ decay, the $\mu^+ \rightarrow e^+ e^+ e^-$ decay has not been observed yet, experiments can set an upper limit or the branching ratio $\mathcal{B}(\mu^+ \rightarrow e^+ e^+ e^-)$. In table 3.2, results from various experiments searching for the decay $\mu^+ \rightarrow e^+ e^+ e^-$ are shown. As for the $\mu^+ \rightarrow e^+ \gamma$ decay, high intensity muon beam line will lead to huge improvements of the sensitivity to the $\mu^+ \rightarrow e^+ e^+ e^-$ decay. The Mu3e experiment at PSI was proposed in 2013 and aims to reach a sensitivity at the level 10^{-16} [131].

3.2.1.3 $\mu^- N \rightarrow e^- N$

Muon to electron conversion is the spontaneous decay of a muon to an electron without the emission of neutrinos. When a negative muon is stopped in a material, it is captured by an atom, and forms a muonic atom. Once captured, the muon cascades down in energy levels to the 1s state, in the muonic atom. In the SM, two processes can occur : the muon can decay in orbit ($\mu^- \rightarrow e^- \nu_\mu \bar{\nu}_e$), or can be captured by a nucleus of mass number A and atomic number Z ($\mu^- + (A, Z) \rightarrow \nu_\mu + (A, Z - 1)$). Considering new physics, a third process is also expected : neutrinoless muon capture ($\mu^- + (A, Z) \rightarrow e^- + (A, Z)$), which is called muon to electron conversion in a muonic atom. Notice that in the final state, the nucleus can be in the ground state or in an excited state. However, most often, the nucleus is in the ground state, in this case, the conversion process is said to be coherent. Notice that experiments do not observe captures on the nucleus, but instead see the signature of a stopped muon : X-rays that are emitted when the muon tumbles down to the 1s state of some target nucleus. The characteristic X-rays spectrum is the signal of a stopped muon. The signature of the coherent conversion in a muonic atom is a monoenergetic single electron emitted from muon capture, whose energy is :

$$(3.7) \quad E = m_\mu - B_\mu - E_{rec}$$

where m_μ is the mas of the muon, B_μ the binding energy of the 1s state of the muonic atom and E_{rec} the nuclear recoil energy. It is important to notice that the peak energy of the conversion signal changes for different nuclei, as B_μ depends on the nucleus.

Experiment (year)	Upper limit	Material
SREL (1972)	1.6×10^{-8} [132]	Cu
SIN (1977)	4.0×10^{-10} [133]	S
SIN (1982)	7.0×10^{-11} [134]	S
TRIUMF (1988)	4.6×10^{-12} [135]	Ti
SINDRUM II (1993)	4.3×10^{-12} [136]	Ti
SINDRUM II (1996)	4.6×10^{-11} [137]	Pb
SINDRUM II (2006)	7.0×10^{-13} [13]	Au

Table 3.3: Historical progress for the upper limit on $\mathcal{B}(\mu^- N \rightarrow e^- N)$

Also, as the signature of the conversion process is a monoenergetic electron, no coincidence measurement is required. It is also very important to notice that contrary to the $\mu \rightarrow e \gamma$ and $\mu \rightarrow e^+ e^+ e^-$ decays, it is possible to improve the sensitivity to the conversion process by using a high muon rate, but without suffering from accidental background.

As the conversion process has not been observed, experiments set upper limit on the branching ratio, that can be written :

$$(3.8) \quad \mathcal{B}(\mu^- N \rightarrow e^- N) = \frac{\Gamma(\mu^- + (A, Z) \rightarrow e^- + (A, Z))}{\Gamma(\mu^- + (A, Z) \rightarrow \text{capture})}$$

The normalization to captures simplify the computations since many details of the nuclear wavefunction cancel in the ratio. In table 3.3, results from various experiments searching for the $\mu \rightarrow e$ conversion process are shown. Several experiments currently under construction will improve the sensitivity to $\mu \rightarrow e$ conversion by several orders of magnitude : the COMET experiment [14] at J-parc and the Mu2e experiment [15] at FNAL aim to reach a sensitivity $\sim 10^{-16}$. The PRISM/PRIME proposal [138] aims to reach a sensitivity $\sim 10^{-18}$ and has the advantage to allow the use of heavy target nuclei with shorter lifetimes of their muonic atoms, because of its designed pure muon beam with no pion contamination. There is also the DeeMe experiment [139] at J-parc, that have a simpler setup but allow an early start of the experiment with a moderate sensitivity, between 10^{-13} and 5×10^{-15} .

3.2.1.4 $\mu^- N \rightarrow e^+ N$

Another neutrinoless muon capture process exist and is a charge-changing reaction : $\mu^- + (A, Z) \rightarrow e^+ + (A, Z - 2)^*$. The final state of the nucleus can be a ground state or an excited state. Contrary to $\mu^- \rightarrow e^-$ conversion, here there is no coherent enhancement, as the initial and final nuclei are not the same. The energy of the positron coming from the $\mu^- \rightarrow e^+$ conversion is :

$$(3.9) \quad E = m_\mu - B_\mu - E_{rec} - \Delta_{Z-2}$$

where Δ_{Z-2} is the difference in the nuclear binding energy between the initial and final nuclei. The branching ratio can be written :

$$(3.10) \quad \mathcal{B}(\mu^- N \rightarrow e^+ N) = \frac{\Gamma(\mu^- + (A, Z) \rightarrow e^+ + (A, Z - 2)^*)}{\Gamma(\mu^- + (A, Z) \rightarrow \text{capture})}$$

Experiment (year)	Upper limit	Material
SREL (1972)	2.6×10^{-8} [132]	Cu
SIN (1978)	1.5×10^{-9} [140]	S
SIN (1980)	9.0×10^{-10} [141]	S
TRIUMF/TPC (1988)	1.7×10^{-10} [135]	Ti
SINDRUM II (1993)	8.9×10^{-11} [136]	Ti
SINDRUM II (1993)	4.3×10^{-12} [136]	Ti
SINDRUM II (1998)	3.6×10^{-11} [142]	Ti
SINDRUM II (1998)	1.7×10^{-12} [142]	Ti

Table 3.4: Historical progress for the upper limit on $\mathcal{B}(\mu^- N \rightarrow e^+ N)$

In table 3.4, results from various experiments searching for the $\mu^- \rightarrow e^+$ conversion process are shown. The $\mu^- \rightarrow e^+$ conversion process also provide complementary informations regarding the Majorana nature of neutrinos. Indeed, this transition violates both lepton number and lepton flavour, and can only proceed if neutrinos are of Majorana nature, as for the neutrinoless double beta decay $(\beta\beta)_{0\nu}$ [143]. Also, the $\mu^- \rightarrow e^+$ conversion process has another similarity with the neutrinoless double beta decay, as both processes require a mechanism involving two nucleons.

3.2.2 Tau channel

In this section, we make a review of some CLFV tau decays and the current upper limits and discuss the prospects.

3.2.2.1 Current experiments and upper limits

The tau lepton is a powerful probe to search for BSM physics, as the mechanisms that govern its production and decay in electroweak interactions are well understood. It is also the only lepton that can decay into hadrons, which allow to study QCD effects in the 1 GeV energy region. However, as explained previously, even if we include neutrino masses only, the SM predicts that the CLFV tau decay branching ratios are too small to be observed with the current experiments. Moreover, many difficulties arise, the tau lepton has a very short lifetime (2.9×10^{-13} s) and is not produced as much as muons are. Taus must be obtained at proton or electron accelerators, and their decay must be measured with detectors that have good particle identification and tracking capabilities, and that are able to constrain the kinematics very well, which require good calorimetry and hermeticity. Even if the large mass of the tau enhance the sensitivity, the number of taus that can be produced and observed is reduced because CLFV tau decay searches have not been performed with dedicated experiments, but with beams and detectors that are used for a broader physics program.

Many experiments have been searching for CLFV tau decays, such as the CLEO experiment at CESR [144]. Nowadays, B factories, using e^+e^- colliders, such as the BaBar experiment at PEP-II collider at SLAC [145], or the Belle experiment at KEKB in Tsukuba [146], that were built to measure the CP-violating parameters in the B-meson systems, are also tau factories. Indeed, at the center-of-mass energy of $\sqrt{s} = 10.58$ GeV ($\Upsilon(4s)$ resonance), the cross section to produce a $\tau^+\tau^-$ pair is 90% of the cross section to produce a $b\bar{b}$ pair. The LHCb [147, 148] and the ATLAS [149] collaborations have also been searching for CLFV tau decays.

Leptonic and radiative CLFV tau decays

In table 3.5, we list some upper limits on various leptonic and radiative CLFV tau decays. More details on the backgrounds and other experimental issued are given in [150–153].

Decay mode	Upper limit
$\tau^- \rightarrow e^- \gamma$	3.3×10^{-8} [150]
$\tau^- \rightarrow \mu^- \gamma$	4.4×10^{-8} [150]
$\tau^- \rightarrow e^- e^- e^+$	2.7×10^{-8} [151]
$\tau^- \rightarrow e^- \mu^- \mu^+$	2.7×10^{-8} [151]
$\tau^- \rightarrow e^+ \mu^- \mu^-$	1.7×10^{-8} [151]
$\tau^- \rightarrow e^+ \mu^- e^-$	1.8×10^{-8} [151]
$\tau^- \rightarrow e^- \mu^+ e^-$	1.5×10^{-8} [151]
$\tau^- \rightarrow \mu^- \mu^+ \mu^-$	2.1×10^{-8} [151]

Table 3.5: Example of current upper limits on selected CLFV leptonic and radiative decays in the tau channel

Semileptonic CLFV tau decays

The tau channel is very promising, as the tau is also the only lepton that can decay into hadrons, which lead to many new modes to study, and allow to study QCD effects in the 1 GeV energy region. In table 3.6, we list some upper limits on various semileptonic CLFV tau decays with pseudoscalar and vector mesons in the final state.

Decay mode	Upper limit
$\tau^- \rightarrow e^- \pi^0$	8.0×10^{-8} [154]
$\tau^- \rightarrow \mu^- \pi^0$	1.1×10^{-7} [155]
$\tau^- \rightarrow e^- \eta$	9.2×10^{-8} [154]
$\tau^- \rightarrow \mu^- \eta$	6.5×10^{-8} [154]
$\tau^- \rightarrow e^- K_S^0$	2.6×10^{-8} [156]
$\tau^- \rightarrow \mu^- K_S^0$	2.3×10^{-8} [156]
$\tau^- \rightarrow e^- \rho^0$	1.8×10^{-8} [157]
$\tau^- \rightarrow \mu^- \rho^0$	1.2×10^{-8} [157]
$\tau^- \rightarrow e^- \phi$	3.1×10^{-8} [157]
$\tau^- \rightarrow \mu^- \phi$	8.4×10^{-8} [157]
$\tau^- \rightarrow e^- K^*(892)^0$	3.2×10^{-8} [157]
$\tau^- \rightarrow \mu^- K^*(892)^0$	5.9×10^{-8} [158]

Table 3.6: Example of current upper limits on selected CLFV semileptonic decays in the tau channel, involving pseudoscalar and vector mesons

The signature of the processes with a neutral pseudoscalar meson in the final state ($\tau \rightarrow lP^0$) is the presence of an lP^0 pair (with $l = e, \mu$ and $P^0 = \pi^0, \eta, K_S^0$) with an invariant mass consistent with $m_\tau = 1,777$ GeV, a total energy of $\sqrt{s}/2$ in the center of mass frame, as well as other particles coming from a tau decay, from the event $e^+ e^- \rightarrow \tau^+ \tau^-$. P^0 candidates are reconstructed in specific mass windows from events such as $\pi^0, \eta \rightarrow \gamma\gamma$, $\eta \rightarrow \pi^0 \pi^+ \pi^-$ or $K_S^0 \rightarrow \pi^+ \pi^-$. More experimental details are given in [154–156, 159].

For processes with a neutral vector meson in the final state ($\tau \rightarrow lV^0$, with $l = e, \mu$ and

$V^0 = \rho^0, \phi, K^{*0}$), V^0 candidates are reconstructed from events such as $\rho^0 \rightarrow \pi^+\pi^-$, $\phi \rightarrow K^+K^-$, $K^{*0} \rightarrow \pi^-K^+$. The signature experiments are looking for is thus three charged particles (from the event $\tau \rightarrow lV^0 \rightarrow lh_1^+h_2^-$ where h_1 and h_2 are charged hadrons) that are identified as the appropriate lepton or hadron and have an invariant mass close to the tau lepton mass. Experimental details are discussed in [157, 160].

Future experiments

Decay mode	Expected limit
$\tau \rightarrow e\gamma$	5×10^{-9} [161]
$\tau \rightarrow \mu\gamma$	10^{-9} [161]
$\tau \rightarrow eee$	5×10^{-10} [161]
$\tau \rightarrow \mu\mu\mu$	5×10^{-10} [161]
$\tau \rightarrow e + hadron$	3×10^{-10} [161]
$\tau \rightarrow \mu + hadron$	3×10^{-10} [161]

Table 3.7: Example of future expected upper limit on CLFV processes in the tau channel from the Belle II experiment

The Belle II experiment at Super KEKB [162] aims to reach a sensitivity $\sim 1 - 5 \times 10^{-9}$ for radiative decays and $\sim 5 \times 10^{-10}$ for three body decays [161]. Despite the improvements, the two body decay still suffers from the backgrounds detailed in [161], while the three body decay are still background free. The Belle II experiment also expect to reach a sensitivity $\sim 3 \times 10^{-10}$ for the semileptonic decays. The expected sensitivities are summarized in table 3.7.

From tables 3.5, 3.6 and 3.7, it is clear that the experimental sensitivity to the various tau decay modes is lower than the sensitivity to CLFV processes in the muon channel. However, the tau channel is a very promising place to probe CLFV effects as there are a large number of processes, and it also allows to study QCD effects in the 1 GeV energy region via the CLFV semileptonic decays.

3.2.3 Meson channel

In this section, we make a review of some CLFV leptonic and semileptonic meson decays, discuss the current upper limits on these processes and discuss the prospects. The meson channel offers many possibilities to study CLFV effects, due to the large number of possible CLFV meson decays. Experiments such as the BES experiment [163, 164] at BEPC and now the BESIII detector at the BEPCII e^+e^- collider [165], the SND detector at VEPP-2M e^+e^- collider [166], the CLEO III detector, at CESR [167] have been searching for CLFV vector meson decays. Experiments such as E871 at BNL [168], LHCb [169], BaBar [145] or Belle [146] have been searching for leptonic

and semileptonic pseudoscalar meson decays. In table 3.8, we list upper limits on some CLFV vector and pseudoscalar meson decays.

Decay mode	Upper limit	Decay mode	Upper limit
$\phi \rightarrow e^+ \mu^-$	2×10^{-6} [170]	$K_J^0 \rightarrow e^\pm \mu^\mp$	4.7×10^{-12} [174]
$J/\psi \rightarrow e^+ \mu^-$	1.6×10^{-7} [171]	$D^0 \rightarrow e^\pm \mu^\mp$	1.3×10^{-8} [17]
$J/\psi \rightarrow e^+ \tau^-$	8.3×10^{-6} [172]	$B_S^0 \rightarrow e^\pm \mu^\mp$	1.1×10^{-8} [175]
$J/\psi \rightarrow \mu^+ \tau^-$	2.0×10^{-6} [172]	$B^0 \rightarrow e^\pm \tau^\mp$	2.8×10^{-5} [176]
$\Upsilon \rightarrow \mu^+ \tau^-$	6.0×10^{-6} [173]	$B^0 \rightarrow \mu^\pm \tau^\mp$	2.2×10^{-5} [176]
Decay mode	Upper limit	Decay mode	Upper limit
$K^+ \rightarrow \pi^+ \bar{\mu} e$	1.3×10^{-11} [16]		
$D_S^+ \rightarrow K^+ \bar{\mu} e$	9.7×10^{-6} [18]		
$B^+ \rightarrow K^+ e^\pm \mu^\mp$	9.1×10^{-8} [177]		
$B^+ \rightarrow K^+ e^\pm \tau^\mp$	3.0×10^{-5} [178]		
$B^+ \rightarrow K^+ \mu^\pm \tau^\mp$	4.8×10^{-5} [178]		

Table 3.8: Example of upper limits on some CLFV processes in the meson channel. Top left pannel : two body decay of vector meson. Top right panel : two body decay of pseudoscalar meson. Bottom panel : three body decay of pseudoscalar meson.

More details on the experimental issues can be found in the references of table 3.8. As there is a large number of experiments searching for these processes, and improving their sensitivity to CLFV mesons decays, the meson channel is another very promising place to look for BSM physics. Indeed, there are many possible processes, and for some of them, the experimental sensitivity is high, especially the leptonic and semileptonic Kaon decays (see table 3.8).

3.3 Future directions

As we have seen in the previous sections, many experiments are searching for various CLFV processes, in the muon channel, in the tau channel, in hadron decays as well as in other channels we did not discuss, such as in Z or H^0 decays. Many significant improvements on the experimental sensitivity are expected for various CLFV processes, such as $\tau \rightarrow lll$, $\mu\gamma$, $e\gamma$, $\mu \rightarrow eee$, $e\gamma$, $\mu N \rightarrow eN$, Z or $H^0 \rightarrow e\mu$, $e\tau$ [179, 180], $\mu\tau$, $K_L \rightarrow e\mu$ and so on.

The large number of possible CLFV processes and associated experiments, as well as the exceptional and promising improvements in experimental sensitivity, strongly motivate our interest in CLFV processes, and their potential to constrain BSM physics.

In chapter 5, we will study the $\mu \rightarrow e$ conversion on nuclei, and use the available and expected upper limit on the branching ratio to constrain a BSM model involving scalar Leptoquarks. We will also study the prospects for discriminating among BSM scenarios once the conversion process is observed.

In chapter 6, we will use the upper limits on various leptonic and semileptonic CLFV pseudoscalar meson decays to constrain coefficients.

EFFECTIVE FIELD THEORY

As we have seen in chapters 1 and 2, even if the SM has been tested successfully at many scales, it is clear that it cannot be a complete theory of everything. The SM can be considered as an effective theory, valid up to a given energy scale Λ , at which a more fundamental theory could enter. The effects of new physics at the electroweak scale can be parametrized by non renormalizable operators, built with the known fields from the SM. In this chapter, we discuss the principles of the Effective Field Theory (EFT) approach [181–183], the framework in which new physics from a given energy scale Λ , can be parametrized at lower scales with effective operators and their associated coefficients. As the notion of EFT is large, we focus on the specific approach we will use in this work

4.1 Effective Lagrangian

In most of the BSM models that have been created, the SM is recovered in the low energy scale via the decoupling of the heavy particles that have a mass much larger than the weak scale : $\Lambda \gg \Lambda_W$ where $\Lambda_W \sim M_W \sim 80$ GeV is the weak scale. If new physics particles are too heavy to be produced at LHC, they could be considered in the decoupling limit [184], by inducing new interactions between SM particles. For example, if a BSM scenario predicts the existence of a new heavy particle, that has not been observed, the EFT formalism allows to describe the indirect effects of that new physics particle between SM particles as corrections to SM observables. The corrections are added in an expansion in inverse power of the new physics scale Λ_{NP} , once the new heavy particles have been integrated out from the theory. There are many benefits in the use of an EFT approach :

- It allows to choose the relevant degrees of freedom to describe the dynamic of a specific

process

- Observables can be parametrized with effective operators and their associated (Wilson) coefficients at a given energy scale
- It allows to describe indirect effects of heavy new physics on interactions between SM particles
- Integrating out the new heavy particles from the theory lead to contact interactions that can be described by an effective Lagrangian that contains effective operators and their coefficients

The higher dimensional operators, suppressed by powers of the new physics scale Λ_{NP} , are added to the SM Lagrangian as follow :

$$(4.1) \quad \mathcal{L}_{EFT} = \mathcal{L}_{SM}^{(4)} + \frac{1}{\Lambda_{NP}} \sum_i C_i^{(5)} \mathcal{O}_i^{(5)} + \frac{1}{\Lambda_{NP}^2} \sum_i C_i^{(6)} \mathcal{O}_i^{(6)} + \mathcal{O}\left(\frac{1}{\Lambda_{NP}^3}\right)$$

where \mathcal{L}_{EFT} is the effective Lagrangian, $\mathcal{L}_{SM}^{(4)}$ is the SM Lagrangian that contains renormalizable four dimensional operators, $\mathcal{O}_i^{(d)}$ are the effective operators of dimension $d > 4$ and $C_i^{(d)}$ are the dimensionless coupling constants associated to the operators, that are also called the Wilson coefficients. Notice that the set of operators that appear at each order is finite.

4.1.1 Contact interactions

When the heavy degrees of freedom have been integrated out from the theory, the usual interactions described in terms of exchange of bosons are replaced by contact interactions in the low energy EFT. Contact interactions are generated by the effective operators and Wilson coefficients. A famous example is the muon decay via the exchange of a W boson. In figure 4.1, we can see the decay of the muon via the usual W boson. However, at the time where the W boson was not discovered yet, the decay of the muon was described in the form of a four-fermion contact interaction in which there is no more the propagation of a W boson, as can be seen in figure 4.1.

Thus a contact interaction is an approximation, but this approximation is widely used in the EFT approach. For example, we can imagine a BSM model that predicts the existence of a new boson, that would mediate new interactions among SM particles. If the boson has not been observed yet, one can assume that the boson is too heavy to be produced at LHC. However, considering contact interactions allow to describe the indirect effects of that new boson, that would induce new interactions between SM particles.

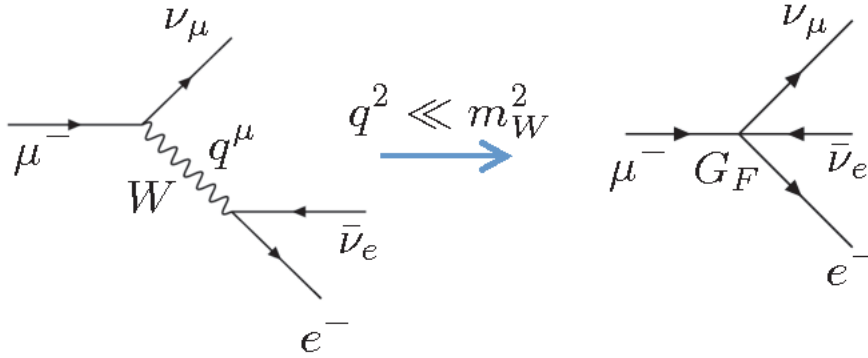


Figure 4.1: Decay of the muon. Left : decay via a W boson. Right : decay described by a four fermion contact interaction.

4.2 Renormalization

A very important feature of quantum field theories, is that all the parameters of the Lagrangian evolve with the energy scale Λ . As a consequence, in the SM, the coupling constant of QED and QCD as well as the Wilson coefficients in the EFT evolve with energy scale, but with a different behavior. The tool used to compute the evolution of the parameters of the Lagrangian with the energy scale is a set of differential equations called renormalization group equations [185–191].

As it is necessary to compute loop diagrams in order to calculate the evolution of a parameter with the scale Λ , we have to treat the divergences that appear in loop calculations. The theory has to be regularized in order to have a parametrization of the singularities, and renormalized to eliminate the divergences. In this work, we will use a regulator called dimensional regularization [192–197] and a renormalization scheme called modified minimal subtraction scheme (\overline{MS} scheme) [198] to subtract divergences.

4.2.1 Dimensional regularization

The idea of dimensional regularization [192–197] is to treat the divergences of loop integrals by continuation to $D = 4 - 2\epsilon$ space-time dimensions. The goal is to compute the loop diagrams as an analytic function of the space time dimension D . The loop integrals will converge for small D , and the final result should be finite and have a well defined limit as $D \rightarrow 4$. The integrals encountered in L-loop calculated in D dimensions are of the form :

$$(4.2) \quad \Lambda^{2\epsilon} \int \prod_{l=1}^L \frac{d^D k_l}{(2\pi)^D} \frac{N}{A_1^{m_1} \dots A_n^{m_n}}$$

where the numerator N is a product of contractions that involve at least one loop momentum, the A_i in the denominator are propagators of the form $(q^2 - m^2)$ where q is a combination of momenta and m a mass and $m_i \in \mathbb{N}^+$ (in most cases, $m_1 = m_N = 1$). Λ is an arbitrary mass scale that is introduced in dimensional regularization in order to keep the dimension of the integrals $(\frac{d^4 k}{(2\pi)^4} \rightarrow \Lambda^{2\epsilon} \frac{d^D k}{(2\pi)^D})$.

Thus, we compute the integral for $D = 4 - 2\epsilon$, and express the result as a Laurent series in ϵ , that we can analytically continue to complex ϵ . Notice that the poles in the Laurent series have two origins :

- Ultraviolet (UV) poles, that come from divergences when the loop momentum goes to infinity.
- Infrared (IR) poles, that come from divergences that can appear when a propagator in the loop integral goes to zero for a finite value of the loop momentum.

The results of a one-loop and a two-loop calculation have the following form

$$(4.3) \quad \begin{aligned} \text{One-loop} &: \frac{a}{\epsilon} + b \\ \text{Two-loop} &: \frac{c}{\epsilon^2} + \frac{d}{\epsilon} + e \end{aligned}$$

where a, b, c, d and e are finite. Singularities are extracted as poles for $\epsilon \rightarrow 0$. Observables and other quantities are made free of the UV divergences in the limit $\epsilon \rightarrow 0$ via the process of renormalization. Notice that even after renormalization, quantities such as amplitudes can still contain IR divergences, as they can not be absorbed by redefining the parameters. However, IR divergences cancel against the singularities that appear in the phase space integration when considering IR-safe observables [199, 200].

4.2.1.1 Feynman parameters

Before using dimensional regularization to compute integrals of the form of eqn 4.2, it is necessary to introduce the method of Feynman parameters, that allows to squeeze the denominators factors in eqn 4.2 into a quadratic polynomial in k . Then the momenta k can be shifted by a constant to complete the square in the polynomial. However, this method require to introduce additional parameters that have to be integrated over : the Feynman parameters.

A simple example is a one-loop integral involving only two propagators in the denominator. In this case, the denominator can be rewritten :

$$(4.4) \quad \frac{1}{A_1 A_2} = \int_0^1 dx \frac{1}{[xA_1 + (1-x)A_2]^2} = \int_0^1 dx dy \delta(x+y-1) \frac{1}{[xA_1 + yA_2]^2}$$

where x and y are Feynman parameters. As an example, we can take $A_1 = (k^2 - m^2)$ and $A_2 = (k+q)^2 - m^2$, using eqn 4.4 lead to

$$(4.5) \quad \int_0^1 dx \frac{1}{[k^2 + 2xk \cdot q + xq^2 - m^2]^2} = \int_0^1 dx \frac{1}{[l^2 + x(1-x)q^2 - m^2]^2} = \int_0^1 dx \frac{1}{[l^2 - \Delta]^2}$$

where we shifted k by $l = k + xq$, $\Delta = m^2 - x(1-x)q^2$ and the denominator depends only on l^2 . In this case, integrating over $d^D k$ is much easier as $d^D k = d^D l$, and the integrand is spherically symmetric with respect to l . One has also to replace the momenta k in the numerator by the shifted momenta l . Thus, after this shift, the denominator in a one-loop integral have the form $(l^2 - \Delta)^n$.

In the case of very complicated integrals with denominators of the form of eqn 4.2, one can use the general formula :

$$(4.6) \quad \frac{1}{A_1^{m_1} \dots A_n^{m_n}} = \int_0^1 dx_1 \dots dx_n \delta(\sum x_i - 1) \frac{\prod x_i^{m_i-1}}{[\sum x_i A_i]^{\sum m_i}} \frac{\Gamma(m_1 + \dots + m_n)}{\Gamma(m_1) \dots \Gamma(m_n)}$$

where the A_i in the denominator are propagators of the form $(q^2 - m^2)$ where q is a combination of momenta and m a mass, and $m_i \in \mathbb{N}^+$.

Using identities such as eqn 4.4 or 4.6, loop integrals of the form of eqn 4.2 are turned into integrals of the form :

$$(4.7) \quad \Lambda^{2\epsilon} \int \frac{d^D l}{(2\pi)^D} \frac{N}{(l^2 - \Delta)^n}$$

where l is the shifted momenta, $D = 4 - 2\epsilon$, Δ is a function of Feynman parameters and of masses and momentum that appear in the loop and the numerator N is a function of l and

Feynman parameters. In the calculation of an integral of the form of eqn 4.7, for example with $N=1$ and $n=2$, the following term appears :

$$(4.8) \quad B \left(\frac{4\pi\Lambda^2}{\Delta} \right)^\epsilon \Gamma(2 - D/2)$$

where B is just a constant. Here, we need the expansion of $\Gamma(x)$ near its poles :

$$(4.9) \quad \Gamma(x) = \frac{1}{x} - \gamma + \mathcal{O}(x)$$

where $\gamma \sim 0,5772$ is the Euler-Mascheroni constant that appears in loop integrals and is also subtracted in \overline{MS} . Thus, in eqn 4.8, for a simple case where $n=2$, the Γ function is the numerator becomes :

$$(4.10) \quad \Gamma(2 - D/2) = \Gamma(\epsilon) = \frac{1}{\epsilon} - \gamma + \mathcal{O}(\epsilon)$$

The term in equation 4.8 becomes :

$$(4.11) \quad B \left(\frac{1}{\epsilon} - \gamma + \log \left(\frac{4\pi\Lambda^2}{\Delta} \right) \right)$$

Notice that in \overline{MS} , the terms $-\gamma + \log(4\pi)$ are subtracted as well. Thus, a singularity in loop integrals can be extracted as a $\frac{1}{\epsilon}$ pole (see eqn 4.3 and 4.11).

4.2.2 Renormalization

It is a well known fact that renormalization is necessary in quantum field theory, in order to treat the divergences that arise in loop diagrams computations. Thus, to eliminate the divergences that come from the loop integrals, it is necessary to renormalize the fields and the parameters of the Lagrangian. In general, this is done by rescaling the parameters with a renormalization constant. For example, in the QED Lagrangian, a fermion ψ of mass m and the coupling constant e are renormalized as follow:

$$(4.12) \quad m_0 = Z_m m, \quad \psi^0 = Z_2^{1/2} \psi, \quad e_0 Z_2 Z_3^{1/2} = e Z_1$$

where the index 0 indicates non renormalized or "bare" quantities and the factors Z_m , Z_1 , Z_2 and Z_3 are renormalization constants. Notice that in order to have a renormalized coupling g independent of the number of dimensions, we have to compensate the dimension of the bare coupling g_0 with an external scale Λ that appears in dimensional regularization :

$$(4.13) \quad g_0 = \Lambda^\epsilon g Z_g$$

where Z_g is the renormalization constant. The bare parameters g_0 and m_0 are independent of the scale Λ . This implies that the renormalized coupling g must be Λ dependent.

A way to implement renormalization is the counter terms method, in which the bare parameters of a Lagrangian are reexpressed via renormalization constants (see eqn 4.12). For example, a mass term of the form $m_0 \psi^0 \bar{\psi}^0$ would become $(Z_2 Z_m - 1) m \psi \bar{\psi} + m \psi \bar{\psi}$. Then, only renormalized quantities are present in the Lagrangian, and the counter term δ is of the form $\delta_i \sim Z_i - 1$. The counter term δ can be considered as an interaction term, and in the case of the mass counter term, the Feynman rule would be $i(Z_2 Z_m - 1)m$. The factors Z have to be determined in order to cancel the divergences coming from the loop integrals.

In the case of the EFT approach, the Wilson coefficients $C_i^{(d)}$ are renormalized in a similar way :

$$(4.14) \quad C_i^{(d),0} = Z_{ij} C_j^{(d)}$$

where Z_{ij} is a renormalization matrix which can also mix operators during renormalization. The idea of renormalization group, renormalization schemes and EFT are closely related, and it is important to choose a specific renormalization scheme when performing an EFT analysis. Many schemes exists :

- A first one is a physical renormalization scheme, such as the momentum space subtraction, that use the Appelquist-Carazzone theorem [184]. In this case, there is no dependence on unphysical parameters. However, physical renormalization schemes are mass dependent, which means that quantities such as the beta function of eqn 4.16 depends on Λ/m . The main issue is that physical renormalization schemes are difficult to use beyond one-loop in theories in which very disparate scales are present. This is due to the fact that the quantities depend on the renormalization scale Λ and on the physical parameters.
- It is thus easier to use a renormalization scheme in which quantities are independent of the scale Λ , but depends only on the physical parameters. These type of schemes are called mass independent subtraction schemes. Famous mass independent schemes are minimal subtraction scheme (MS) [189] and modified minimal subtraction scheme \overline{MS} [198]. There are many advantages to use the \overline{MS} scheme, as calculations are easier, the subtraction is automatic and moreover, dimensional analysis works.

In the \overline{MS} scheme, a renormalization constant Z is chosen to absorb the pure pole divergences $\frac{1}{\epsilon^k}$ (see eqn 4.3 and 4.11). Thus, Z can be expanded in inverse powers of ϵ :

$$(4.15) \quad Z = 1 + \sum_{k=1}^{\infty} \frac{1}{\epsilon^k} Z_k$$

The ϵ dependent renormalization constants, such as in eqn 4.12 and 4.14, are determined as an expansion in the renormalized coupling constant by imposing that all the transitions amplitudes, once expressed in terms of the renormalized coupling, are free of the UV divergences when $\epsilon \rightarrow 0$. As we saw, the renormalization constants depend on the renormalization scheme, that is to say on the way the divergences are absorbed.

In the EFT approach we will use in the rest of the manuscript, and especially in chapters 5 and 6, we will use dimensional regularization as a regulator and use the \overline{MS} scheme to subtract the divergences.

4.3 Running of the QED and QCD coupling constants

In this section we discuss the evolution of the QED and QCD coupling with energy scale Λ via the renormalization group equations.

In the process of renormalization (see eqn 4.12 and 4.13), we have introduced an arbitrary scale Λ . The running of a coupling constant with the scale Λ is given by the renormalization group beta function [201], that can be written :

$$(4.16) \quad \beta(g, \epsilon) = \frac{dg(\Lambda)}{d \log \Lambda}$$

where g is a coupling constant and Λ is the energy scale (see eqn 4.12 and 4.13). The beta function is calculated as :

$$(4.17) \quad \beta(g, \epsilon) = -g\epsilon + \beta(g), \quad \beta(g) = -g \frac{1}{Z_g} \frac{dZ_g}{d \log \Lambda}$$

where Z_g is the renormalization constant associated to the coupling constant g . This means that the beta function can be directly obtained from the $\frac{1}{\epsilon}$ pole parts of the renormalization constant Z_g . Notice that in four dimensions, $\beta(g, \epsilon)$ reduces to $\beta(g)$.

4.3.1 Running of the QED coupling constant

In the case of the QED coupling constant, the leading term of the beta function for N_f Dirac fields of charge $Q_i e$ is positive :

$$(4.18) \quad \beta(e) = \frac{e^3 \sum_{i=1}^{N_f} Q_i^2}{12\pi^2}$$

The fact that the beta function of QED (eqn 4.18) is positive means that the coupling constant $\alpha_e = e^2/4\pi$ increases with the energy scale Λ . However, the running of the coupling constant in QED is small, as the value of α_e varies from $\sim 1/137$ at low energy to $\sim 1/128$ at high energy.

4.3.2 Running of the QCD coupling constant

The leading term of the QCD beta function is given by :

$$(4.19) \quad \beta(g_s) = -\beta_0 \frac{g_s^3}{16\pi^2}, \quad \beta_0 = \frac{11N_c - 2N_f}{3}$$

where N_c is the number of colors and N_f the number of quark flavours.

Using eqn 4.16, eqn 4.19 and $\alpha_s = g_s^2/4\pi$, the running of the strong coupling constant at one-loop can be written :

$$(4.20) \quad \alpha_s(\Lambda) = \frac{4\pi}{\beta_0 \log(\Lambda^2/\Lambda_\infty^2)}$$

where β_0 is defined in eqn 4.19 and Λ_∞ is the scale where $\alpha_s \rightarrow \infty$. The fact that the beta function of QCD (eqn 4.19) is negative means that the coupling constant α_s decreases with the energy scale Λ . In figure 4.2 [38], we can see the that running of the strong coupling constant is very large, as α_s evolve a lot from low to high energies. We also see that QCD becomes non perturbative below one GeV.

This is a striking result of QCD, as the running of α_s is large, which lead to very different behavior at low and high energies. Indeed, at high energy, α_s is small, leading to an important feature of QCD, called asymptotic freedom. It means that at high energies or short distances (large momentum transfers), quarks behave like free particles, as observed in deep inelastic scattering experiments.

However, at low energies, QCD has a very different behavior due to a phenomenon called confinement, which means that quarks and gluons are confined into colorless bound states called hadrons. However, as α_s becomes very large at low energies, the perturbativity is lost. Thus describing the behavior of hadrons is a very difficult task. A current and powerful approach is lattice QCD, which attempts to evaluate the path integral by discretizing space time.

4.4 Running of the Wilson coefficients

In this section, we describe the evolution of the Wilson coefficients associated to the operators with the energy scale Λ via the renormalization group equations, that require to compute a function

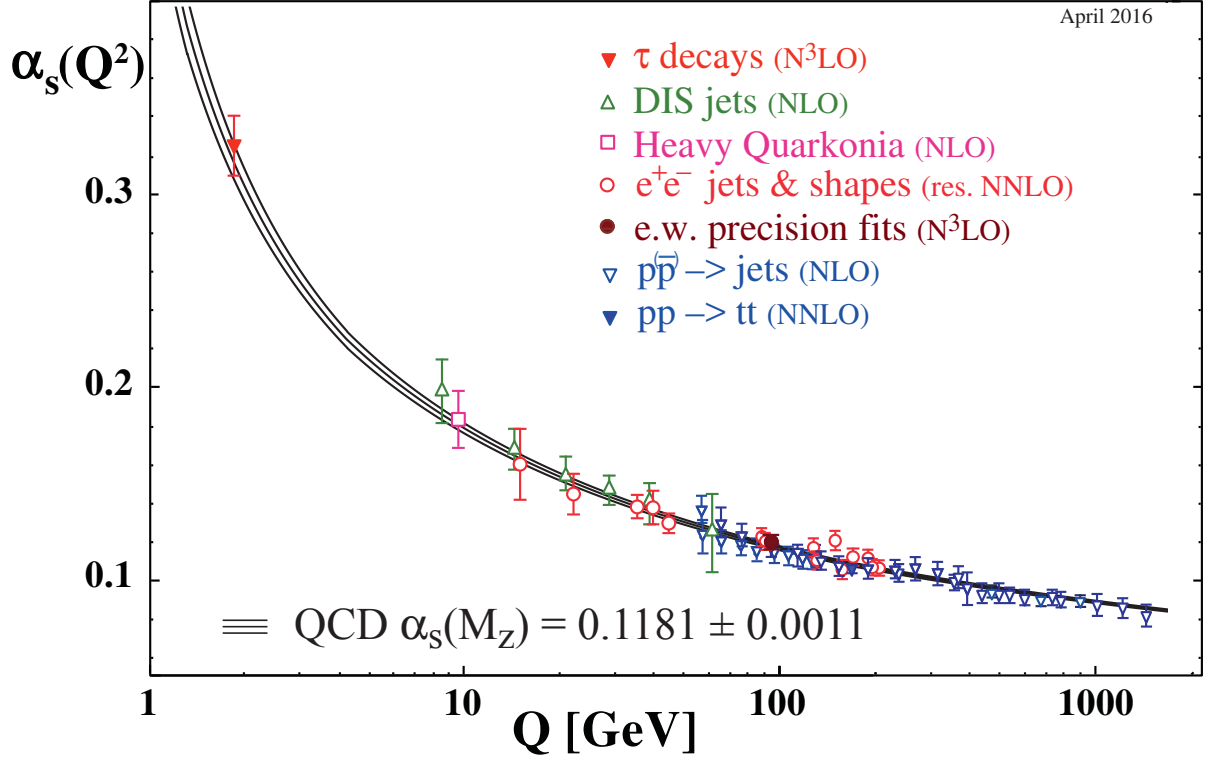


Figure 4.2: Evolution of the strong coupling α_s with the energy scale \mathcal{Q} (from Phys. Rev., D98(3):030001, 2018).

called anomalous dimension. As a first example, let us consider the anomalous dimension of a mass term. Indeed, as the renormalization constants have a perturbative expansion in the renormalized coupling constant (see 4.12 and 4.13), they must depend on Λ , which means that the renormalized mass is also Λ dependent. The running is given by :

$$(4.21) \quad \frac{dm(\Lambda)}{d \log(\Lambda)} = -\gamma_m m(\Lambda)$$

where γ_m is the anomalous dimension of a mass that can be written

$$(4.22) \quad \gamma_m = \frac{1}{Z_m} \frac{dZ_m}{d \log(\Lambda)}$$

where Z_m is defined in eqn 4.12.

Similarly, the anomalous dimension of a Wilson coefficient can be written :

$$(4.23) \quad \gamma = \frac{1}{Z} \frac{dZ}{d \log(\Lambda)}$$

Thus, as for the beta function, the anomalous dimension of a mass or a Wilson coefficient can be obtained from the $\frac{1}{\epsilon}$ poles of the associated renormalization constant. However, from eqn 4.14, we see that the running of Wilson coefficients is more complicated, as the coefficients of the operators can also mix during renormalization.

4.4.1 Renormalization Group evolution of the Wilson coefficients

We have now to discuss the computation of the running of the Wilson coefficients with the energy scale Λ , via the appropriate renormalization group equations. We saw that the running of a coupling constant is govern by a quantity called the beta function (eqn 4.16). The renormalization group function describing the evolution of the Wilson coefficients is called an anomalous dimension (see eqn 4.23). We saw in eqn 4.14 that Wilson coefficients can mix under renormalization, which means that the anomalous dimensions will be organized in a matrix. As for the running of a coupling constant, it is also necessary to compute loop diagrams that diverge in order to solve the renormalization group equations for the Wilson coefficients. As explained, we will use the \overline{MS} scheme and dimensional regularization to treat the divergences that appear in loop diagrams involved in the evolution of the Wilson coefficients with the energy scale.

When considering a specific basis of operators, the Wilson coefficients associated to the operators of the basis can be organized in a row vector \vec{C} . In the case of one-loop corrections that are included in the \overline{MS} scheme, the running of the Wilson coefficients with the scale Λ is given by

$$(4.24) \quad \Lambda \frac{\partial}{\partial \Lambda} (C_I, \dots C_J, \dots) = \frac{\alpha_e}{4\pi} \vec{C} \Gamma^e + \frac{\alpha_s}{4\pi} \vec{C} \Gamma^s$$

where I, J represent the super- and subscripts which label operator coefficients, Γ^e and Γ^s are the QED and QCD anomalous dimension matrices that contribute to the running and the mixing of the Wilson coefficients.

In chapters 5 and 6, we will study the effects of the running and the mixing of Wilson coefficients, which are also reviewed in appendix C and F.

4.4.2 Why do we need EFT?

In chapters 5 and 6, we will study two CLFV processes in an EFT approach. As no CLFV processes have been observed, experiments have set upper limits on observables, such as branching ratios for CLFV decays, as we saw in chapter 3. In this case, the goal of an EFT approach is to compute

an observable, such as a cross section or a branching ratio, as a function of the Wilson coefficients. Then, we will use the available experimental upper limits on the observables we computed in order to constrain the Wilson coefficients. This will allow us to constrain the parameter space of BSM scenarios that aim at explaining CLFV processes.

As we have seen, the running of the strong coupling constant is large, and QCD has a very different behavior at low and high energies. Indeed, we saw that at high energies, quarks behaves like free particles, whereas at low energies quarks and gluons are confined into hadrons. This is of great importance in the use of an EFT approach, as the question we ask is "what is the scale of the physics we are interested in?", or equivalently, "what can experiments observe?" : free quarks exchanging gluons? or bound states of quarks?

For example, experiments searching for the $\mu \rightarrow e$ conversion on nuclei are not sensitive to free quarks exchanging gluons, but rather to the nucleons. Another similar example would be experiments searching for the CLFV decays of meson.

Consider again a BSM scenario that predicts the existence of a new boson, that would mediate new interactions among SM particles. The boson has not been observed yet, thus, we assume that the boson is too heavy to be produced at LHC. The next step is to consider contact interactions in order to describe the indirect effects of that new boson, that would induce new interactions between SM particles. This means that we have to compute the effective operators and their associated Wilson coefficients to describe the contact interactions induced by the new boson. Assuming that the scale of that BSM scenario, or equivalently the mass of the new boson is at the TeV, it means that the Wilson coefficients we computed are also at the TeV scale.

As we saw in figure 4.2, at the TeV scale, quarks behave like free particle as α_s is small. But in the case of CLFV mesons decays or $\mu \rightarrow e$ conversion on nuclei, we know that experiments are not sensitive to free quarks, but to bound state of quarks. This means that we need to evolve the Wilson coefficients from the TeV scale down to the GeV scale in order to correctly describe the physics experiments can observe. Indeed, the GeV scale is the scale at which QCD becomes strongly coupled, as α_s becomes very large (see figure 4.2); which means that quarks are confined into hadrons.

Once the Wilson coefficients are evolved to the experimental scale ($\Lambda_{exp} \sim GeV$) and describe the physics experiments can observe, that is to say hadrons, we can compute an observable (as a function of the Wilson coefficients) that can be measured by experiments. Again, in the case of unobserved processes, such as CLFV processes, experiments set upper limits on observables, that we will use in order to constrain the Wilson coefficients.

4.5 Matching

It is also important to notice that when we compute the evolution of the coefficients between the new physics scale $\Lambda_{NP} \sim TeV$ and the experimental scale $\Lambda_{exp} \sim GeV$, we have to consider the intermediate scales, each time a particle mass is encountered, such as the top and bottom quark mass. For simplicity, we will consider only the intermediate weak scale $\Lambda_W \sim m_W$. In this case, the evolution is in two steps : first we compute the evolution between Λ_{NP} and Λ_W , then between Λ_W and Λ_{exp} , or vice versa. Indeed, between Λ_{exp} and Λ_W , the W, the Z and Higgs boson do not participate to the loop diagrams, but they will between Λ_W and Λ_{NP} . As long as no particle masses are encountered, the evolution of the coefficients is described by the renormalization group equations (eqn. 4.24). However, when the scale Λ reaches the mass M of a particle, we have to change the effective theory to a new theory without the particle of mass M .

Let us consider the following example. First, we start at a very high scale, with new heavy particles of mass M (for example $M \sim TeV$). When Λ goes below the mass M , the parameters of the theory change and new non renormalizable interactions are introduced. At the scale $\Lambda = M$, the particles of mass M are integrated out. These changes in the parameters and the coefficients that describe the new interactions have to be computed by "matching" (for $\Lambda = M$) the physics just below the boundary $\Lambda = M$ in both theories. The matching condition of the two theories at the boundary $\Lambda = M$ is that S-matrix elements for light particle scattering in the low energy theory without the heavy particle must match those in the high-energy theory with the heavy particle(s) of mass M . Then, we have to compute the running of the coefficients of the new effective theory from the scale M down to a smaller scale until another particle mass is encountered, which is $\Lambda_W \sim 80 GeV$ in this example. The renormalization group also introduces additional factors into the coefficients, including the mass of the heavy particle.

This means that a heavy particle mass appears in the coefficients in two ways :

- From matching conditions, in the form of a power dependence
- From the renormalization group running in the form of a logarithmic dependence (eqn. 4.24)

Then, we have to repeat this procedure each time a mass is encountered. Thus, the calculation is done by using a sequence of effective field theories with fewer and fewer particles. For example, at the scale Λ_W , we first have to compute the matching so that the physics of the light particles is the same in the two theories, at the boundary $\Lambda = \Lambda_W$. Then, we have to use the renormalization group to compute the running of the coefficients from Λ_W to the scale of interest, in our case, $\Lambda_{exp} \sim GeV$.

4.6 Bottom-up vs top-down approach

In this section, we discuss two approaches that we will use in our EFT analyses.

4.6.1 Top-down EFT

In the top-down approach, the aim is to start directly from a BSM Lagrangian of a specific model, that would for example predict the existence of a new heavy boson, that, for the purpose of this manuscript could mediate CLFV processes.

As explained in the previous sections, the assumption is that the new boson has not been observed yet, as it is too heavy to be produced. We have to compute the effective operators and their associated coefficients in order to describe the indirect effects of the boson among SM particles. The goal is then to compute an observable that can be measured, as a function of the coefficients, and use experimental data to constrain the coefficients. The steps of the top-down approach are :

- Compute the effective operators from the BSM Lagrangian \mathcal{L}_{BSM} at the new physics scale Λ_{NP} (in general $\Lambda_{NP} \sim \text{TeV}$).
- Compute the Wilson coefficients associated to the operators, at Λ_{NP} . Notice that the Wilson coefficients are proportional to the parameters of \mathcal{L}_{BSM} , like coupling constants or masses.
- As the Wilson coefficients are at the new physics scale Λ_{NP} , they do not describe the physics experiments can observe, which is bound states of quarks rather than free quarks exchanging gluons. Thus, we have to run the coefficients down to the experimental scale $\Lambda_{exp} \sim \text{GeV}$, via eqn 4.24.
- Compute an observable proportional to the Wilson coefficients once they are evolved to the experimental scale Λ_{exp} .
- Finally, as we are interested in CLFV processes, that have not been observed, we use the experimental upper limits on the observable to constrain the coefficients at Λ_{exp} .

Notice that as the coefficients are proportional to the parameters of \mathcal{L}_{BSM} , the top-down approach is model dependent.

In chapter 5, we will apply the top-down approach to the $\mu \rightarrow e$ conversion on nuclei, in a BSM scenario involving scalar Leptoquarks.

4.6.2 Bottom-up EFT

In the bottom-up approach, the aim is to start directly from the experimental scale $\Lambda_{exp} \sim \text{GeV}$. In this case, we make absolutely no assumption of the new physics and on the scale Λ_{NP} . We have thus to write the most general operators describing the contact interactions, in our case, for CLFV

processes. We can then compute an observable proportional to the coefficients at Λ_{exp} , using the experimental upper limits on the observable to constrain the coefficients at Λ_{exp} . Finally, the aim is to evolve the bounds on the coefficients to an arbitrary new physics scale $\Lambda_{NP} \sim TeV$. The steps of the bottom-up approach are :

- Write the most general operators at $\Lambda_{exp} \sim GeV$, that describe the process of interest, with no assumption on the new physics at high energy.
- The coefficients associated to the operators at Λ_{exp} do not depend on any parameters of a BSM Lagrangian.
- Compute an observable proportional to the coefficients, as they are already at Λ_{exp} .
- Constrain the coefficients at Λ_{exp} using experimental upper limits on the observables.
- Evolve the bounds on the coefficients from Λ_{exp} to a scale Λ_{NP} , at which new physics could enter.
- The final step is to reconstruct the fundamental Lagrangian of the new physics from the operator coefficients.

Notice that as we made no assumption on the high energy theory, the coefficients do not depend on the parameters of a BSM Lagrangian. This means the bottom-up approach is model independent, and will allow to test several BSM scenarios.

In chapter 6, we will apply the bottom-up approach to CLFV leptonic and semileptonic pseudoscalar meson decays.

It is important to notice that the running of the Wilson coefficients via the renormalization group equations of eqn 4.24 will be always model dependent. Indeed, we saw that in order to solve the renormalization group equations, we have to compute loop diagrams. In this manuscript, we will assume that only SM particles are involved in the loop diagrams when we compute the evolution of the coefficients between the experimental scale and the new physics scale.

SPIN-DEPENDENT $\mu \rightarrow e$ CONVERSION ON LIGHT NUCLEI

AUTHORS : Sacha Davidson ¹, Yoshitaka Kuno ², and Albert Saporta¹.

PUBLISHED IN : The European Physical Journal C ¹

The experimental sensitivity to $\mu \rightarrow e$ conversion will improve by four or more orders of magnitude in coming years. It is thus interesting to consider the “spin-dependent” (SD) contribution to the rate. This process does not benefit from the atomic-number-squared enhancement of the spin-independent (SI) contribution, but probes different operators. We give details of our recent estimate of the spin dependent rate, expressed as a function of operator coefficients at the experimental scale. Then we explore the prospects for distinguishing coefficients or models by using different targets, both in an EFT perspective, where a geometric representation of different targets as vectors in coefficient space is introduced, and also in three leptoquark models. It is found that comparing the rate on isotopes with and without spin could allow to detect spin dependent coefficients that are at least a factor of few larger than the spin independent ones. Distinguishing among the axial, tensor and pseudoscalar operators that induce the SD rate would require calculating the nuclear matrix elements for the second two. Comparing the SD rate on nuclei with an odd proton vs odd neutron could allow to distinguish operators involving u quarks from those involving d quarks; this is interesting because the distinction is difficult to make for SI operators.

¹<https://doi.org/10.1140/epjc/s10052-018-5584-8>

5.1 Introduction

Charged Lepton Flavour Violation (CLFV) is New Physics that must exist; only the rates are unknown. In this paper, we consider $\mu \leftrightarrow e$ flavour change, and assume that it can be parametrised by contact interactions involving Standard Model particles. Flavour change $\mu \leftrightarrow e$ can be probed in the decays $\mu \rightarrow e\gamma$ [123] and $\mu \rightarrow ee\bar{e}$ [129], in $\mu \rightarrow e$ conversion [13, 137, 202] and in various meson decays such as $K \rightarrow \bar{\mu}e$ [38]. In $\mu \rightarrow e$ conversion, a beam of μ^- impinges on a target, where the μ is captured by a nucleus, and can convert to an electron while in orbit. The COMET [14] and Mu2e [15] experiments, currently under construction, plan to improve the sensitivity by four orders of magnitude, reaching a branching ratio $\sim 10^{-16}$. The PRISM/PRIME proposal [138] aims to probe $\sim 10^{-18}$. These exceptional improvements in experimental sensitivity motivate our interest in subdominant contributions to $\mu \rightarrow e$ conversion. Initial analytic estimates of the $\mu \rightarrow e$ conversion rate were performed by Feinberg and Weinberg [203], for promising operators and nuclei. A wider range of nuclei were studied numerically by Shanker [204], and estimates for many operators and nuclei can be found in the review [8]. Relativistic effects relevant in heavier nuclei were included in [205]. The matching of CLFV operators constructed with quarks and gluons, onto operators constructed with nucleons, was performed in [206]. The current state of the art is the detailed numerical calculations of Kitano, Koike and Okada (KKO) [207], who studied all the CLFV nucleon operators that contribute coherently to $\mu \rightarrow e$ conversion, for nuclei from Helium to Uranium. In such processes, the amplitude for $\mu \rightarrow e$ conversion on each nucleon is coherently summed over the whole nucleus. Like “spin-independent”(SI) dark matter scattering, the final rate therefore is enhanced by a factor $\sim A^2$, where A is the atomic number of the nucleus. However, other conversion processes are possible. For instance, incoherent $\mu \rightarrow e$ conversion, where the final-state nucleus is in an excited state, has been discussed by various people [204, 208, 209], and is expected to be subdominant with respect to the coherent process. In a previous letter [210], some of us noted that “spin-dependent”(SD) $\mu \rightarrow e$ conversion can also occur, if the target nuclei have spin (as is the case for Aluminium, the target of the upcoming COMET and Mu2e experiments). Although this process does not benefit from the $\sim A^2$ enhancement associated to SI rates, it has the interest of being mediated by different CLFV operators from the coherent process.

The aim of this manuscript is to give details of our calculation, and explore whether the SD process could help distinguish models or operators, should $\mu \rightarrow e$ conversion be observed. The operators which could induce SD $\mu \rightarrow e$ conversion are listed in section 5.2. The conversion rate in Aluminium is estimated in section 5.3, and the extrapolation to other nuclei is discussed in subsection 5.3.2. The theoretical uncertainties in our estimates are briefly discussed in section 5.4. Section 5.5 explores the consequences of including the SD contribution to the $\mu \rightarrow e$ conversion rate, both in the perspective of obtaining constraints on operator coefficients from an upper bound on the branching ratio, and for discriminating models when $\mu \rightarrow e$ conversion is observed. This section comes in three parts: we study three leptoquark models which induce SD and

SI conversion, then consider the same operators but with arbitrary coefficients, and calculate a covariance matrix. Finally, we allow all possible operators with arbitrary coefficients. We summarise in section 5.6.

In our previous letter [210], we showed that the SI and SD operator coefficients mix under Renormalisation Group(RG) evolution between the experimental and weak scales. The effects of this mixing are significant: the largest contribution to the $\mu \rightarrow e$ conversion rate from an ‘‘SD’’ coefficient at the weak scale, would be via the RG mixing to an SI coefficient (for example, a tensor coefficient at the weak scale induces a SI contribution to the rate which is $\sim A^2$ larger than the SD contribution). In this paper, we focus on operator coefficients at the experimental scale, only including the RG evolution in the leptoquark models of section 5.5.1. The RG evolution of the operator coefficients is summarised in Appendix C.

5.2 Operators

We are interested in contact interactions that can mediate $\mu \rightarrow e$ conversion on nuclei, at a scale $\Lambda_{exp} \sim 2$ GeV. The focus of this manuscript is the subset of ‘‘spin-dependent’’ interactions, but for completeness, all QED \times QCD invariant operators that mediate $\mu \rightarrow e$ conversion on nuclei are included. The relevant operators in the quark-level Lagrangian are [206, 207]:

$$(5.1) \quad \delta\mathcal{L} = -2\sqrt{2}G_F \sum_{Y \in L,R} \left[C_{D,Y} \mathcal{O}_{D,Y} + \frac{1}{m_t} C_{GG,Y} \mathcal{O}_{GG,Y} + \sum_{q=u,d,s} \sum_{O'} C_{O',Y}^{qq} \mathcal{O}_{O',Y}^{qq} \right] + h.c.$$

where the two-lepton operators are

$$(5.2) \quad \mathcal{O}_{D,Y} = m_\mu (\bar{e} \sigma^{\alpha\beta} P_Y \mu) F_{\alpha\beta} \quad \mathcal{O}_{GG,Y} = (\bar{e} P_Y \mu) G_{\alpha\beta} G^{\alpha\beta}$$

and $O' \in \{V, A, S, P, T\}$ labels 2-lepton 2-quark operators in a basis where only the lepton currents are chiral:

$$(5.3) \quad \begin{aligned} \mathcal{O}_{V,Y}^{qq} &= (\bar{e} \gamma^\alpha P_Y \mu) (\bar{q} \gamma_\alpha q) & \mathcal{O}_{A,Y}^{qq} &= (\bar{e} \gamma^\alpha P_Y \mu) (\bar{q} \gamma_\alpha \gamma_5 q) \\ \mathcal{O}_{S,Y}^{qq} &= (\bar{e} P_Y \mu) (\bar{q} q) & \mathcal{O}_{P,Y}^{qq} &= (\bar{e} P_Y \mu) (\bar{q} \gamma_5 q) \\ \mathcal{O}_{T,Y}^{qq} &= (\bar{e} \sigma^{\alpha\beta} P_Y \mu) (\bar{q} \sigma_{\alpha\beta} q) \end{aligned}$$

with $\sigma^{\alpha\beta} = \frac{i}{2}[\gamma^\alpha, \gamma^\beta]$ and $P_L = (1 - \gamma_5)/2$. This choice of non-chiral quark currents is convenient for matching onto nucleons. However, often an operator basis with chiral quark currents is added to the Lagrangian as $\delta\mathcal{L} = -2\sqrt{2}G_F \sum C_{O,YX} \mathcal{O}_{O,YX}^{qq}$ [8, 211, 212], where for instance, $\mathcal{O}_{V,YX}^{qq} \equiv (\bar{e} \gamma^\alpha P_Y \mu) (\bar{q} \gamma_\alpha P_X q)$. In this case, the coefficients are related as (recall that $\mathcal{O}_{T,LR}^{qq}$ vanishes—see appendix C of [211]):

$$(5.4) \quad \begin{aligned} C_{V,Y}^{qq} &= \frac{1}{2}(C_{V,YR}^{qq} + C_{V,YL}^{qq}) & C_{A,Y}^{qq} &= \frac{1}{2}(C_{V,YR}^{qq} - C_{V,YL}^{qq}) \\ C_{S,Y}^{qq} &= \frac{1}{2}(C_{S,YR}^{qq} + C_{S,YL}^{qq}) & C_{P,Y}^{qq} &= \frac{1}{2}(C_{S,YR}^{qq} - C_{S,YL}^{qq}) \\ C_{T,Y}^{qq} &= C_{T,YY}^{qq} \quad . \end{aligned}$$

In eqn (5.1), the coefficients and operators are evaluated close to the experimental scale, at $\Lambda_{exp} \simeq 2$ GeV. The scale is relevant, because Renormalisation Group running mixes the tensor and axial vector operators (that induce SD $\mu \rightarrow e$ conversion) into the scalar and vector operators (who mediate the SI process)[210]². This is reviewed in Appendix C. Throughout the paper, coefficients without an explicit scale are assumed to be at Λ_{exp} .

To compute the rate for $\mu \rightarrow e$ conversion, the operators containing quarks should be matched at the scale Λ_{exp} onto CLFV operators involving nucleons and mesons. The relevant nucleon operators are the four-fermion operators of eqn (5.3) with $q \rightarrow N$ and $N \in \{n, p\}$. As discussed below, rather than include mesons in the Lagrangian, we approximate their effects by form factors for some nucleon operators and two additional operators given in eqn (5.10). So the nucleon-level Lagrangian will be

$$(5.5) \quad \delta\mathcal{L} = -2\sqrt{2}G_F \sum_{Y \in L,R} \left[C_{D,Y} \mathcal{O}_{D,Y} + \sum_{N=p,n} \sum_{O''} \tilde{C}_{O'',Y}^{NN} \mathcal{O}_{O'',Y}^{NN} \right] + h.c.$$

where $O'' \in \{V, A, S, P, T, Der\}$.

At zero momentum transfer ($\vec{P}_f - \vec{P}_i \rightarrow 0$), we match onto operators with nucleon currents, by replacing

$$(5.6) \quad \bar{q}(x)\Gamma_O q(x) \rightarrow G_O^{N,q} \bar{N}(x)\Gamma_O N(x)$$

such that $\langle N | \bar{q}(x)\Gamma_O q(x) | N \rangle = G_O^{N,q} \langle N | \bar{N}(x)\Gamma_O N(x) | N \rangle = G_O^{N,q} \bar{u}_N(P_f)\Gamma_O u_N(P_i)e^{-i(P_f - P_i)x}$, with $\Gamma_O \in \{I, \gamma_5, \gamma^\alpha, \gamma^\beta \gamma_5, \sigma^{\alpha\beta}\}$. The constants $G_O^{N,q}$ obtained at zero-recoil are given in appendix A, and we will assume that they are an acceptable approximation at the momentum-transfer of $\mu \rightarrow e$ conversion, which is $|\vec{P}_f - \vec{P}_i|^2 = m_\mu^2$.

Various mesons are present in the low energy theory at Λ_{exp} , so in principle the quark operators of eqn (5.1) should be also matched onto meson operators. χ PT [215] involving nucleons (see *e.g.* the review [216]) would be the appropriate formalism for this calculation, and has been used to calculate WIMP scattering on nuclei [217–220], neutrinoless-double-beta-decay [221], and SI $\mu \rightarrow e$ conversion [222]. However, to avoid more notation, here we just give results for the simple diagrams of interest. We only consider the CLFV decays of pions, because the effects of heavier mesons would be suppressed by their masses, and diagrams where a pion is exchanged

²The analogous mixing of SD WIMP scattering operators into SI operators was discussed in [213, 214].

between two nucleons are suppressed by more propagators, and would require two nucleons in the initial and final states³. Pion decay can contribute to $\mu \rightarrow e$ conversion via the second diagram of figure 5.1, in the presence of a pseudoscalar or axial vector quark current. We follow the notation of [215, 216] in matching the axial vector and pseudoscalar quark currents onto the pion, at $P^2 = m_\pi^2$, as

$$(5.7) \quad \bar{q}(x)\tau^b\gamma^\alpha\gamma_5q(x) \rightarrow f_\pi i\partial^\alpha\pi^b(x) \quad , \quad 2m_q\bar{q}(x)\tau^3\gamma_5q(x) \rightarrow f_\pi m_\pi^2\pi^0$$

in order to obtain the usual expectation values $\langle 0|\bar{u}(x)\gamma^\alpha\gamma_5d(x)|\pi^-(P)\rangle = \sqrt{2}P^\alpha f_\pi e^{-iP\cdot x}$, $\langle 0|\bar{u}(x)\gamma^\alpha\gamma_5u(x)|\pi^0(P)\rangle = P^\alpha f_\pi e^{-iP\cdot x}$, and $\langle 0|\bar{u}(x)\gamma_5u(x)|\pi(P)\rangle = f_\pi m_\pi^2 e^{-iP\cdot x}/2m_u$, where $f_\pi \simeq 92.4$ MeV. Later in the manuscript, the matrix element for $\mu \rightarrow e$ conversion on a nucleon, $\mathcal{M}(\mu + N(P_i) \rightarrow e(k) + N(P_f))$ will be required. In the case of vector, scalar or tensor interactions, it is straightforward because conversion proceeds via a 2-nucleon-2-lepton contact interaction. In the case of axial vector and pseudoscalar interactions, there is a pion exchange contribution, as illustrated in figure 5.1, so we give the matrix elements here. The pion-nucleon interaction term in the Lagrangian is taken as $ig_{\pi NN}\bar{N}\gamma_5\vec{\tau}\cdot\vec{\pi}N$, and the Goldberger-Treiman relation gives $g_{\pi pp} \simeq (G_A^{pu} - G_A^{pd})m_p/f_\pi$.

In the following two equations, $u_N = (u_p, u_n)$ represents a vector of spinors in isospin space. The matrix element $\mathcal{M}(\mu + N(P_i) \rightarrow e_X(k) + N(P_f))$ mediated by the axial up quark current, can be written [217, 223] :

$$(5.8) \quad \left(\overline{u_N}(P_f) \frac{[a_0 I + a_1 \tau_3]}{2} \gamma^\alpha \gamma_5 u_N(P_i) + C_{A,X}^{uu} \frac{g_{\pi NN} f_\pi q^\alpha}{|\vec{q}^2| + m_\pi^2} \overline{u_N}(P_f) [\tau_3] \gamma_5 u_N(P_i) \right) \overline{u_e} \gamma_\alpha P_X u_\mu$$

where $q = (0, -\vec{q}) = P_f - P_i$, the first term is written in terms of iso-scalar and iso-vector contributions $(a_0 + a_1)/2 = C_{A,X}^{uu} G_A^{p,u}$, $(a_0 - a_1)/2 = C_{A,X}^{uu} G_A^{n,u}$, whereas the pion contribution is only isovector.

In the case of the pseudoscalar operator $\mathcal{O}_{P,Y}^{uu}$, the pion exchange diagram is non-vanishing at $|\vec{q}|^2 = 0$, so at finite momentum transfer, only the additional contribution $\propto 1/(|\vec{q}|^2 + m_\pi^2) - 1/m_\pi^2$ should be included. This gives :

$$(5.9) \quad C_{P,Y}^{uu} \left(\overline{u_N}(P_f) \begin{bmatrix} G_P^{p,u} & 0 \\ 0 & G_P^{n,u} \end{bmatrix} \gamma_5 u_N(P_i) - \frac{m_N(G_A^{p,u} - G_A^{n,u})|\vec{q}|^2}{2m_u(|\vec{q}|^2 + m_\pi^2)} \overline{u_N}(P_f) [\tau_3] \gamma_5 u_N(P_i) \right) \overline{u_e} P_Y u_\mu$$

In summary, the axial vector and pseudoscalar quark operators could equivalently have been matched at Λ_{exp} to an EFT without pions, but with a q^2 -dependent ‘‘form factor’’ for the pseudoscalar nucleon operator, and an additional dimension seven derivative operator

³Such two-nucleon contributions, which arise at NLO, have been studied in WIMP scattering [217–219], and recently considered for coherent $\mu \rightarrow e$ conversion in [222].

$$(5.10) \quad \mathcal{O}_{Der,Y}^{NN} = i(\bar{e}\gamma^\alpha P_Y \mu)(\bar{N} \vec{\partial}_\alpha \gamma_5 N)$$

such that $i\langle N(P_f, s') | \bar{N}(x) \vec{\partial}_\alpha \gamma_5 N(x) | N(P_i, s) \rangle = \bar{u}_N^{s'}(P_f) q_\alpha \gamma_5 u_N^s(P_i) e^{-i(P_f - P_i) \cdot x}$. In this extended basis, the nucleon coefficients are :

$$(5.11) \quad \begin{aligned} \tilde{C}_{A,Y}^{NN} &= G_A^{N,u} C_{A,Y}^{uu} + G_A^{N,d} C_{A,Y}^{dd} + G_A^{N,s} C_{A,Y}^{ss} \\ \tilde{C}_{Der,Y}^{NN} &= \frac{m_\mu m_N}{(m_\mu^2 + m_\pi^2)} (G_A^{N,u} - G_A^{N,d}) (C_{A,Y}^{uu} - C_{A,Y}^{dd}) \\ \tilde{C}_{P,Y}^{NN} &= G_P^{N,u} C_{P,Y}^{uu} + G_P^{N,d} C_{P,Y}^{dd} + G_P^{N,s} C_{P,Y}^{ss} - \left(\frac{C_{P,Y}^{uu}}{2m_u} - \frac{C_{P,Y}^{dd}}{2m_d} \right) \frac{m_N (G_A^{N,u} - G_A^{N,d}) m_\mu^2}{(m_\mu^2 + m_\pi^2)} \\ \tilde{C}_{T,Y}^{NN} &= G_T^{N,u} C_{T,Y}^{uu} + G_T^{N,d} C_{T,Y}^{dd} + G_T^{N,s} C_{T,Y}^{ss} \\ \tilde{C}_{V,Y}^{NN} &= G_V^{N,u} C_{V,Y}^{uu} + G_V^{N,d} C_{V,Y}^{dd} \end{aligned}$$

$\tilde{C}_{Der,Y}^{NN}$ was evaluated at $q^2 = -m_\mu^2$, and the scalar nucleon coefficients, to which contribute also gluon operator of eqn (5.2), are given in [206].

To obtain the $\mu \rightarrow e$ conversion rate, the expectation values of the nucleon operators in the nucleus are required. This is discussed in the next section. We were unable to find nuclear expectation values of the tensor and pseudoscalar operator, so $\mathcal{O}_{P,Y}^{NN}$ will be neglected, and the tensor included in the scalar and axial operators, as described in eqn (5.19).



Figure 5.1: Diagrams contributing to $\mu \rightarrow e$ conversion in the presence of axial and pseudoscalar CLFV operators (represented by the grey blob)

5.3 Estimating the SD and SI rate in light nuclei

In our previous paper [210], we gave analytic estimates of the SI and SD conversion rates on Aluminium. The aim of section 5.3.1 is to give details of the calculation in the notation of

relativistic, second-quantised Field Theory. The results can then be matched onto the nuclear physics calculations of [207] (for SI conversion), and SD WIMP scattering [217, 223–225] (for SD conversion). In subsection 5.3.1.3, the estimates are mapped onto the numerical results of KKO [207], and SD conversion in heavier targets is discussed in section 5.3.2.

5.3.1 Estimating the SD and SI rate in Aluminium

We define the bound state of momentum P_i composed of an Aluminium nucleus and a muon in the $1S$ orbital as $\equiv |Al\mu(P_i)\rangle$. We are interested in the S -matrix element for $Al\mu(P_i) \rightarrow Al(P_f) + e_X^-(q)$ induced either by the dipole operator (which we discuss later), or by a four-fermion operator $(\bar{e}_X \Gamma_l \mu)(\bar{N} \Gamma_n N)$. To be concrete, we consider the S -matrix element where the nucleon N is a proton:

$$(5.12) \quad i2\sqrt{2}G_F \tilde{C}_F^{pp} \langle Al(P_f), e(q, s) | \int d^4 y [\bar{e}_X^-(y) \Gamma_l \hat{\mu}(y)] [\bar{p}(y) \Gamma_n \hat{p}(y)] | Al\mu(P_i) \rangle$$

where s is the spin of the electron selected by the chiral projector P_X , field operators wear hats, and $\Gamma_n \in \{I, \gamma_5, \gamma^\alpha, \gamma^\beta \gamma_5, \sigma^{\alpha\beta}\}$, $\Gamma_l \in \{I, \gamma^\alpha, \sigma^{\alpha\beta}\}$.

5.3.1.1 four-fermion operators

A first step is to write the motionless bound state $|Al\mu(0)\rangle$ as

$$(5.13) \quad |Al\mu(\vec{P}_i = 0)\rangle = \sqrt{\frac{2(M_{Al} + m_\mu)}{4M_{Al}m_\mu}} \sum_w \int \frac{d^3 k}{(2\pi)^3} \tilde{\psi}_\mu(\vec{k}) |Al(-\vec{k})\rangle \otimes |\mu(\vec{k}, w)\rangle$$

where w is the spin of the muon, the square-root prefactor accounts for one vs two-body normalisation of states in Lorentz-covariant field theory conventions where states are normalised $\propto \sqrt{2E}$ [226], and $\tilde{\psi}_\mu(\vec{l}) = \int d^3 z e^{-i\vec{l}\cdot\vec{z}} \psi_\mu(\vec{z})$ is the fourier transform of the Schrodinger wavefunction $\psi_\mu(\vec{z})$ for a muon in a central potential of charge Z .

For $Z\alpha \ll 1$, the unit-normalised wavefunction, for either spin state, can be approximated [227–229] as

$$(5.14) \quad \psi_\mu(r, \theta, \phi) \simeq \frac{[m\alpha Z]^{3/2}}{\sqrt{\pi}} e^{-Z\alpha m r} .$$

We approximate the outgoing electron as a free particle (plane wave), which should be acceptable for an Aluminium target. For heavy nuclei, the Dirac equation for the electrons outgoing in the field of the nucleus should be solved [205], allowing to express the electron as a superposition of free states. This approach was followed in KKO [207].

In the same non-relativistic bound state formalism (see *e.g.*, Appendix B of [224] for more details), the Aluminium nucleus, of spin J_A , can be written as a bound state composed of a proton of spin t , with another state M_1 of mass M_1 and spin J_M containing $Z - 1$ protons and $A - Z$ neutrons:

$$(5.15) \quad \langle Al(P_f), J_A | = \sqrt{\frac{2M_{Al}}{4M_1 m_p}} \sum_{t, J_M} \int \frac{d^3 l}{(2\pi)^3} \tilde{f}_p^*(\vec{l}, t, J_M, J_A) \langle M_1(-\vec{l} + M_1 \vec{v}_f), J_M | \times \langle p(\vec{l} + m_p \vec{v}_f), t |$$

where $\tilde{f}_p(\vec{l}, t, J_M, J_A)$ is the fourier transform of the (unknown) wavefunction of the proton in the potential of M_1 , and $P_f = (M_{Al}, M_{Al} \vec{v}_f)$.

The fermion operators can be expanded as [226]

$$(5.16) \quad \hat{\mu}(y) = \sum_w \int \frac{d^3 p}{(2\pi)^3} \frac{1}{\sqrt{2E}} \left(\hat{a}_p^w u_p^w e^{-ip \cdot y} + \hat{b}_p^{w\dagger} v_p^w e^{ip \cdot y} \right)$$

and act on states as $\hat{\mu}(y)|\vec{k}, w\rangle = u_k^w e^{-ik \cdot y} |0\rangle$, where the spinors are normalised as $u_k^\dagger u_k = 2k_0$. The S-matrix element of eqn (5.12) can then be evaluated as

$$(5.17) \quad i(2\pi)^4 \delta^4(P_i - P_f - q) 2\sqrt{2} G_F \tilde{C}_\Gamma^{pp} \frac{M_{Al}}{m_p \sqrt{2m_\mu}} \sum_{p \in Al} \sum_{spins} \int d^3 x \psi_\mu(\vec{x}) |f_p(\vec{x}, J_A, J_M, t)|^2 e^{-i\vec{q} \cdot \vec{x}} (\bar{u}_e^s \Gamma u_\mu^w) (\bar{u}_p^o \Gamma u_p^t)$$

where the spinors subscripts are particle names rather than momenta, and $P_i \simeq (M_{Al} + m_\mu, \vec{P}_i)$, $P_f \simeq (M_{Al}, \vec{P}_f)$. To obtain this approximation, the states were taken to be non-relativistic, the wavefunctions expressed in position space, the proton wavefunction was assumed independent of the proton spin, and the dependence of spinors on three-momenta was neglected in many integrals. Notice the M_{Al}/m_p enhancement factor that arises automatically for both spin-dependent and spin-independent interactions, and that the usual $(2\pi)^4 \delta^4(P_i - P_f - q)$, which accounts for four-momentum conservation, appears despite that there is a spatial integral over the nucleus. In the following, we drop the spin indices in the nucleon distribution in the nucleus $|f_N|^2$.

The leptonic spinor contraction is independent of \vec{x} and can be factored out of the spatial integral in eqn (5.17). In light nuclei such as Aluminium, the muon wavefunction can also be factored out [203], because the muon wavefunction decreases on the scale $\sim 1/(Z\alpha m_\mu)$, which is larger than the radius of the Aluminium nucleus, given in [230] as ≤ 6 fm. On the other hand, the first zero of the electron plane wave (the $e^{-i\vec{q} \cdot \vec{x}}$ of eqn (5.17)) would occur at $r \sim \pi/(m_\mu) \sim 6$ fm.

The nucleon spinor contractions, in the non-relativistic limit, can be written (see eqn (47) of [231]):

$$\begin{aligned}
 (5.18) \quad & \bar{u}_N^o(P_f)u_N^t(P_i) && \rightarrow 2m_N\delta^{ot} \\
 & \bar{u}_N^o(P_f)\gamma_5 u_N^t(P_i) && \rightarrow 2\vec{q} \cdot \vec{S}_N \\
 & \bar{u}_N^o(P_f)\gamma^\alpha u_N^t(P_i) && \rightarrow 2m_N\delta^{o\alpha}\delta^{\alpha 0} \\
 & \bar{u}_N^o(P_f)\gamma^j\gamma_5 u_N^t(P_i) && \rightarrow 4m_N S_N^j \\
 & \bar{u}_N^o(P_f)\sigma_{ik} u_N^t(P_i) && \rightarrow 4m_N \epsilon_{ikj} S_N^j \\
 & \bar{u}_N^o(P_f)\sigma^{0k} u_N^t(P_i) && \rightarrow iq^k
 \end{aligned}$$

where the spin vector of the nucleon is defined as $2\vec{S}_N = u_N^\dagger \vec{\Sigma} u_N / 2E_N$, and the rotation generator $S^{ij} = \frac{i}{4}[\gamma^i, \gamma^j] = \frac{1}{2}e^{ijk}\Sigma^k$. The momentum transfer $q = P_i - P_f$ has been neglected, except in the case of the pseudoscalar, where the leading term is $\mathcal{O}(\vec{q} \cdot \vec{S}_N)$, and in the case of the tensor, where there is a ‘‘spin-independent’’ contribution $\propto \vec{q}$.

These spinor identities allow the tensor interaction involving nucleons to be absorbed into the scalar and axial vector coefficients. Following [210], we define

$$(5.19) \quad \tilde{C}_{S,Y}^{NN} = \tilde{C}_{S,Y}^{NN} + 2\frac{m_\mu}{m_N}\tilde{C}_{T,Y}^{NN}, \quad \tilde{C}'_{A,Y}{}^{NN} = \tilde{C}_{A,Y}^{NN} + 2\tilde{C}_{T,X}^{NN}$$

where in both cases the 2 arises from the two antisymmetric contributions of the tensor, the unprimed \tilde{C} s are defined in eqn (5.11), $X, Y \in \{L, R\}$, and $X \neq Y$ because only operators with electrons of the same chirality can interfere. Notice that there is an error in [210], where is written $\tilde{C}_{A,Y}^{NN'} = \tilde{C}_{A,Y}^{NN} + 2\tilde{C}_{T,Y}^{NN}$.

It remains to evaluate the expectation value of the nucleon currents in the nucleus.

- In the case of the scalar or vector operators, the matrix element of eqn (5.17) becomes

$$(5.20) \quad \mathcal{M} = 2\sqrt{2}G_F \tilde{C}_{S,V}^{pp'} \frac{2M_{Al}}{\sqrt{2m_\mu}} \psi_\mu(0) \sum_{p \in A} \int d^3x |f_p(r)|^2 \frac{\sin(qr)}{qr} \sum_{s,r} \begin{cases} (\bar{u}_e^s u_\mu^r) & \text{scalar} \\ (\bar{u}_e^s \gamma^0 u_\mu^r) & \text{vector} \end{cases}$$

where the sum over protons in the nucleus will give a factor Z , we drop the spin indices because the sum and average give one, and assume a spherically symmetric nucleon distribution $|f_p(r)|^2$ in the nucleus, which allows to replace⁴ $e^{-i\vec{q}\cdot\vec{x}} \rightarrow \frac{\sin(qr)}{qr}$. The ‘‘form factors’’

$$(5.21) \quad F_N(m_\mu) = \int d^3x |f_N(r)|^2 \frac{\sin(m_\mu r)}{m_\mu r}$$

are defined in eqns (29) and (30) of [207]: $F_p(m_\mu) \sim .53$ for Al, and $\sim .35$ for Ti.

⁴Recall that a plane wave can be expanded on spherical harmonics as $e^{iqz} = \sum_{\ell=0}^{\infty} i^\ell \sqrt{(4\pi)(2\ell+1)} j_\ell(qr) Y_\ell^0(\theta)$, and $Y_0^0(\theta) = 1/\sqrt{4\pi}$.

- The expectation value of the axial current in Aluminium ($A = 27, Z = 13, \vec{J}_{Al} = 5/2$) was calculated by Engel *et.al* [225] and Klos *et.al* [217] using the shell model. In the zero-momentum transfer limit, where the spin expectation values S_N^A are defined by:

$$(5.22) \quad \sum_{N \in A} \int d^3x |f_N(\vec{x})|^2 (\bar{u}_N \gamma^k \gamma_5 u_N) = 4m_N S_N^A \frac{J_A^k}{|J_A|},$$

they obtain $S_n^{Al} = 0.0296$, $S_p^{Al} = 0.3430$. (J_A^k is a quantum mechanical operator, to be evaluated in the ground state of the nucleus A). At finite momentum transfer, references [217, 225] include the nucleon axial vector operators $\mathcal{O}_{A,X}^{NN}$ and the pion exchange operator $\mathcal{O}_{Der,X}^{NN}$, in the combination induced by axial vector quark operators. The various terms in the matrix-element-squared have different spin sums, so the finite momentum transfer correction depends on $\tilde{C}_{A,X}^{pp'}$ and $\tilde{C}_{A,X}^{nn'}$, and is quoted as a multiplicative factor $S_A(m_\mu)/S_A(0)$ in the rate (see eqn (5.26)). Neglecting $S_n^{Al} \ll S_p^{Al}$, the results of Engel *et. al* for Aluminium give [225]

$$(5.23) \quad S_{Al}(k) \propto (0.31500480 - 1.857857y + 4.86816y^2 - 5.422770y^3)$$

where $y = (m_\mu b/2)^2$ and $b = 1.73$ fm. This gives $S_{Al}(m_\mu)/S_{Al}(0) = 0.29$.

- At zero momentum transfer, the nuclear expectation value of tensor operators $\mathcal{O}_{T,X}^{NN}$ is proportional to that of axial vector operators, as accounted for in eqn (5.19). However, at finite momentum transfer, there is no pion exchange contribution for the tensor operator (while pion exchange induces $\mathcal{O}_{Der,X}^{NN}$ in the presence of the axial vector quark operators), so the redefinition of eqn (5.19) is not valid. Indeed, the tensor and axial vector operators are distinct at finite momentum transfer.

However, we did not find nuclear calculations of SD scattering on Aluminium mediated by the tensor operator. We can try to estimate the error from using the axial results for the tensor: at $q^2 = -m_\mu^2$, the pion exchange contribution to the matrix element in eqn (5.8) is comparable to the four-fermion contact interaction. Also, the finite-momentum-transfer suppressions of the axial and scalar rates on Aluminium are comparable ($S_{Al}(m_\mu)/S_{Al}(0) \simeq |F_N(m_\mu)|^2$), despite that one might expect the oscillations of the electron wavefunction to suppress the SD rate more than the SI rate, because spin-carrying nucleons are likely to be at large radii. So we interpret that axial matrix element is amplified by a factor ~ 2 at $q^2 = -m_\mu^2$ (due to the pion), and suppressed by an extra factor $\sim 1/2$ (as compared to the scalar matrix element) due to the oscillations of the electron wavefunction, and estimate that the identification of eqn (5.19) could overestimate the tensor contribution to the branching ratio by a factor $\sim 2 \rightarrow 4$ (depending on whether the pseudoscalar and axial matrix elements interfere).

- The pseudoscalar operator $\mathcal{O}_{P,X}^{NN}$ is proportional to the nucleon spin, is only present at finite momentum transfer, and at $q^2 = -m_\mu^2$, is enhanced by a pion exchange contribution of comparable magnitude. Since the magnitude of the pseudoscalar spinor contraction in eqn (5.18) is suppressed with respect to the axial vector by $\sim m_\mu/2m_N$, its contribution to the SD branching ratio could be $\sim m_\mu^2/4m_N^2 \times$ the axial vector contribution. However, the identification $\tilde{C}'_{A,Y}{}^{NN} = \tilde{C}'_{A,Y}{}^{NN} + \frac{m_\mu}{2m_N} \tilde{C}_{P,X}^{NN}$ does not work, because the spin sums suppress the axial-pseudoscalar interference term. A dedicated nuclear calculation would seem required for both the pseudoscalar and tensor operators.

To obtain the matrix-element-squared, the lepton spinor part can be evaluated by Dirac traces. Then to perform the nuclear spin sums in the SD case, the identity

$$(5.24) \quad \frac{1}{(2J_\mu + 1)(2J_A + 1)} \sum_{spins} \sum_{k,i} \langle J_\mu | \hat{J}_\ell^k | J'_e \rangle \langle J'_e | \hat{J}_\ell^i | J_\mu \rangle \langle J'_A | \hat{J}_A^k | J_A \rangle \langle J_A | \hat{J}_A^i | J'_A \rangle = \frac{1}{3} J_\mu (J_\mu + 1) J_A (J_A + 1)$$

can be used.

Finally, the conversion rate is obtained as

$$\Gamma = \frac{1}{2M_{Al}} \int d\Pi |\overline{\mathcal{M}}|^2 = \frac{m_\mu}{8M_{Al}^2 \pi} |\overline{\mathcal{M}}|^2$$

where $|\overline{\mathcal{M}}|^2$ is averaged over the incident spins, and $d\Pi$ gives the integration over the final state phase space of the nucleus and electron.

These steps give an analytic estimate for the four-fermion contributions to the SI conversion rate on a nucleus of atomic number A and charge Z :

$$(5.25) \quad \frac{\Gamma_{SI}}{\Gamma_{capt}} = 2B_0 |Z(\tilde{C}'_{S,L}{}^{pp} + \tilde{C}_{V,R}{}^{pp} + 2eC_{D,L})F_p(m_\mu) + (A-Z)(\tilde{C}'_{S,L}{}^{nn} + \tilde{C}_{V,R}{}^{nn})F_n(m_\mu)|^2 + \{L \leftrightarrow R\} .$$

where the F_N are defined in eqn (5.21) and related to the overlap integrals of KKO in (5.34), the contribution of the dipole operator (estimated in subsection 5.3.1.2) was also included, and

$$B_0 = \frac{G_F^2 m_\mu^5}{\Gamma_{capt} \pi^2} (Z\alpha)^3 \simeq \begin{cases} 0.310 & Al (Z = 13) \\ 0.438 & Ti (Z = 22) \end{cases} ,$$

where Γ_{capt} is the rate for the Standard Model process of muon capture [207, 232]. Similarly, the SD conversion rate on a nucleus of atomic number A , charge Z and spin J_A is

$$(5.26) \quad \frac{\Gamma_{SD}}{\Gamma_{capt}} = 8B_0 \frac{J_A + 1}{J_A} \left| S_p^A \tilde{C}'_{A,L}{}^{pp} + S_n^A \tilde{C}'_{A,L}{}^{nn} \right|^2 \frac{S_A(m_\mu)}{S_A(0)} + \{L \leftrightarrow R\} .$$

where the spin expectation values S_N^A and the finite momentum transfer correction $S_A(k)$ are given for Aluminium at eqn (5.23).

5.3.1.2 the dipole

In the case of the dipole operator of eqn (5.2), the S-matrix element can be written

$$(5.27) \quad i \frac{2\sqrt{2}G_F}{\sqrt{2m_\mu}} C_{D,Y} m_\mu \langle e(q, s) | \int d^4y 2(\overline{e\hat{X}}(y)) \sigma^{0i} \cdot E_i(y) P_Y \hat{\mu}(y) | \mu(q) \rangle$$

$$(5.28) \quad = i \frac{2\sqrt{2}G_F}{\sqrt{2m_\mu}} C_{D,Y} m_\mu 2\pi \delta(E_e - m_\mu) \int d^3y e^{-i\vec{q}\cdot\vec{y}} \psi_\mu(\vec{y}) 2(\overline{u_e} \sigma^{0i} \cdot E_i(y) P_Y u_\mu(y))$$

$$(5.29) \quad \equiv i 2\pi \delta(E_e - m_\mu) \tilde{\mathcal{M}} \quad , \quad \tilde{\mathcal{M}} = \frac{2\sqrt{2}G_F}{\sqrt{2m_\mu}} 2C_{D,Y} m_\mu \int d\Omega r^2 dr \frac{\sin m_\mu r}{m_\mu r} \psi_\mu(r) (\overline{u_e} \sigma^{0i} P_Y u_\mu) E_i(r)$$

where the 2 under the integral is to account for $E_i = F_{0i} = F_{i0}$, and the magnitude of the radial electric field induced by the nucleus is [207]

$$(5.30) \quad E(r) = \frac{Ze}{r^2} \int_0^r r'^2 |f_p(r')|^2 dr' \quad .$$

To estimate the dipole matrix element analytically, we suppose that the electric field only contributes at radii within the first zero of the electron wavefunction r_e , because outside the rapid oscillation of the electron wavefunction gives an approximate cancellation in \mathcal{M} . The muon wavefunction is approximately constant at such radii. The radius of the Aluminium nucleus is comparable to r_e , but if we nonetheless approximate the nucleon distribution $|f_p(r)|^2$ as a constant for $r < r_e$, we obtain

$$(5.31) \quad E(r) \simeq \frac{Zer}{3} |f_p(r)|^2 \quad , \quad \tilde{\mathcal{M}} \simeq \frac{2\sqrt{2}G_F}{\sqrt{2m_\mu}} 2C_{D,Y} m_\mu \psi_\mu(0) \int d\Omega \frac{r^3 dr}{3} |f_p(r)|^2 \frac{\sin m_\mu r}{m_\mu r} (\overline{u_e} \sigma^{0i} P_Y u_\mu) Z e \hat{r}_i$$

where \hat{r} is a radial unit vector.

The ‘‘matrix element’’ $\tilde{\mathcal{M}}$ neglects recoil of the nucleus, so the final state phase space in the rate is only one-body, and we reproduce the analytic estimate of [207] for light nuclei ($D \sim 8eS^p$ given above eqn (29) of [207]):

$$(5.32) \quad BR_{SI} = \frac{\overline{|\tilde{\mathcal{M}}|^2} m_\mu}{2\pi} = \frac{8G_F^2 m_\mu^5}{\pi^2 \Gamma_{capt}} (\alpha Z)^3 |Z e C_{D,Y} F_p(m_\mu)|^2$$

This estimate uses $\int r^3 dr/3 \simeq \int r^2 dr$, and applies in the absence of other contributions; the dipole coefficient sums with the scalar and vector coefficients in the amplitude, as given in eqn (5.25).

5.3.1.3 Comparing to KKO

This section compares our estimates to the more exact formulae of [207] (KKO). Our estimates use a solution of the Schrodinger equation for the muon, a plane wave for the electron, and chiral γ -matrices. KKO solve the Dirac equation in the potential of the nucleus, both for the electron and muon, use Bjorken and Drell γ -matrix conventions, and give the branching ratio as:

$$(5.33) \quad BR(A\mu \rightarrow Ae) = \frac{32G_F^2 m_\mu^5}{\Gamma_{cap}} \left[|\tilde{C}_{V,R}^{pp} V^{(p)} + \tilde{C}_{S,L}^{pp} S^{(p)} + \tilde{C}_{V,R}^{nn} V^{(n)} + \tilde{C}_{S,L}^{nn} S^{(n)} + C_{D,L} \frac{D}{4}|^2 + \{L \leftrightarrow R\} \right]$$

where Γ_{cap} is the rate for the muon to transform to a neutrino by capture on the nucleus (see [207, 232]), and the nucleus- and nucleon-dependent ‘‘overlap integrals’’ $V_X^{(N)}$, $S_X^{(N)}$, $D^{(N)}$ correspond to the integral over the nucleus of the lepton wavefunctions and the appropriate nucleon density (vector, scalar, electric field for the dipole operator; the definitions and numerical values are given in KKO [207]). The numerical coefficient in eqn (5.33) differs from the result given in KKO, because $4\tilde{C}|_{here} = \tilde{g}|_{KKO}$.

Our unit-normalised nuclear density $|f_N(r)|^2$ can be identified with the similarly normalised density $\rho_N(r)$ of KKO [207]. Our Schrodinger approximation for the muon wavefunction can be identified to the upper component (in Bjorken and Drell γ conventions) of the Dirac wavefunction obtained by [207]. Then the normalisation conventions of eqn (5) and (7) of [207] identify

$$\psi_\mu(r, \theta, \phi) \leftrightarrow \frac{g_\mu(r)}{\sqrt{4\pi}} .$$

In the limit of massless electron, the upper (g_e) and lower components (if_e) of the electron wave function of [207] are comparable. The electron normalisation condition given in eqn (8) of [207] then implies that we can identify our electron plane wave as

$$if_e = g_e(r) \leftrightarrow \sqrt{2} \frac{\sin m_\mu r}{r} \leftrightarrow \sqrt{2} m_\mu e^{-i\vec{k}\cdot\vec{r}} .$$

In the approximation where the muon wavefunction is constant in the nucleus, the overlap integrals of [207] can be identified to our approximations as

$$(5.34) \quad \begin{aligned} S^{(p)}, V^{(p)} &\rightarrow \frac{m_\mu |\psi_\mu(0)|}{4\sqrt{\pi}} Z \int d^3x e^{-i\vec{k}\cdot\vec{x}} |f_p|^2 \\ S^{(n)}, V^{(n)} &\rightarrow \frac{m_\mu^{5/2} (Z\alpha)^{3/2}}{4\pi} (A-Z) \int d^3x e^{-i\vec{k}\cdot\vec{x}} |f_n|^2 , \end{aligned}$$

as given in eqns (29) - (31) of KKO.

5.3.2 Spin-dependent conversion in other light nuclei

In this section we consider how the estimates of the previous section could be applied to other nuclei. Recall that light nuclei are interesting for SD detection, because the SD rate is relatively suppressed by $1/A^2$ compared to the SI rate: the ratio Γ_{SD}/Γ_{SI} is largest for light nuclei.

The matrix element given in eqn (5.17) for SD $\mu \rightarrow e$ conversion contains the integral of the axial current over the nucleus, weighted by the lepton wavefunctions. In the case of light nuclei ($Z \leq 20$), as discussed in the previous section, the muon wavefunction can be taken constant in the nucleus, and the electron can be treated as a plane wave. This allows to use the results of nuclear calculations [223] of matrix elements for spin-dependent WIMP scattering at finite-momentum-transfer. The zero-momentum-transfer matrix elements (spin expectation values; see eqn (5.22)), have been calculated for a wide variety of nuclei [233], and finite momentum transfer results also been obtained for some nuclei [234]. For $\mu \rightarrow e$ conversion in heavier nuclei, a dedicated nuclear calculation would be required to obtain the expectation values of the SD operators weighted by the lepton wavefunctions.

An interesting light nucleus for SD $\mu \rightarrow e$ conversion could be Titanium ($Z=22$)⁵, because it has isotopes with and without spin, so targets of different isotopic abundances could allow to distinguish SD from SI operators. Titanium has a spin-zero isotope with $A = 48$ and 74% natural abundance [235], an isotope with $A = 47, J = 5/2$, 7.5% abundance, and another isotope with $A = 49, J = 7/2$, 5.4 % abundance. These natural abundances of more than 5 % are large enough to make sufficiently-enriched sample targets.

In the Odd Group Model, Engel and Vogel [236] obtained spin expectation values $S_n^{Ti,47} = 0.21, S_p^{Ti,47} = 0$, and $S_n^{Ti,49} = 0.29, S_p^{Ti,49} = 0$. Unfortunately, we were unable to find finite-momentum-transfer corrections to the spin expectation values in Titanium. However, we observe that in Aluminium, the SI and SD form factors are comparable: $0.28 = |F_p(m_\mu)|^2 \approx S_{Al}(m_\mu)/S_{Al}(0) = 0.29$. A similar relation appears to hold [207, 234] for Florine, where $|F_n(m_\mu)|^2 \approx S_{Fl}(m_\mu)/S_{Fl}(0) \approx .36$. This suggests that for light nuclei, the spin-expectation-squared at $|\vec{q}|^2 \neq 0$ (that is, $S_A(m_\mu)$), is similar to the square of the spin-expectation-value at zero momentum transfer, multiplied by the square of the SI $|\vec{q}|^2 \neq 0$ form-factor. Or taking the square root:

$$(5.35) \quad \sum_{p \in A} \int d^3x |f_p(\vec{x})|^2 e^{-i\vec{q} \cdot \vec{x}} (\bar{u}_p \gamma^k \gamma_5 u_p) \approx \sum_{p \in A} \int d^3y |f_p(\vec{y})|^2 (\bar{u}_p \gamma^k \gamma_5 u_p) \times \int d^3z |f_p(\vec{z})|^2 e^{-i\vec{q} \cdot \vec{z}} .$$

So we apply this approximation to Titanium, and estimate $S_{Ti}(m_\mu)/S_{Ti}(0) \approx 0.12$.

⁵Titanium was used as a target by SINDRUMII [13, 137, 202], who set an upper bound $BR(\mu Ti \rightarrow e Ti) < 4.3 \times 10^{-12}$.

5.4 Parametric expansions and uncertainties

Once $\mu \rightarrow e$ conversion is observed, the aim will be to determine (or constrain) as many operator coefficients as possible. This would require at least as many “independent” observations as operators, where observations are independent if, in spite of uncertainties, they depend on a different combination of coefficients. So the purpose of this section, is to estimate the uncertainties in relating the conversion rate to operator coefficients.

The inputs for this calculation, (equivalently, the theoretical parameters to be extracted from data) are the coefficients of either the quark operators (see eqn 5.1), or of the nucleon operators (see eqns 5.11,5.19), in both cases at the experimental scale Λ_{exp} . So uncertainties associated to the Renormalisation Group evolution from the New Physics scale to the experimental scale are not considered. In the remainder of this paper, we will sometimes use the quark operator basis, and sometimes the nucleon basis. As discussed below, there are significant uncertainties in some of the $\{G_O^{N,q}\}$, which are required to extract the coefficients of the quark operators, but can be avoided by using the nucleon operators.

- There are uncertainties in some of the matching coefficients that relate quark to hadron operators (see eqn (5.6) and appendix A). The $G_V^{N,q}$ are from charge conservation, so should be exact. For the axial and scalar coefficients, the determinations from data (see eqn (A.6)) and from the lattice (A.7,A.9) are quoted with smaller uncertainties than their differences (this is especially flagrant for the $G_S^{N,q}$, whose lattice and data values differ by 30-50%, and are both quoted with $\leq 10\%$ uncertainties). First, it can be hoped that these discrepancies will be reduced in the future. Secondly, in some models (or equivalently, for some choices of coefficients), these factors can be cancelled by taking ratios. Finally, if we are only interested in discriminating SD from SI contributions to the rate, this distinction exists at the nucleon level, so the matching to quark operators is not required.
- The lepton interactions with nucleons are calculated at Leading Order (LO) in χPT . At NLO, arise pion loops as well as processes with two nucleons in the initial and final states which exchange a pion that interacts with the leptons. For the case of WIMP scattering, such NLO contributions for the scalar quark operator have been discussed [218, 219, 237] and reference [218] estimates them to be a higher order effect ($\leq 10\%$), provided there are no cancellations among the LO contributions. The two-nucleon contributions were also calculated to be unexpectedly small for WIMP scattering on few-nucleon nuclei [238]. However, after this manuscript was completed, appeared a study of the $\mu \rightarrow e$ conversion rate mediated by the scalar and vector interactions [222], where the authors estimate that the NLO effects associated to pion exchange between two nucleons can reduce the scalar matrix element by 20→ 30% (NLO corrections vanish for the vector). We will account for these nucleon/ χPT uncertainties by including them in the uncertainties in the overlap integrals.

- The $\mu \rightarrow e$ conversion matrix element, expressed as a function of nucleon operator coefficients, relies on many perturbative expansions, among which an expansion in the finite-momentum-transfer $|\vec{q}|^2 = m_\mu^2$. Naively such corrections are $\mathcal{O}(m_\mu^2/m_N^2)$ (so negligible), however in practise there are various effects which are not so suppressed. First, the finite momentum transfer gives a significant suppression of the matrix element. In our analytic approximations, where the muon is at rest and the electron momentum $\vec{k} = \vec{q}$, this is encoded in the form factors F_N (see eqn (5.21)), which are $\sim .2 \rightarrow 0.7$. KKO include this effect more accurately, by solving the Dirac equation for the leptons. Secondly, finite momentum transfer effects can change the nucleon and lepton spinor algebra. This is discussed for Dark Matter in [224, 231], and gives the $\mathcal{O}(m_\mu/m_N)$ contribution of the tensor to the scalar coefficient given in eqn (5.19). We include this correction, because the tensor operator at zero momentum transfer contributes to the SD matrix element (suppressed by $1/A$), whereas this (m_μ/m_N) -suppressed contribution gains a relative factor A because it contributes to the SI matrix element. The ratio of these contributions to the conversion rate is estimated in appendix B. Finally, pion exchange becomes relevant at $|\vec{q}|^2 = m_\mu^2$ for the axial vector and pseudoscalar operators (see eqns (5.8,5.9)), and is included in the nuclear matrix elements of [225] that we use for the axial vector in Aluminium. Pion contributions at $|\vec{q}| \neq 0$ to the SI rate are discussed above. We hope that these are the dominant finite-momentum-transfer corrections, such that any other effects are negligible ($< 10\%$) corrections.
- In our calculation of the SD matrix element, the velocity of the initial muon was neglected. This may seem doubtful, by analogy with the extended basis of WIMP scattering operators constructed in [224], because these authors expand in both the momentum transfer between the WIMP and nucleon, and the incoming velocity difference. However, in our case, the muon velocity is parametrically smaller: writing the binding energy of the $1s$ state as $\pi Z\alpha m_\mu \sim m\vec{v}^2$, gives $|\vec{v}| \sim \sqrt{Z\alpha}$. We neglect any effects related to this velocity.
- There could be nuclear uncertainties in the SI overlap integrals S^N, V^N, D , in addition to the effects discussed above. These were estimated by [207] to be \sim a few % in most cases, $\leq 10\%$ in the case of some heavier nuclei

Consider first the uncertainty on the SI rate, because, when $\mu \rightarrow e$ conversion is observed in a nucleus with spin, the SD conversion rate can only be observed, if it is larger than the uncertainty in the ubiquitous A^2 -enhanced SI rate. The uncertainty in Γ_{SI} , written as a function of the quark operator coefficients $C_{O,X}^{qq}$, would arise from the $G_O^{N,q}$, from the overlap integrals S^N, V^N, D of [207], and from NLO contributions in χPT :

$$(5.36) \quad \frac{\delta\Gamma_{SI}}{\Gamma_{SI}}(C_{O,X}^{qq}) \simeq 2 \left(\sum_{X=L,R} \frac{|F_X|}{|F_L|^2 + |F_R|^2} \left(C_{S,X}^{qq} S^N \delta G_S^{N,q} + \tilde{C}_{S,X}^{NN} [\delta S^N]_{NLO} \right) + \frac{\delta I_A}{I_A} \right)$$

where $F_L = \tilde{C}_{V,L}^{NN} V^{(N)} + \tilde{C}_{S,R}^{NN} S^{(N)} + \tilde{C}_{D,R} D$, sums on $N \in \{n, p\}$ and $q \in \{u, d, s\}$ are implicit, the gluon contribution to the scalar [206] was neglected, for simplicity a common uncertainty $\frac{\delta I_A}{I_A}$ was assigned to the overlap integrals in nucleus A , except for the effect of neglecting pion exchange between two nucleons [218, 222] (discussed above), which is parametrised as an uncertainty $[\delta S^N]_{NLO}$ in the scalar overlap integrals. Expressed this way, the uncertainty depends on the quark coefficients present: for $C_{S,X}^{qq} \gg C_{V,X}^{qq}, C_{D,X}$, the current discrepancies in the determination of the $G_S^{N,q}$ and $[\delta S^N]_{NLO}$ give an $\mathcal{O}(1)$ uncertainty on the conversion rate, whereas if only the $C_{V,X}^{qq}$ and $C_{D,X}$ were present, the rate uncertainty would come from the overlap integrals. The $G_S^{N,q}$ uncertainties can be avoided by expressing the rate in terms of the coefficients of the nucleon Lagrangian; if in addition, $[\delta S^N]_{NLO}/S_N < 10\%$, then the uncertainty in the SI rate comes from the overlap integrals. From the KKO discussion, $2\frac{\delta I_A}{I_A} \leq 10\%$ in most cases, $< 20\%$ in all cases. In order to be concrete, we assume in the remainder of this paper, that the uncertainty on the SI rate expressed in terms of coefficients on nucleons, is $\leq 10\%$. This suggests that the SD rate would need to be $\geq 10 - 20\%$ of the SI rate, to be observed.

A better sensitivity to the SD rate could be obtained by using isotopes with and without spin as targets: consider for instance, $^{48}\text{Titanium}$ (without spin), and $^{47}\text{Titanium}$ (with spin), whose SI matrix elements differ by one neutron. Using the analytic approximation of eqn (5.25), the ratio of the SI conversion rates, for real coefficients and left-handed electrons, is

$$(5.37) \quad \frac{\Gamma_{SI}(^{47}\text{Ti})}{\Gamma_{SI}(^{48}\text{Ti})} \simeq 1 - 2 \frac{|(\tilde{C}'_{S,L}{}^{nn} + \tilde{C}_{V,R}{}^{nn})F_n(m_\mu)|}{|Z(\tilde{C}'_{S,L}{}^{pp} + \tilde{C}_{V,R}{}^{pp} + 2eC_{D,L})F_p(m_\mu) + (A - Z)(\tilde{C}'_{S,L}{}^{nn} + \tilde{C}_{V,R}{}^{nn})F_n(m_\mu)|} + \dots$$

where the second term⁶ is $\mathcal{O}(1/A)$. The theoretical uncertainty in this ratio will arise from the overlap integrals (equivalently, form factors F_N), so should be of order $\frac{1}{A} \frac{\delta I_{Ti}}{I_{Ti}} \leq 0.002$. This greatly improves the sensitivity to the SD rate, although it is unlikely to allow as good a sensitivity to SD as SI coefficients, because the SD rate is parametrically suppressed as $1/A^2$ which is $\leq \frac{1}{A} \frac{\delta I_{Ti}}{I_{Ti}}$.

Some prospects for distinguishing among SI operators by using different targets will be discussed in section 5.5.3. For this, the various targets need to probe different combinations of operator coefficients, and this difference needs to be larger than the theoretical uncertainty. In section 5.5.3, targets are parametrised as vectors in coefficient space, whose components are the overlap integrals (see eqn (5.54)), and targets are assumed to probe different combinations of operator coefficients if the angle between the vectors is $\geq 10\% \geq \frac{\delta I_A}{I_A}$. This estimate can be obtained in the 2-dimensional plane of the vectors, where the uncertainty on the angle θ of a point $(I_1 \pm \delta I_1, I_2 \pm \delta I_2)$ is

$$(5.38) \quad \delta\theta \simeq \frac{\delta I_i}{I_i} \times \frac{I_1 I_2}{I_1^2 + I_2^2}$$

⁶Since ^{47}Ti and ^{48}Ti only differ by one neutron, there would be no $\mathcal{O}(1/A)$ term if the CLFV operators only involved protons or the dipole.

5.5 Implications of including the SD rate

The aim of this section is to explore the implications of including the SD contribution to $\mu \rightarrow e$ conversion. At first sight, it appears to be of limited interest: the ratio of SD to SI rates is

$$\frac{\Gamma_{SD}}{\Gamma_{SI}} \sim \frac{|C_{SD}|^2}{A^2|C_{SI}|^2}$$

so for a SI operator coefficient C_{SI} comparable to C_{SD} , the SD contribution to the branching ratio is much smaller than the $\sim 10\%$ theory uncertainty of the SI contribution, estimated in the previous section. Furthermore, as discussed in [210], renormalisation group running between the New Physics scale and low energy mixes the tensor and axial vector (“SD”) operators to the scalars and vectors, so even in a New Physics model that only induces SD operators, their dominant contribution to $\mu \rightarrow e$ conversion is via the SI operators that arise due to RG running. This perspective that SD conversion can be ignored is illustrated in section 5.5.1, where we consider three leptoquark models. They give negligible SD branching ratios, but we explore the prospects of distinguishing them by comparing the SI rates in various nuclei.

The SD conversion rate is nonetheless interesting, because it is an independent observable, that can be observed by comparing targets with and without spin. As in the case of dark matter, it is sensitive to different operator coefficients (evaluated at the experimental scale) from the SI process, so provides complementary information. In section 5.5.2 we allow $C_{SD} \gg C_{SI}$ such that the SD rate can be observable, and discuss the constraints that could be obtained from upper bounds on $\mu \rightarrow e$ conversion. Finally in section 5.5.3, we allow arbitrary coefficients to all the operators of the nucleon-level Lagrangian, and explore the prospects for identifying coefficients should $\mu \rightarrow e$ conversion be observed.

5.5.1 Leptoquarks

We consider three possible leptoquark scenarios, each containing an SU(2) singlet leptoquark, whose mass $M \geq \text{few TeV}$ respects direct search constraints [239–241], and which has only one coupling to electrons and one to muons. The scenarios are represented by adding to the Standard Model the following Lagrangians

$$(5.39) \quad \mathcal{L}_1 = D^\mu S^\dagger D_\mu S + M^2 S^\dagger S + [\lambda_R^*]_{eu} \bar{e} u^c S + [\lambda_R^*]_{\mu u} \bar{\mu} u^c S + h.c. \quad ,$$

$$(5.40) \quad \mathcal{L}_2 = D^\mu S^\dagger D_\mu S + M^2 S^\dagger S + [\lambda_L^*]_{\mu d} \bar{\ell}_\mu i \tau_2 q_{L,u}^c S + [\lambda_R^*]_{eu} \bar{e} u^c S + h.c. \quad ,$$

$$(5.41) \quad \mathcal{L}_3 = D^\mu \tilde{S}^\dagger D_\mu \tilde{S} + \tilde{M}^2 \tilde{S}^\dagger \tilde{S} + [\tilde{\lambda}^*]_{ed} \bar{e} d^c \tilde{S} + [\tilde{\lambda}^*]_{\mu d} \bar{\mu} d^c \tilde{S} + h.c. \quad .$$

where D^μ is the appropriate covariant derivative of QCD and QED. At the leptoquark mass scale, we match these scenarios onto the SM extended by QED*QCD invariant operators, which mediate $\mu \rightarrow e$ conversion. The coefficients and operators are given in table 5.1.

	operators	coefficients at M
\mathcal{L}_1	$-\frac{[\lambda_R]_{eu}^*[\lambda_R]_{\mu u}}{M^2}(\bar{e}_R u^c)(\bar{u}^c \mu_R) = \frac{[\lambda_R]_{eu}^*[\lambda_R]_{\mu u}}{2M^2}(\bar{e}_R \gamma^\alpha \mu_R)(\bar{u} \gamma_\alpha P_R u)$	$C_{V,R}^{uu} = C_{A,R}^{uu} = \frac{[\lambda_R]_{eu}^*[\lambda_R]_{\mu u}}{4M^2}$
\mathcal{L}_2	$-\frac{[\lambda_R]_{eu}^*[\lambda_L]_{\mu u}}{M^2}(\bar{e}_R u^c)(\bar{u}^c \mu_L) = \frac{[\lambda_R]_{eu}^*[\lambda_L]_{\mu u}}{2M^2}((\bar{e}_R P_L \mu)(\bar{u} P_L u) + \frac{1}{4}(\bar{e}_R \sigma P_L \mu)(\bar{u} \sigma P_L u))$	$C_{S,L}^{uu} = 2C_{T,L}^{uu} = \frac{[\lambda_R]_{eu}^*[\lambda_L]_{\mu u}}{4M^2}$
\mathcal{L}_3	$-\frac{[\tilde{\lambda}]_{ed}^*[\tilde{\lambda}]_{\mu d}}{M^2}(\bar{e}_R d^c)(\bar{d}^c \mu_R) = \frac{[\tilde{\lambda}]_{ed}^*[\tilde{\lambda}]_{\mu d}}{2M^2}(\bar{e}_R \gamma^\alpha \mu_R)(\bar{d} \gamma_\alpha P_R d)$	$C_{V,R}^{dd} = C_{A,R}^{dd} = \frac{[\tilde{\lambda}]_{ed}^*[\tilde{\lambda}]_{\mu d}}{4M^2}$

Table 5.1: Lepton flavour-changing operators induced in the leptoquark scenarios of equations (5.39 -5.41). The coefficients are given at the leptoquark mass scale M , in the basis of section 5.2.

In each scenario, we translate the coefficients down to the experimental scale $\Lambda_{exp} = 2 \text{ GeV}$ via an approximate analytic solution to the one-loop RGEs of QED and QCD [211, 212]:

$$(5.42) \quad C_I(\Lambda_{exp}) \simeq C_J(M) \lambda^{a_J} \left(\delta_{JI} - \frac{\alpha_e \tilde{\Gamma}_{JI}^e}{4\pi} \log \frac{M}{\Lambda_{exp}} \right)$$

where $\lambda = \frac{\alpha_s(M)}{\alpha_s(\Lambda_{exp})} \simeq 1/3$ for $M = \text{TeV}$, and I, J represent the super- and subscripts which label operator coefficients. The a_I describe the QCD running and are only non-zero for scalars and tensors. We suppose five quark flavours for the running, which gives $a_I = \frac{\Gamma_{II}^s}{2\beta_0} = \{-\frac{12}{23}, \frac{4}{23}\}$ for $I = S, T$. Γ^e is the one-loop QED anomalous dimension matrix, $\tilde{\Gamma}^e$ is this matrix with an additional factor multiplying the TS and ST entries [242, 243] in order to account for the QCD running:

$$(5.43) \quad \tilde{\Gamma}_{JI}^e = \Gamma_{JI}^e f_{JI}, f_{JI} = \frac{1}{1+a_J-a_I} \frac{\lambda^{a_I-a_J} - \lambda}{1-\lambda} = \begin{cases} \frac{23}{7} \frac{\lambda^{16/23} - \lambda}{1-\lambda} & JI = ST \\ \frac{23}{39} \frac{\lambda^{-16/23} - \lambda}{1-\lambda} & JI = TS \\ 1 & otherwise \end{cases}$$

We neglect the RG mixing out of our operator basis, because it is small: tensor mixing to the dipole is suppressed by light quark masses, and the mixing via the penguin diagram to vector operators $\mathcal{O}_{V,X}^{ff}$ is a few %, and does not generate operators interesting to us here. The RG evolution is described in more detail in appendix C.

This formalism allows to predict the ratio of SD to SI contributions to the branching ratio for $\mu \rightarrow e$ conversion. In Aluminium, we find for the three scenarios, taking $M = 1 \text{ TeV}$:

$$\begin{aligned}
 (5.44) \quad & \text{for } \mathcal{L}_1 : \quad \frac{BR_{SD}}{BR_{SI}} \sim 1.5 \times 10^{-4} \\
 & \text{for } \mathcal{L}_2 : \quad \frac{BR_{SD}}{BR_{SI}} \sim 4.4 \times 10^{-6} \\
 & \text{for } \mathcal{L}_3 : \quad \frac{BR_{SD}}{BR_{SI}} \sim 3.2 \times 10^{-5}
 \end{aligned}$$

so we see that the SD rate is smaller than the current $\sim 10\%$ uncertainties on the SI rate, so cannot be observed in these models. This is as expected, because the leptoquark model imposes that the tensor/axial coefficients are comparable to the scalar/vector coefficients, so the SD rate is relatively suppressed with respect to the SI rate by $1/(AG_S^{N,q})^2$ for tensor coefficients, and $1/A^2$ for axial vector coefficients.

It is interesting to explore whether the three leptoquark scenarios could be distinguished by comparing the SI rates in various nuclei. We imagine that $\mu \rightarrow e$ conversion has been observed in Aluminium ($Z_{Al}=13, A_{Al} = 27$), the target of the upcoming COMET and Mu2e experiments. We wish to identify alternative target materials, which could allow to distinguish our leptoquark scenarios.

A simple distinction between the leptoquarks S and \tilde{S} , is that the former couples to u quarks, and the latter to d quarks. To identify an appropriate target (A, Z) , where the $\mu \rightarrow e$ conversion rates induced by S and \tilde{S} would be significantly different (subject to the constraint that both reproduced the Aluminium observations), we consider the double ratio:

$$(5.45) \quad \frac{\frac{\Gamma(AI\mu \rightarrow Ale)}{\Gamma((A,Z)\mu \rightarrow (A,Z)e)} \Big|_S}{\frac{\Gamma(AI\mu \rightarrow Ale)}{\Gamma((A,Z)\mu \rightarrow (A,Z)e)} \Big|_{\tilde{S}}} \simeq \left(\frac{2A_{Al} - Z_{Al}}{A_{Al} + Z_{Al}} \right)^2 \left(\frac{A + Z}{2A - Z} \right)^2 = \left(\frac{2V_{Al}^{(p)} + V_{Al}^{(n)}}{V_{Al}^{(p)} + 2V_{Al}^{(n)}} \right)^2 \left(\frac{V_A^{(p)} + 2V_A^{(n)}}{2V_A^{(p)} + V_A^{(n)}} \right)^2$$

where the operator coefficients cancel because we compare two models that each induce a single SI operator. This ratio should differ from 1 by $\geq 20\%$, in order to unambiguously distinguish the S from \tilde{S} , given the $\sim 10\%$ uncertainties on the theory calculation. The first approximate equality in eqn (5.45), applies for light nuclei, where the conversion rate can be written as eqn (5.25). The second equality uses the KKO conversion rate given in eqn (5.33) in terms of the overlap integrals $V^{(N)}$, and applies for all nuclei.

The continuous green line (with stars) of figure 5.2 is the ratio of $\mu \rightarrow e$ conversion rates mediated by S and \tilde{S} , assuming equal operator coefficients. It corresponds to the second fraction in the products appearing in eqn (5.45), so the double ratio of eqn (5.45) is simply obtained by dividing by the ratio for Aluminium. The stars are the light nucleus approximation, the green continuous line is the ratio of overlap integrals. This shows that the approximation is very similar to the numerical results of KKO, and that a target with $Z \geq 40$ could allow to distinguish the first and third leptoquark scenarios. In the following, we take Niobium (Nb, $Z=41, A=93$) as a $Z \geq 40$ target.

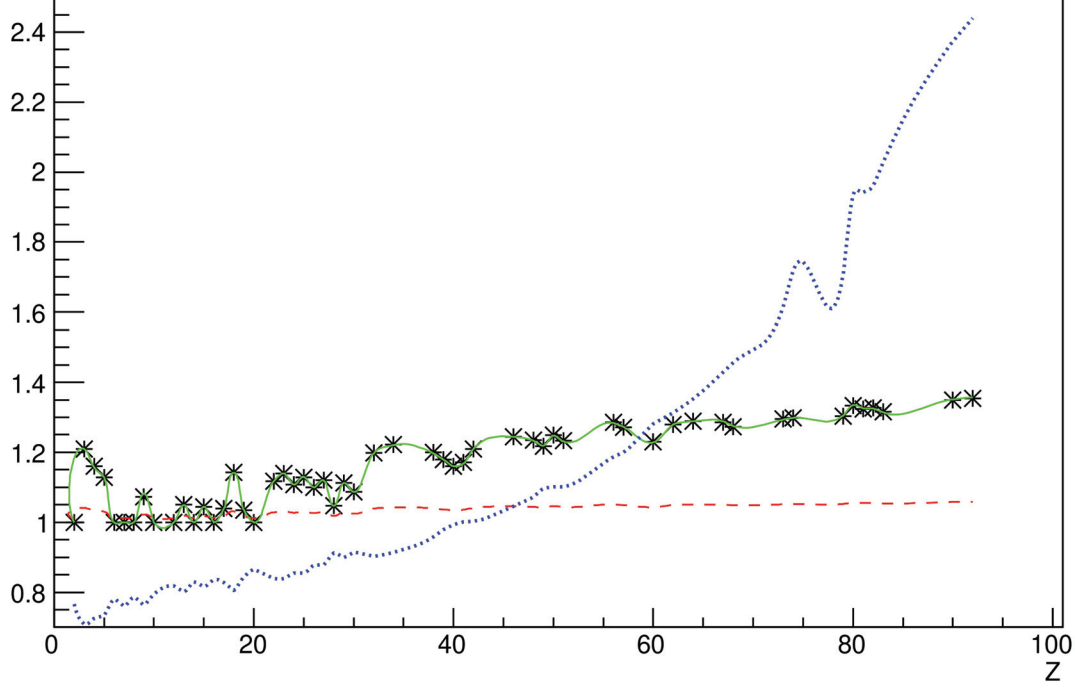


Figure 5.2: This plot illustrates the prospects for distinguishing SI operators involving up quarks, from those involving down quarks, and vector operators from scalars. The continuous green [dashed red] line is the ratio, given in eqn (5.45) [eqn (5.46)], of $\mu \rightarrow e$ conversion rates induced by $\mathcal{O}_{V,X}^{uu}$ and $\mathcal{O}_{V,X}^{dd}$ [$\mathcal{O}_{S,X}^{uu}$ and $\mathcal{O}_{S,X}^{dd}$], assuming equal coefficients. The stars on the green line are an analytic approximation. The dotted blue line is the ratio, given in eqn (5.47), of $\mu \rightarrow e$ conversion rates induced by $\mathcal{O}_{V,X}^{uu}$ and $\mathcal{O}_{S,X}^{uu}$, with coefficients selected to give the same rate on Niobium ($Z=41$).

It is also interesting to explore the prospects of distinguishing scalar operators involving u vs d quarks. So we also plot in figure 5.2, as a dashed red line, the ratio of $\mu \rightarrow e$ conversion rates mediated upstairs by $\mathcal{O}_{S,X}^{uu}$ and downstairs by $\mathcal{O}_{S,X}^{dd}$:

$$(5.46) \quad \frac{\Gamma((A,Z)\mu \rightarrow (A,Z)e) \Big|_{\mathcal{O}_{S,X}^{uu}}}{\Gamma((A,Z)\mu \rightarrow (A,Z)e) \Big|_{\mathcal{O}_{S,X}^{dd}}} = \left(\frac{G_S^{p,d} S_A^{(p)} + G_S^{n,d} S_A^{(n)}}{G_S^{p,u} S_A^{(p)} + G_S^{n,u} S_A^{(n)}} \right)^2 .$$

For the $G_S^{N,q}$ values given in appendix A, the scalar ratio is close to one (because $G_S^{p,q} \simeq G_S^{n,q}$), suggesting that changing the target in $\mu \rightarrow e$ conversion does not help distinguish $\mathcal{O}_{S,X}^{uu}$ from $\mathcal{O}_{S,X}^{dd}$.

The first and second leptoquark scenarios respectively induce scalar and vector operators. As discussed in [206, 207], these can be distinguished by comparing the conversion rates in light and heavy targets. This is illustrated in figure 5.2, by the blue dotted line, which gives the double ratio normalised to Niobium

$$(5.47) \quad \frac{\frac{\Gamma(Nb\mu \rightarrow Nbe)}{\Gamma((A,Z)\mu \rightarrow (A,Z)e)} \Big|_{scalar}}{\frac{\Gamma(Nb\mu \rightarrow Nbe)}{\Gamma((A,Z)\mu \rightarrow (A,Z)e)} \Big|_{vector}} = \left(\frac{G_S^{p,u} S_{Nb}^{(p)} + G_S^{n,u} S_{Nb}^{(n)}}{G_S^{p,u} S_A^{(p)} + G_S^{n,u} S_A^{(n)}} \right)^2 \left(\frac{2V_A^{(p)} + V_A^{(n)}}{2V_{Nb}^{(p)} + V_{Nb}^{(n)}} \right)^2.$$

We see that measuring the $\mu \rightarrow e$ conversion rate on Aluminium, some intermediate target around $Z \sim 40$ and on a heavy nucleus like lead or gold ($Z = 79$), could distinguish the three leptoquark scenarios, that is a vector operator involving ds , vs vector operator involving us , vs a scalar operator involving us .

5.5.2 Bounds on arbitrary coefficients of four operators

This section considers the operators induced by the second and third leptoquark models (see equations (5.40),(5.41)) which are added simultaneously to the Lagrangian with arbitrary coefficients:

$$(5.48) \quad \mathcal{L}_{EFT} = C_{S,L}^{uu} \mathcal{O}_{S,L}^{uu} + C_{T,L}^{uu} \mathcal{O}_{T,L}^{uu} + C_{V,R}^{dd} \mathcal{O}_{V,R}^{dd} + C_{A,R}^{dd} \mathcal{O}_{A,R}^{dd} + h.c.$$

This is clearly an incomplete basis (the complete basis of dimension six operators at Λ_{exp} is given in eqns (5.1,5.3)); however, it is sufficient for our purpose⁷, which is to explore which constraints can be obtained on quark-level operators from the non-observation of $\mu \rightarrow e$ conversion in targets with and without spin.

We suppose that $\mu \rightarrow e$ conversion has not been observed on Aluminium, Titanium (enriched in isotopes with spin) and Lead targets. These targets are chosen because heavy and light targets have different sensitivities to vector and scalar coefficients, and because the spin of Titanium and Aluminium is respectively associated to an odd neutron and an odd proton. In order to check that upper bounds on these branching ratios can constrain all the operator coefficients which we consider, we set the branching ratios to zero, and check that this forces the coefficients to vanish.

Setting the SD conversion rates in Titanium and Aluminium to zero gives two equations:

$$(5.49) \quad 0 \simeq C_{A,R}^{dd} \left(G_A^{p,d} + \frac{S_n^{Al}}{S_p^{Al}} G_A^{n,d} \right) + 2C_{T,L}^{uu} \left(G_T^{p,u} + \frac{S_n^{Al}}{S_p^{Al}} G_T^{n,u} \right)$$

$$(5.50) \quad 0 \simeq C_{A,R}^{dd} G_A^{n,d} + 2C_{T,L}^{uu} G_T^{n,u}$$

⁷In a later publication, we may try to constrain operator coefficients and count ‘‘flat directions’’, for which a complete basis would be required.

where $\frac{S_n^{Al}}{S_p^{Al}} \simeq 0.1$ is the ratio of spin expectation values in Aluminium. These equations have solutions

$$2C_{A,R}^{dd} \simeq C_{T,L}^{uu} \quad , \quad C_{A,R}^{dd} \simeq 2C_{T,L}^{uu}$$

so even allowing for a 10% theory uncertainty on the coefficients, it is clear that the only solution is for both coefficients to vanish. This is because the spin of Titanium isotopes arises from the odd number of neutrons, whereas in Aluminium the spin is from the odd proton, so these two conversion rates probe the SD coefficients $\tilde{C}_{A,X}^{NN}$ for both neutrons and protons. Then, since the matching coefficients $G_{A,X}^{Nu}$ and $G_{A,X}^{Nd}$ (equivalently $G_{T,X}^{Nu}$ and $G_{T,X}^{Nd}$) are of opposite sign and different magnitude, $C_{A,X}^{uu} + 2C_{T,X}^{uu}$ and $C_{A,X}^{dd} + 2C_{T,X}^{dd}$ can be distinguished.

It is straightforward to check that setting the SI rates on Al, Ti and Pb to zero, forces $C_{V,R}^{dd}, C_{S,L}^{uu} \rightarrow 0$.

A more informative way to present the constraints on coefficients arising from the experimental bounds is to give the covariance matrix. We suppose an upper bound of BR (for instance, 10^{-14}) on the SI branching ratios on Pb and Al, and on the SD branching ratios on Al and Ti. The tensor operator gives comparable contributions to both SI and SD processes (see Appendix B), so the 4×4 covariance matrix does not split into 2×2 subblocks. Nonetheless, it is interesting to give the covariance matrices for different cases, in order to see the variation of the bounds, when different theoretical information is included.

First, the tensor contribution to the SI rates is neglected, in which case the covariance matrices for $(C_{V,R}^{dd}, C_{S,L}^{uu})$ and $(C_{T,L}^{uu}, C_{A,R}^{dd})$ are:

$$(5.51) \quad BR \begin{bmatrix} 0.012 & -.0028 \\ -.0028 & .0007 \end{bmatrix} \quad , \quad BR \begin{bmatrix} 9.1 & 20 \\ 20 & 73.6 \end{bmatrix} \quad .$$

So, for instance, $|C_{S,L}^{uu}|$ is excluded above $\sqrt{0.0007 \times BR}$, and $|C_{A,R}^{dd}| < \sqrt{73.6 \times BR}$.

If now the SD rates are neglected, but the tensor contribution to SI is included, then the covariance matrix for $(C_{V,R}^{dd}, C_{S,L}^{uu}, C_{T,L}^{uu})$ is

$$(5.52) \quad BR \begin{bmatrix} 0.47 & -.24 & 23 \\ -.24 & .13 & -14 \\ 23 & -14 & 1400 \end{bmatrix} \quad ,$$

which shows that the exclusions become weaker due to potential cancellations between a large $C_{T,L}^{uu}$ and the vector or scalar coefficients. Finally the full covariance matrix arising from imposing $BR_{SI}(\mu Pb \rightarrow ePb) \leq 10^{-14}$, $BR_{SI}(\mu Ti \rightarrow eTi) \leq 10^{-14}$, $BR_{SD}(\mu^{47}Ti \rightarrow e^{47}Ti) \leq 10^{-14}$,

$BR_{SI}(\mu Al \rightarrow eAl) \leq 10^{-14}$, and $BR_{SD}(\mu Al \rightarrow eAl) \leq 10^{-14}$, for the coefficients $(C_{V,R}^{dd}, C_{S,L}^{uu}, C_{T,L}^{uu}, C_{A,R}^{dd})$, is

$$(5.53) \quad BR \begin{bmatrix} 0.010 & -0.0029 & 0.12 & 0.26 \\ -0.0029 & 0.0011 & -0.078 & -0.17 \\ 0.12 & -0.078 & 9.0 & 19.6 \\ 0.26 & -0.17 & 19.6 & 73 \end{bmatrix}.$$

Comparing to the bounds of eqn (5.51), shows that the tensor contribution to the SI rate is of little importance, provided the SD bounds are included. However, if the SD bounds are neglected, including the tensor in the SI rate significantly weakens the constraints, as can be seen in eqn (5.52). We also checked that including $BR_{SI}(\mu Au \rightarrow eAu) \leq 10^{-14}$ only changes a few entries by about 25%, as expected, because Al, Ti and Pb were chosen as targets for their discriminating power.

5.5.3 Reconstructing nucleon coefficients

We now suppose that $\mu \rightarrow e$ conversion is observed in Aluminium, where there can be SI and SD contributions to the rate, and that the New Physics is described by the nucleon-level Lagrangian of eqn (5.5) with arbitrary operator coefficients. It is interesting to consider which subsequent targets, in what order, would be required to distinguish the SD and SI contributions, and then to discriminate among the SI operators?

We first introduce a geometric representation of models and targets, which allows to visualize the ability of various targets to discriminate among models. A New Physics scenario can be represented as a two 5-dimensional vectors, each composed of SI coefficients which interfere $\vec{C}_X \equiv (C_{D,X}, \tilde{C}_{S,X}^{pp}, \tilde{C}_{V,Y}^{pp}, \tilde{C}_{S,X}^{nn}, \tilde{C}_{V,Y}^{nn})$, and two two-component vectors of SD coefficients $(\tilde{C}_{A,X}^{nn}, \tilde{C}_{A,X}^{pp})$.

For simplicity, we focus on $X = L$, and drop this electron chirality subscript. Then we focus on discriminating among SI operators, because the spin of target nuclei is usually associated to either an unpaired n or p , giving an order of magnitude better sensitivity to the coefficient corresponding to the unpaired nucleon (see, *e.g.* the spin expectation values given after eqn (5.22)). This means that discriminating $\tilde{C}_{A,X}^{nn}$ vs $\tilde{C}_{A,X}^{pp}$ should be a straightforward matter of using targets with an unpaired p and n .

For the spin independent process, a target nucleus (Z, A) can be envisaged as a vector

$$(5.54) \quad \vec{v}_{(Z,A)} = (D_{(Z,A)}, S_{(Z,A)}^{(p)}, V_{(Z,A)}^{(p)}, S_{(Z,A)}^{(n)}, V_{(Z,A)}^{(n)})$$

in the five-dimensional coefficient space, whose components are the appropriate overlap integrals. (In the following, the vectors and components are indiscriminately labelled by A or

Z because we use the overlap integrals of KKO, obtained for a single abundant isotope.) The matrix element for $\mu \rightarrow e$ conversion on target A , mediated by a combination of coefficients \vec{C} , is proportional to $\vec{C} \cdot \vec{v}_A$, and target nucleus A allows to probe coefficients in the direction \vec{v}_A . If we define the unit-normalised $\hat{e}_A = \vec{v}_A/|\vec{v}_A|$, then target A probes the same combination of coefficients as Aluminium if \hat{e}_A is parallel to \hat{e}_{Al} , and the difference

$$(5.55) \quad 1 - \hat{e}_A \cdot \hat{e}_{Al} \approx \frac{\theta^2}{2}$$

gives an invariant measure of whether the target A has sensitivity to an orthogonal direction in coefficient space. In eqn (5.55), θ is the angle between \hat{e}_A and \hat{e}_{Al} . Figure 5.3 gives $\hat{e}_A \cdot \hat{e}_{Al}$ as a function of Z . From eqn (5.38), the uncertainty in the direction of \hat{e}_A is $\leq 10\%$, so target A is indistinguishable from Aluminium for $\hat{e}_A \cdot \hat{e}_{Al} \geq 0.995$, or $Z \leq 25 - 30$.

Perhaps a more transparent measure of the change of direction of \hat{e}_A in coefficient space, is given in figure 5.4 by the ratio

$$(5.56) \quad \frac{e_A^O}{e_{Al}^O}$$

where $O = \tilde{C}_{S,X}^{pp}$ (continuous black), $O = \tilde{C}_{S,X}^{nn}$ (dotted green), $\tilde{C}_{V,X}^{pp}$ (dashed red) and $O = \tilde{C}_{V,X}^{nn}$ (dot-dashed blue). Recall that e_A^O parametrises the fraction of the sensitivity of target A to operator O . So figure 5.4 shows that heavier targets have greater sensitivity to \mathcal{O}_V^{nn} and less to \mathcal{O}_S^{pp} . (Unfortunately, this figure also suggests that \mathcal{O}_V^{nn} and \mathcal{O}_S^{pp} with comparable coefficients could be difficult to distinguish from \mathcal{O}_V^{pp} .) This normalised ratio of overlap integrals is interesting, because the normalisation ‘‘factors out’’ the growth with Z shared by all the overlap integrals, so this ratio parametrises the difference in direction in coefficient space, which allows different targets to discriminate among coefficients. This ratio also indicates that targets of $Z \leq 25$ cannot distinguish operators, if one admits a theory uncertainty of $\sim 10\%$ in the calculation of the components e_A^O .

Assisted by the measures of discriminating power given in eqns (5.55) and (5.56), we now speculate on a possible series of targets. A light nucleus without spin could be an interesting second target, because it would allow to distinguish whether the rate in Aluminium was dominantly SD or SI. In particular, the SI rate in Aluminium could be approximately predicted from the the rate observed in another spinless light nucleus. This is because the SI rate in all targets with $Z \leq 20$ is sensitive to a similar linear combination of operator coefficients, as illustrated in figures 5.3 and 5.4.

An interesting choice for the second target could be Titanium ($Z=22$, $A = 48$). As illustrated in figures 5.3 and 5.4, it of sufficiently low Z that the SI rate probes the same combination of operator coefficients as the SI rate in Aluminium. So measuring the SI rate in Titanium-48 would

allow to determine whether there was a significant SD contribution to the $\mu \rightarrow e$ conversion rate observed on Aluminium.

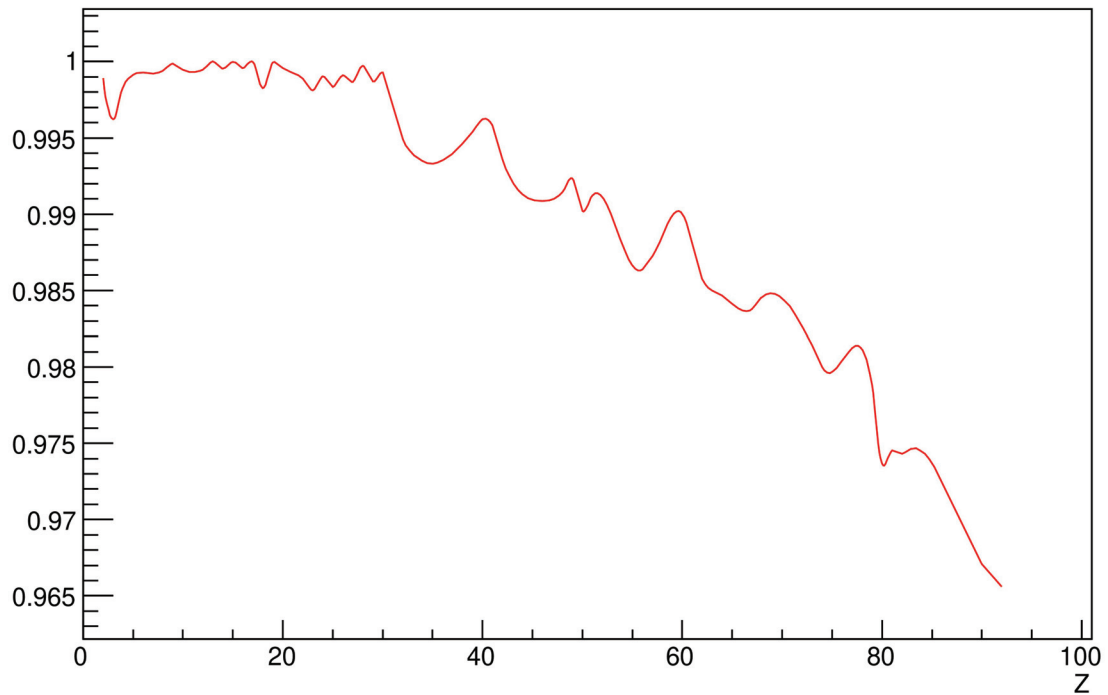


Figure 5.3: A representation of the discriminating power of a target (labelled by Z), with respect to Aluminium. On the vertical axis is the invariant measure, given in eqn (5.55), of the misalignment in coefficient space of the target with respect to Aluminium.

If there is indication for an SD contribution in Aluminium, then it could be interesting to measure the rate on a Titanium target enriched with the spin-carrying isotopes 47 and 49. This would give complementary information on the quark flavour of the tensor and/or axial vector operators, because the spin of Aluminium is largely due to the odd proton, whereas for Titanium, there is an odd neutron. So the SD rate in Aluminium is mostly sensitive to $\tilde{C}_{A,X}^{pp}$, whereas the SD rate in Titanium depends on $\tilde{C}_{A,X}^{nn}$.

Finally, if there is no evidence of an SD rate in Aluminium, a heavy target such as lead could be interesting to discriminate the scalar vs vector coefficients in the SI rate.

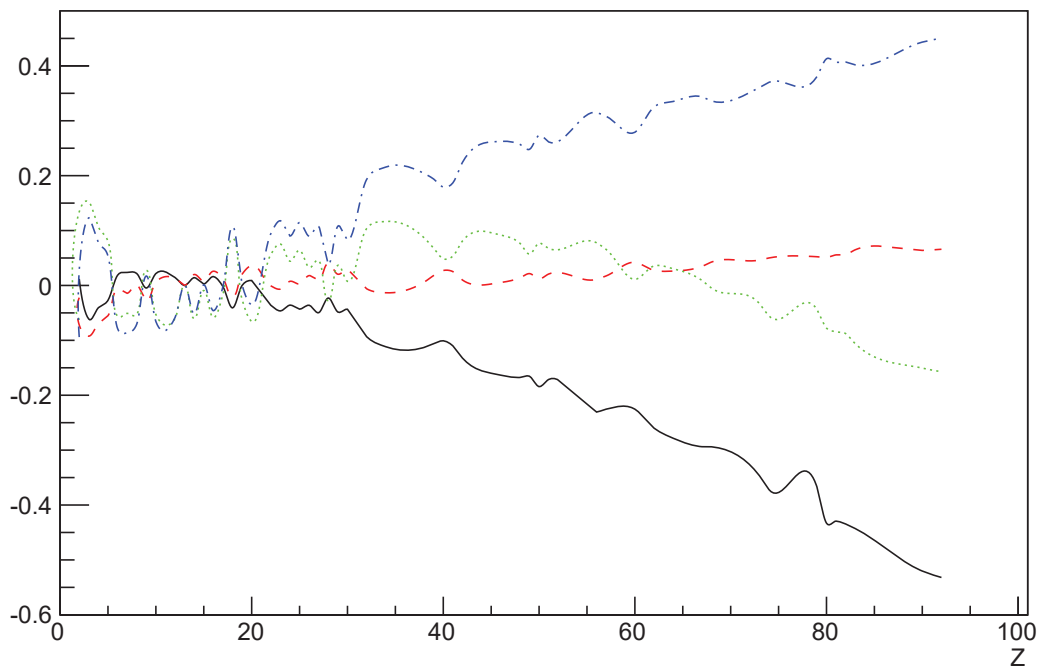


Figure 5.4: An operator-dependent measure of the discriminating power of a targets (labelled by Z). On the vertical axis is the measure given in of eqn (5.56), of the relative sensitivity(normalised to Aluminium) of a target to the operators $O = \tilde{C}_{S,X}^{pp}$ (continuous black), $O = \tilde{C}_{S,X}^{nn}$ (dotted green), $\tilde{C}_{V,X}^{pp}$ (dashed red) and $O = \tilde{C}_{V,X}^{nn}$ (dot-dashed blue).

5.6 Summary

This paper gives some details of the calculation of the Spin Dependent (SD) $\mu \rightarrow e$ conversion rate in light nuclei, previously outlined in [210]. Section 5.2 reviews the operators involving quarks and gluons that contribute [206, 207] at the experimental scale ($\Lambda_{exp} = 2$ GeV), and matches them onto the nucleon operators which enter the nuclear physics calculation. Some attempt is made to include pion exchange in this matching (it is relevant because the momentum-transfer is m_μ^2).

Section 5.3 calculates as much as possible of the conversion rate in the notation of relativistic, second-quantised, QFT [226]; in the last steps, the results of nuclear calculations are included. The final rate is given in equation (5.26). This section is not original; its purpose is to make the result accessible to aficionados of QFT. We recall the SD $\mu \rightarrow e$ conversion is incoherent, like SD WIMP scattering, so it is best searched for in light nuclei, where the $1/A^2$ suppression with respect to the coherent Spin Independent (SI) rate (given in eqns (5.25,5.33)) is less significant.

Our SD rate estimate relies on nuclear physics calculations of the expectation value of nucleon axial currents in the nucleus. The results we use were obtained for SD WIMP scattering, which are often at zero momentum transfer. As discussed in section 5.3.1, additional nuclear calculations seem required to include tensor and pseudoscalar operators at finite momentum transfer, in light targets such as Aluminium and Titanium. In this paper, we did not discuss SD conversion on heavy nuclei; however, one can speculate that the nuclear expectation values could be of interest, because heavy nuclei could be sensitive to a different combination of tensor and axial operators from light nuclei. This is because the anti-lepton wavefunction contributes with opposite sign to the tensor vs axial operators, and is more relevant in heavy nuclei (this sign difference allows to discriminate scalar and vector operators in SI conversion on light and heavy nuclei [207]). Of course, the SD rate might be unobservably small (due to the $1/A^2$ suppression), but heavy nuclei could nonetheless give an independent constraint on the many operator coefficients.

Both the SD and SI conversion rates depend on the modulus-squared of a sum of coefficients, weighted by nucleus-dependent numbers— see equations (5.25,5.26,5.33). This allows for cancellations, making it difficult to constrain individual coefficients, or identify the operators responsible for $\mu \rightarrow e$ conversion when it is observed. In the SI case, Kitano Koike and Okada (KKO)[207] pointed out that scalar vs dipole vs vector operators could be distinguished by changing the nuclear target. Section 5.5 explores, from various approaches, the prospects of distinguishing a wider variety of operators, including SD vs SI, and u - vs d - quark operators.

The prospects for discriminating vector or scalar operators involving either u or d quarks are illustrated in figure 5.2: vector operators involving u or d quarks could be distinguished by comparing the $\mu \rightarrow e$ conversion rate in light ($Z \leq 20$) and intermediate ($Z \sim 40$) targets, but distinguishing scalar u versus d operators seems difficult. Curiously, the u vs d distinction is more transparent in the SD rates, as discussed after eqn (5.50). So if both SD and SI conversion are observed, possibly the quark flavour could be extracted from the SD rates ⁸.

⁸Recall that SD and SI operators mix in the RG evolution, but without changing the quark flavour, as shown in

The SD and SI contributions to the conversion rate could be distinguished (if the SD rate is large enough) by comparing the conversion rate in nuclei with and without spin. Section 5.4 reviews the theoretical uncertainties in the calculation of the $\mu \rightarrow e$ conversion rate, in order to estimate the sensitivity to the subdominant SD process. Comparing $\mu \rightarrow e$ conversion on isotopes with and without spin would cancel the leading theory uncertainties, giving a sensitivity (see the discussion after eqn 5.37) to $\Gamma_{SD}/\Gamma_{SI} \geq \frac{0.1}{A}$, assuming a 10% uncertainty on Γ_{SI} . Among the SD operators, it is not currently possible to distinguish pseudoscalar, axial and tensor coefficients, because only the nuclear expectation value of the axial operator has been calculated. However, as mentioned in the previous paragraph, it could be possible to discriminate SD operators involving u vs d quarks, because they contribute differently in nuclei where the odd nucleon is a proton or neutron.

The upcoming COMET and Mu2e experiments will initially search for $\mu \rightarrow e$ conversion on Aluminium, a target which has spin — so if they observe a signal, it could be mediated by the SD or SI operators. So in section 5.5.3, we considered what series of subsequent targets could give information about the dominant coefficients. To this purpose, we represent a target material as a vector in the space of nucleon-level operators, whose components are numbers which multiply the operator coefficient in the rate (overlap integrals, in the SI case). Different targets can discriminate between operators, if they point in different directions of operator space. We plot in figures 5.3 and 5.4 two different measures of the misalignment between target vectors.

If $\mu \rightarrow e$ conversion is observed on Aluminium, the following sequence of targets could be interesting: as second target, a light nucleus without spin, such as Titanium-48, would discriminate whether the dominant contribution was from the SD rate, because the SI rate in Titanium is comparable to Aluminium (see figures 5.3 and 5.4). If there is an SD contribution to the rate in Aluminium, then Titanium isotopes with spin, could be an interesting target: the spin of Titanium is related to the odd neutron (whereas in Aluminium there is an odd proton), so this could discriminate whether the SD operators involved u or d quarks. Finally, a heavy target such as gold or lead could allow to discriminate scalar vs vector operators, as pointed out in [207].

Acknowledgements

We greatly thank Vincenzo Cirigliano for his participation in the early stages of this project, and for insightful discussions afterwards. SD acknowledges the partial support and hospitality of the Mainz Institute for Theoretical Physics (MITP) during the initial stages of this work. The work of Y.K. is supported in part by the Japan Society of the Promotion of Science (JSPS) KAKENHI Grant No. 25000004.

appendix C. The only flavour change is via the first two “penguin” diagrams of figure C.1, which could change the flavour of vector operators.

CONSTRAINTS ON $2l2q$ OPERATORS FROM $\mu \leftrightarrow e$ FLAVOUR-CHANGING MESON DECAYS

AUTHORS : Sacha Davidson¹ and Albert Saporta²,

PUBLISHED IN : Physical Review D¹

We study lepton flavour violating two- and three-body decays of pseudoscalar mesons in Effective Field Theory (EFT). We give analytic formulae for the decay rates in the presence of a complete basis of QED×QCD-invariant operators. The constraints are obtained at the experimental scale, then translated to the weak scale via one-loop RGEs. The large RG-mixing between tensor and (pseudo)scalar operators weakens the constraints on scalar and pseudoscalar operators at the weak scale.

6.1 Introduction

As we have seen in chapter 2 and 3, the discovery of neutrino oscillations [36, 37] established non zero neutrino masses and mixing angles [38]. If neutrinos are taken massless in the Standard Model (SM), then New Physics (NP) is required to explain the oscillation data. There are several possibilities to search for NP signatures, such as looking for new particles at the LHC [244, 245]. Another possibility is to look for new processes among known SM particles, such as Charged Lepton Flavour Violation (CLFV) [8, 9], which we define to be a contact interaction that changes the flavour of charged leptons. If neutrinos have renormalizable masses via the Higgs mechanism,

¹<https://doi.org/10.1103/PhysRevD.99.015032>

then their contribution to CLFV rates is GIM suppressed by a factor $\propto (m_\nu/M_W)^4 \sim 10^{-48}$. However, various extensions of the Standard Model that contain heavy new particles (see *e.g.* [8, 9, 246, 247] and references therein), can predict CLFV rates comparable to the current experimental sensitivities. Indeed, low energy precision experiments searching for forbidden SM modes, are sensitive to NP scales \sim TeV [8]. Many experiments search for CLFV processes; for example, $\mu \leftrightarrow e$ flavour change can be probed in the decays $\mu \rightarrow e\gamma$ [10] and $\mu \rightarrow 3e$ [12, 129], in $\mu \rightarrow e$ conversion on nuclei [13, 248, 249] and also in meson decays such as $K, D, B \rightarrow \bar{\mu}e$ [19, 38, 174, 175, 177, 250–252].

In this paper, we focus on leptonic and semileptonic pseudoscalar meson decays with a $\mu^\pm e^\mp$ in the final state [38]. We assume that these decays could be mediated by two-lepton, two-quark contact interactions, induced by heavy New Particles at the scale $\Lambda_{NP} > m_W$. The contact interactions are included in a bottom-up Effective Field Theory (EFT) [253–255] approach, as a complete set of dimension six, QED \times QCD-invariant operators [8], containing a muon, an electron and one of the quark-flavour-changing combinations ds, bs, bd or cu .

Many studies on related topics can be found in the literature. The experimental sensitivity to the coefficients of four-fermion operators (sometimes referred to as one-operator-at-a-time bounds), evaluated at the experimental scale, has been compiled by various authors [256–258]. Reference [259] compared the sensitivities of the LHC vs low-energy processes, to quark flavour-diagonal scalar operators. The constraints on combinations of lepton-flavour-changing operator coefficients, which can be obtained from the decays of same-flavour mesons, were studied in [260], and the radiative decays of B, D and K mesons were discussed in [261]. Lepton flavour-conserving, but quark flavour-changing meson decays (which occur in the Standard Model), are widely studied [262]. In particular, B decays attract much current interest, due to the observed anomalies [49, 50, 55, 263, 264] which suggest lepton universality violation [59, 265–270]. Lepton flavour change has been widely studied in various models (see *e.g.* references of [8, 9, 271]). More model-independent studies, that take into account loop corrections (or equivalently, renormalization group running) have also been performed for $\mu \leftrightarrow e$ flavour change [211, 212]. Finally, with respect to the calculations in this manuscript, the leptonic branching ratio of pseudoscalar mesons is well-known, and can be found in [256, 258, 272, 273] and semi-leptonic branching ratios in various scenarios can be found in [274–282].

The aim of this paper is to obtain constraints on the operator coefficients describing meson decays at the experimental scale, and then transport the bounds to the weak scale². The four fermion operators that could induce the meson decays are listed in section 6.2. Section 6.3 gives the branching ratios for the leptonic and semileptonic decays as a function of the operator coefficients. In section 6.4, we then use the available bounds to constrain the coefficients at the experimental scale ($\Lambda_{exp} \sim 2$ GeV) by computing a covariance matrix, which allow us to take into account the interferences among the operators. The bounds are then evolved from the

²In a future publication, we will give the evolution from the weak scale to the NP scale, and discuss the prospects for reconstructing the fundamental Lagrangian of the New Physics from the operator coefficients.

experimental scale to the weak scale ($\Lambda_W \sim m_W$) in section 6.5, using the Renormalization Group Equations (RGEs) of QED and QCD for four-fermion operators [211, 212]. As discussed in the final section, these equations give a significant mixing of tensor operators into the (pseudo)scalars between Λ_{exp} and Λ_W , which significantly weakens the bounds on (pseudo)scalar coefficients at Λ_W .

6.2 A basis of $\mu - e$ interactions at low energy

We are interested in four-fermion operators involving an electron, a muon and two quark of different flavours, which are constructed with chiral fermions, because the lepton masses are frequently neglected, and it simplifies the matching at the weak scale onto SU(2)-invariant operators. The operators are added to the Lagrangian as

$$(6.1) \quad \delta\mathcal{L} = +2\sqrt{2}G_F \sum_O \sum_\zeta C_O^\zeta \mathcal{O}_O^\zeta + h.c.$$

where the subscript O identifies the Lorentz structure, the superscript $\zeta = l_1 l_2 q_i q_j$ gives the flavour indices, and both run over the possibilities in the lists below, extrapolated from [8, 207]:

$$(6.2) \quad \begin{aligned} \mathcal{O}_{V,YY}^{e\mu uc} &= (\bar{e}\gamma^\alpha P_Y \mu)(\bar{u}\gamma_\alpha P_Y c), & \mathcal{O}_{V,YX}^{e\mu uc} &= (\bar{e}\gamma^\alpha P_Y \mu)(\bar{u}\gamma_\alpha P_X c) \\ \mathcal{O}_{V,YY}^{e\mu cu} &= (\bar{e}\gamma^\alpha P_Y \mu)(\bar{c}\gamma_\alpha P_Y u), & \mathcal{O}_{V,YX}^{e\mu cu} &= (\bar{e}\gamma^\alpha P_Y \mu)(\bar{c}\gamma_\alpha P_X u) \\ \mathcal{O}_{S,YY}^{e\mu uc} &= (\bar{e}P_Y \mu)(\bar{u}P_Y c), & \mathcal{O}_{S,YX}^{e\mu uc} &= (\bar{e}P_Y \mu)(\bar{u}P_X c) \\ \mathcal{O}_{S,YY}^{e\mu cu} &= (\bar{e}P_Y \mu)(\bar{c}P_Y u), & \mathcal{O}_{S,YX}^{e\mu cu} &= (\bar{e}P_Y \mu)(\bar{c}P_X u) \\ \mathcal{O}_{T,YY}^{e\mu uc} &= (\bar{e}\sigma P_Y \mu)(\bar{u}\sigma P_Y c) \\ \mathcal{O}_{T,YY}^{e\mu cu} &= (\bar{e}\sigma P_Y \mu)(\bar{c}\sigma P_Y u) \end{aligned}$$

$$(6.3) \quad \begin{aligned} \mathcal{O}_{V,YY}^{e\mu ds} &= (\bar{e}\gamma^\alpha P_Y \mu)(\bar{d}\gamma_\alpha P_Y s), & \mathcal{O}_{V,YX}^{e\mu ds} &= (\bar{e}\gamma^\alpha P_Y \mu)(\bar{d}\gamma_\alpha P_X s) \\ \mathcal{O}_{V,YY}^{e\mu sd} &= (\bar{e}\gamma^\alpha P_Y \mu)(\bar{s}\gamma_\alpha P_Y d), & \mathcal{O}_{V,YX}^{e\mu sd} &= (\bar{e}\gamma^\alpha P_Y \mu)(\bar{s}\gamma_\alpha P_X d) \\ \mathcal{O}_{S,YY}^{e\mu ds} &= (\bar{e}P_Y \mu)(\bar{d}P_Y s), & \mathcal{O}_{S,YX}^{e\mu ds} &= (\bar{e}P_Y \mu)(\bar{d}P_X s) \\ \mathcal{O}_{S,YY}^{e\mu sd} &= (\bar{e}P_Y \mu)(\bar{s}P_Y d), & \mathcal{O}_{S,YX}^{e\mu sd} &= (\bar{e}P_Y \mu)(\bar{s}P_X d) \\ \mathcal{O}_{T,YY}^{e\mu ds} &= (\bar{e}\sigma P_Y \mu)(\bar{d}\sigma P_Y s) \\ \mathcal{O}_{T,YY}^{e\mu sd} &= (\bar{e}\sigma P_Y \mu)(\bar{s}\sigma P_Y d) \end{aligned}$$

where $YY \in \{LL, RR\}$, and $XY \in \{LR, RL\}$, and the list is given explicitly for the Kaon and D -meson operators. The lists for the B_d and B_s are obtained from eqn. (6.3) by replacing $ds \rightarrow db, sb$. The operators are normalised such that the Feynman rule will be $+iC/\Lambda^2$. The operators in the lists (6.2) and (6.3) transform a muon into an electron; the $e \rightarrow \mu$ operators arise in the $+h.c.$ of eqn (6.1). So in these conventions, the lepton flavour indices are always $e\mu$, and do not need to be given. In the following sections, we give the decay rates of pseudoscalar mesons, composed of constituent quarks \bar{q}_i and q_j , into $e^+\mu^-$ or $e^-\mu^+$. Then we obtain constraints on the operator coefficients by comparing to the experimental upper bounds on the branching ratios, e.g. $BR(P_1 \rightarrow e^\pm \mu^\mp) = BR(P_1 \rightarrow e^+\mu^-) + BR(P_1 \rightarrow e^-\mu^+) < \dots$ which we suppose to apply independently to both decays. This gives independent and identical bounds on $e^{\mu q_i q_j}$ and $e^{\mu q_j q_i}$.

In this work, we choose an operator basis with non-chiral quark currents, which is convenient for the non-chiral hadronic matrix elements involved in meson decays. Thus, the operators describing the contact interactions that can mediate leptonic ($\bar{q}_i q_j \rightarrow \bar{\mu} e$) and semileptonic ($q_i \rightarrow q_j \bar{\mu} e$) CLFV pseudoscalar meson decays at a scale $\Lambda_{exp} \sim 2 \text{ GeV}$ ($\Lambda_{exp} \sim m_b \simeq 4.2 \text{ GeV}$ for bs and bd) are written:

$$(6.4) \quad \begin{aligned} \mathcal{O}_{S,X}^{e\mu q_i q_j} &= (\bar{e} P_X \mu) (\bar{q}_i q_j), & \mathcal{O}_{P,X}^{e\mu q_i q_j} &= (\bar{e} P_X \mu) (\bar{q}_i \gamma^5 q_j) \\ \mathcal{O}_{V,X}^{e\mu q_i q_j} &= (\bar{e} \gamma^\alpha P_X \mu) (\bar{q}_i \gamma_\alpha q_j), & \mathcal{O}_{A,X}^{e\mu q_i q_j} &= (\bar{e} \gamma^\alpha P_X \mu) (\bar{q}_i \gamma_\alpha \gamma^5 q_j) \\ \mathcal{O}_{T,X}^{e\mu q_i q_j} &= (\bar{e} \sigma^{\alpha\beta} P_X \mu) (\bar{q}_i \sigma_{\alpha\beta} P_X q_j) \end{aligned}$$

where $q_{i,j} \in \{u, d, s, c, b\}$, $P_X = P_{R,L} = \frac{1 \pm \gamma_5}{2}$ and $\sigma^{\mu\nu} = \frac{i}{2}[\gamma^\mu, \gamma^\nu]$.

In this case, the coefficients ϵ of the operators in eqn. (6.4) are :

$$(6.5) \quad \begin{aligned} \epsilon_{S,X}^{e\mu q_i q_j} &= \frac{1}{2}(C_{S,XR}^{e\mu q_i q_j} + C_{S,XL}^{e\mu q_i q_j}), & \epsilon_{P,X}^{e\mu q_i q_j} &= \frac{1}{2}(C_{S,XR}^{e\mu q_i q_j} - C_{S,XL}^{e\mu q_i q_j}) \\ \epsilon_{V,X}^{e\mu q_i q_j} &= \frac{1}{2}(C_{V,XR}^{e\mu q_i q_j} + C_{V,XL}^{e\mu q_i q_j}), & \epsilon_{A,X}^{e\mu q_i q_j} &= \frac{1}{2}(C_{V,XR}^{e\mu q_i q_j} - C_{V,XL}^{e\mu q_i q_j}) \\ \epsilon_{T,X}^{e\mu q_i q_j} &= C_{T,XX}^{e\mu q_i q_j} \end{aligned}$$

In the next section, we compute the branching ratio for the (semi)leptonic decays as a function of the coefficients of eqn. (6.5).

6.3 Leptonic and semileptonic pseudoscalar meson decays

There are a multitude of bounds on rare meson decays coming from precision experiments [38, 258]. The aim of this paper is to use these bounds to constrain the coefficients of eqn. (6.5). Thus, in this section, we compute the leptonic and semileptonic pseudoscalar meson decay branching ratio as a function of these coefficients.

6.3.1 Leptonic decay branching ratio

We are interested in decays such as : $P_1 \rightarrow l_1 \bar{l}_2$ where $\{l_1, l_2\}$ are leptons of mass m_1, m_2 and P_1 is a pseudoscalar meson of mass M ($P_1 \in \{K_L^0(\frac{\bar{d}s+\bar{s}d}{\sqrt{2}}), D^0(\bar{u}c), B^0(\bar{b}d)\}$). In the presence of New Physics, the leptonic decay branching ratio of a pseudoscalar meson P_1 of mass M is written [256, 258, 273]:

$$(6.6) \quad \frac{BR(P_1 \rightarrow l_1 \bar{l}_2)}{C_{2\text{body}}} = (|\epsilon_{P,L}|^2 + |\epsilon_{P,R}|^2) \tilde{P}'^2 (M^2 - m_1^2 - m_2^2) \\ + (|\epsilon_{A,L}|^2 + |\epsilon_{A,R}|^2) \tilde{A}'^2 [(M^2 - m_1^2 - m_2^2)(m_1^2 + m_2^2) + 4m_1^2 m_2^2] \\ - 2(\epsilon_{P,L} \epsilon_{A,R} + \epsilon_{P,R} \epsilon_{A,L}) \tilde{P}' \tilde{A}' m_2 (M^2 + m_1^2 - m_2^2) \\ + 2(\epsilon_{P,L} \epsilon_{A,L} + \epsilon_{P,R} \epsilon_{A,R}) \tilde{P}' \tilde{A}' m_1 (M^2 + m_2^2 - m_1^2) \\ - 4\epsilon_{P,L} \epsilon_{P,R} \tilde{P}'^2 m_1 m_2 \\ - 4\epsilon_{A,L} \epsilon_{A,R} \tilde{A}'^2 M^2 m_1 m_2$$

where $C_{2\text{body}} = \frac{\tau r^* G_F^2}{\pi M^2}$, $r^* = \frac{1}{2M} \sqrt{(M^2 - (m_1 + m_2)^2)(M^2 - (m_1 - m_2)^2)}$, $m_{1,2}$ are the masses of the leptons and τ is the lifetime of P_1 . For simplicity, we dropped the flavour superscript ($\zeta = l_1 l_2 q_i q_j$) of the coefficients.

The expectation values of the quark current for a pseudoscalar meson are written [258, 273] :

$$(6.7) \quad \tilde{P}' = \frac{1}{2} \langle 0 | \bar{q}_i \gamma^5 q_j | P_1 \rangle = \frac{f_{P_1} M^2}{2(m_i + m_j)}, \quad \tilde{A}' k^\mu = \frac{1}{2} \langle 0 | \bar{q}_i \gamma^\mu \gamma^5 q_j | P_1 \rangle = \frac{f_{P_1} k^\mu}{2}$$

where $m_{i,j}$ are the masses of the quarks, f_{P_1} is the decay constant of the meson and k^μ the momentum of the meson. These formulae are used for pions, Kaons, D and B mesons. The values of the constants are given in appendix D. Note that tensor operators do not contribute to the leptonic decay, because the trace of product of the Dirac matrices contained in the tensor operator vanishes in this case.

6.3.2 Semileptonic decay branching ratio

We are interested in decays such as : $P_1 \rightarrow l_1 \bar{l}_2 P_2$ where $\{l_1, l_2\}$ are leptons of mass m_1, m_2 and $\{P_1, P_2\}$ are pseudoscalar mesons of mass M, m_3 ($P_1 \in \{K^+(u\bar{s}), D^+(c\bar{d}), B^+(u\bar{b}), B_s^+(s\bar{b})\}$ and $P_2 \in \{\pi^+(u\bar{d}), K^+(u\bar{s})\}$). The semileptonic decay branching ratio is written [283]:

$$(6.8) \quad BR(P_1 \rightarrow l_1 \bar{l}_2 P_2) = \frac{\tau}{512\pi^3 M^3} \frac{1}{2J+1} \int_{(m_1+m_2)^2}^{(M-m_3)^2} dq^2 \int_{-1}^1 d\cos\theta \frac{|\mathcal{M}|^2 \sqrt{\lambda(M^2, m_3^2, q^2)} \sqrt{\lambda(q^2, m_1^2, m_2^2)}}{q^2}$$

where $q = (p_1 + p_2)$ is the transferred momentum, θ the angle between the direction of propagation of the lighter meson (P_2) and the antilepton (l_2) in the leptons reference frame, τ and J the lifetime and the spin of P_1 and $|\mathcal{M}|^2$ the matrix element of the semileptonic decay. The Kallen function is defined as $\lambda(x, y, z) = (x - y - z)^2 - 4yz$. In the presence of New Physics, the matrix element in the semileptonic decay branching ratio of eqn. (6.8) is written :

$$\begin{aligned}
 \frac{|\mathcal{M}|^2}{8G_F^2} &= 2(|\epsilon_{S,L}|^2 + |\epsilon_{S,R}|^2)\tilde{S}^2(p_1 \cdot p_2) \\
 &+ \frac{1}{4}(|\epsilon_{V,L}|^2 + |\epsilon_{V,R}|^2)[f_+^2(4(p_1 \cdot P)(p_2 \cdot P) - 2P^2(p_1 \cdot p_2)) + f_-^2(4(p_1 \cdot q)(p_2 \cdot q) - 2q^2(p_1 \cdot p_2))] \\
 &+ 4f_+f_-((p_1 \cdot q)(p_2 \cdot P) + (p_1 \cdot P)(p_2 \cdot q) - (p_1 \cdot p_2)(P \cdot q))] \\
 &+ 4(|\epsilon_{T_R}|^2 + |\epsilon_{T_L}|^2)\tilde{T}'^2[4(p_1 \cdot q)(p_2 \cdot P)(P \cdot q) + 4(p_1 \cdot P)(p_2 \cdot q)(P \cdot q) - 2(p_1 \cdot p_2)(P \cdot q)^2 \\
 &+ 2P^2q^2(p_1 \cdot p_2) - 4P^2(p_1 \cdot q)(p_2 \cdot q) - 4q^2(p_1 \cdot P)(p_2 \cdot P)] \\
 &- 2(\epsilon_{S,L}\epsilon_{V,R} + \epsilon_{S,R}\epsilon_{V,L})\tilde{S}m_2[(f_+(p_1 \cdot P) + f_-(p_1 \cdot q))] \\
 (6.9) \quad &+ 2(\epsilon_{S,L}\epsilon_{V,L} + \epsilon_{S,R}\epsilon_{V,R})\tilde{S}m_1[(f_+(p_2 \cdot P) + f_-(p_2 \cdot q))] \\
 &+ 8(\epsilon_{S,R}\epsilon_{T_R} + \epsilon_{S,L}\epsilon_{T_L})\tilde{S}\tilde{T}'[(p_1 \cdot P)(p_2 \cdot q) - (p_1 \cdot q)(p_2 \cdot P)] \\
 &- 4\epsilon_{S,L}\epsilon_{S,R}\tilde{S}^2m_1m_2 \\
 &- \epsilon_{V,L}\epsilon_{V,R}m_1m_2[f_-^2q^2 + f_+^2P^2 + 2f_+f_-(P \cdot q)] \\
 &+ 4(\epsilon_{V,L}\epsilon_{T_R} + \epsilon_{V,R}\epsilon_{T_L})\tilde{T}'m_2[f_+((p_1 \cdot q)p^2 - (P \cdot p_1)(P \cdot q)) + f_-((p_1 \cdot q)(P \cdot q) - (p_1 \cdot P)q^2)] \\
 &+ 4(\epsilon_{V,R}\epsilon_{T_R} + \epsilon_{V,L}\epsilon_{T_L})\tilde{T}'m_1[(f_+((P^2)(p_2 \cdot q) - (p_2 \cdot P)(P \cdot q)) + f_-((p_2 \cdot q)(P \cdot q) - q^2(p_2 \cdot P)))] \\
 &+ 16\epsilon_{T_R}\epsilon_{T_L}\tilde{T}'^2m_1m_2[(P \cdot q)^2 - P^2q^2]
 \end{aligned}$$

where p_1, p_2, k, p_3 are respectively the 4-momentum of the leptons 1 and 2, and the 4-momenta

of P_1 and P_2 , $P = k + p_3$ and the hadronic matrix elements are written [258, 273–276] :

$$\begin{aligned}
 \tilde{V}^\mu &= \frac{1}{2} \langle P_2 | \bar{q}_i \gamma^\mu q_j | P_1 \rangle = \frac{1}{2} (P^\mu f_+^{P_1 P_2}(q^2) + q^\mu f_-^{P_1 P_2}(q^2)) \\
 \tilde{S} &= \frac{1}{2} \langle P_2 | \bar{q}_i q_j | P_1 \rangle = \frac{1}{2} \frac{(M^2 - m_3^2)}{(m_{q_i} - m_{q_j})} f_0^{P_1 P_2}(q^2) \\
 \tilde{T}^{\mu\nu} &= \frac{1}{2} \langle P_2 | \bar{q}_i \sigma^{\mu\nu} q_j | P_1 \rangle = -\frac{i}{2} \frac{(f_+^{P_1 P_2}(q^2) - f_-^{P_1 P_2}(q^2))}{M^*} (P^\mu q^\nu - P^\nu q^\mu) \\
 \tilde{T}'^\nu &= \frac{1}{2} \frac{(f_+^{P_1 P_2}(q^2) - f_-^{P_1 P_2}(q^2))}{M^*}
 \end{aligned}
 \tag{6.10}$$

For simplicity, we suppressed the q^2 dependence of the form factors $f_{+,-,0}$ in eqn. (6.9), and the flavour superscript ($\zeta = l_1 l_2 q_i q_j$) of the coefficients. Notice there is no interference between $\epsilon_{S,L}$ ($\epsilon_{S,R}$) and ϵ_{T_R} (ϵ_{T_L}) because the trace of the product of Dirac matrices involved in tensor and scalar operators of different chirality vanishes. The form factors and the scalar product in eqn. (6.9) are given in appendix E.

For simplicity, we do not give the analytic expression of the integrated semileptonic decay branching ratio, but only perform the integrals numerically.

6.4 Covariance matrix

In this section, we use the Branching Ratios (BRs) of eqns (6.6) and (6.8) to compute a covariance matrix, that will give constraints on the coefficients that account for possible interferences. We note BR_2^{exp} [BR_3^{exp}] the experimental upper limit on the leptonic decay $P_1 \rightarrow \bar{l}_1 l_2$ [semileptonic decay $P_1 \rightarrow P_2 \bar{l}_1 l_2$] branching ratio and M_2 [M_3] the associated covariance matrix.

We can write the decay branching ratio of eqn. (6.6) and (6.8) in the form

$$\vec{\tilde{c}}^T M^{-1} \vec{\tilde{c}} = 1
 \tag{6.11}$$

where $\vec{\tilde{c}}^T$ ($\vec{\tilde{c}}$) is a row (column) vector of coefficients, and M^{-1} is the inverse of the covariance matrix. The explicit form of the 4×4 and 6×6 matrices is given in appendix G. The diagonal elements of the covariance matrix M represent the squared bounds on our coefficients, and the off-diagonal elements represent the correlation between coefficients.

<i>Decay</i>	<i>Leptonic</i>	<i>Semileptonic</i>
K	$BR_2^{exp}(K_L^0 \rightarrow \mu^\pm e^\mp) < 4.7 \times 10^{-12}$ [174] -	$BR_3^{exp}(K^+ \rightarrow \pi^+ \bar{\mu} e) < 1.3 \times 10^{-11}$ $BR_3^{exp}(K^+ \rightarrow \pi^+ \bar{e} \mu) < 5.2 \times 10^{-10}$ [251]
D	$BR_2^{exp}(D^0 \rightarrow \mu^\pm e^\mp) < 1.3 \times 10^{-8}$ [250] -	$BR_3^{exp}(D^+ \rightarrow \pi^+ \bar{\mu} e) < 3.6 \times 10^{-6}$ $BR_3^{exp}(D^+ \rightarrow \pi^+ \bar{e} \mu) < 2.9 \times 10^{-6}$ [252]
D_s	- -	$BR_3^{exp}(D_S^+ \rightarrow K^+ \bar{\mu} e) < 9.7 \times 10^{-6}$ $BR_3^{exp}(D_S^+ \rightarrow K^+ \bar{e} \mu) < 1.4 \times 10^{-5}$ [252]
B	$BR_2^{exp}(B^0 \rightarrow \mu^\pm e^\mp) < 2.8 \times 10^{-9}$ [175] -	$BR_3^{exp}(B^+ \rightarrow \pi^+ \mu^\pm e^\mp) < 1.7 \times 10^{-7}$ [19] $BR_3^{exp}(B^+ \rightarrow K^+ \mu^\pm e^\mp) < 9.1 \times 10^{-8}$ [177]
B_s	$BR_2^{exp}(B_S^0 \rightarrow \mu^\pm e^\mp) < 1.1 \times 10^{-8}$ [175]	-

Table 6.1: Experimental bounds on leptonic and semileptonic decays.

6.4.1 Bounds on the coefficients

In this section, we give constraints on the coefficients for Kaon, D and B meson leptonic and semileptonic decays. As explained in section 6.3, tensor operators do not contribute to the leptonic decays of mesons. Thus, the available upper limits on leptonic [semileptonic] pseudoscalar meson branching ratios will give constraints on the $\epsilon_{P,X}$ and $\epsilon_{A,X}$ [$\epsilon_{S,X}$, $\epsilon_{V,X}$ and $\epsilon_{T,X}$] coefficients. Indeed, hadronic matrix elements with scalar, vector or tensor quark current structure vanish in the leptonic case, while hadronic matrix elements with pseudoscalar or axial structure vanish in the semileptonic case. We consider the CLFV decays with the associated experimental upper limits given in table 6.1 [38].

The bounds in table 6.1 will be used to constrain the coefficients at Λ_{exp} and the at Λ_W after the RGEs evolution of the coefficients (see section 6.5). The covariance matrices at Λ_{exp} for the (semi)leptonic meson decays are given in appendix H, and the bounds on coefficients are summarized in table 6.2, 6.3 and 6.4.

6.5 Renormalization Group Equations (RGEs)

In this section, we review the evolution of operator coefficients from the experimental scale ($\Lambda_{exp} \sim 2$ GeV) up to the weak scale ($\Lambda_W \sim 80$ GeV) via the one-loop RGEs of QED and QCD [211, 212]. We only consider the QED \times QCD invariant operators of eqn. (6.4). The matching onto the SMEFT basis [284] and the running above m_W [285] will be studied at a later date.

6.5.1 Anomalous dimensions for meson decays

Figure 6.1 illustrates some of the one-loop diagrams that renormalize our operators below the weak scale. Operator mixing is induced by photon loops, whereas the QCD corrections only rescale the S,P and T operator coefficients. After including one-loop corrections in the \overline{MS} scheme, the operator coefficients will run with scale Λ according to [211] :

$$(6.12) \quad \Lambda \frac{\partial}{\partial \Lambda} \vec{c} = \frac{\alpha_e}{4\pi} \vec{c} \Gamma^e + \frac{\alpha_s}{4\pi} \vec{c} \Gamma^s$$

where Γ^e and Γ^s are the QED and QCD anomalous dimension matrices and \vec{c} is a row vector that contains the operator coefficients of eqn. (6.5). In this work, we use the approximate analytic solution [210] of eqn. (6.12) to compute the running and mixing of the coefficients between Λ_{exp} and Λ_W :

$$(6.13) \quad c_I(\Lambda_{exp}) = c_J(\Lambda_W) \lambda^{\alpha_J} \left(\delta_{JI} - \frac{\alpha_e \tilde{\Gamma}_{JI}^e}{4\pi} \log \frac{\Lambda_W}{\Lambda_{exp}} \right)$$

where I,J represent the super- and sub-scripts which label operator coefficients, λ encodes the QCD corrections, and $\tilde{\Gamma}_{JI}^e$ is the ‘‘QCD-corrected’’ one-loop, anomalous dimension matrix for QED [286, 287] . The elements of $\tilde{\Gamma}_{JI}^e$ are defined as:

$$(6.14) \quad \tilde{\Gamma}_{JI}^e = \Gamma_{JI}^e f_{JI}, \quad f_{JI} = \frac{1}{1 + \alpha_J - \alpha_I} \frac{\lambda^{\alpha_I - \alpha_J} - \lambda}{1 - \lambda}, \quad \Gamma^e = \begin{bmatrix} \Gamma_{SPT} & 0 \\ 0 & \Gamma_{VA} \end{bmatrix}.$$

where there is no sum on I, J , $\lambda = \frac{\alpha_s(\Lambda_W)}{\alpha_s(\Lambda_{exp})}$, and $\alpha_J = \frac{\Gamma_{JJ}^s}{2\beta_0} = \{-\frac{12}{23}, -\frac{12}{23}, \frac{4}{23}\}$ for $J \in \{S, P, T\}$. The QED anomalous dimensions are

$$(6.15) \quad \Gamma_{SPT} = \begin{bmatrix} \gamma_{PP}^{l_1 l_2 q_i q_j} & 0 & \gamma_{PT}^{l_1 l_2 q_i q_j} \\ 0 & \gamma_{SS}^{l_1 l_2 q_i q_j} & \gamma_{ST}^{l_1 l_2 q_i q_j} \\ \gamma_{TP}^{l_1 l_2 q_i q_j} & \gamma_{TS}^{l_1 l_2 q_i q_j} & \gamma_{TT}^{l_1 l_2 q_i q_j} \end{bmatrix}, \quad \Gamma_{VA} = \begin{bmatrix} \gamma_{AA}^{l_1 l_2 q_i q_j} & \gamma_{AV}^{l_1 l_2 q_i q_j} \\ \gamma_{VA}^{l_1 l_2 q_i q_j} & \gamma_{VV}^{l_1 l_2 q_i q_j} \end{bmatrix}$$

where the matrix elements in Γ_{SPT} and Γ_{VA} are defined in section 6.5.

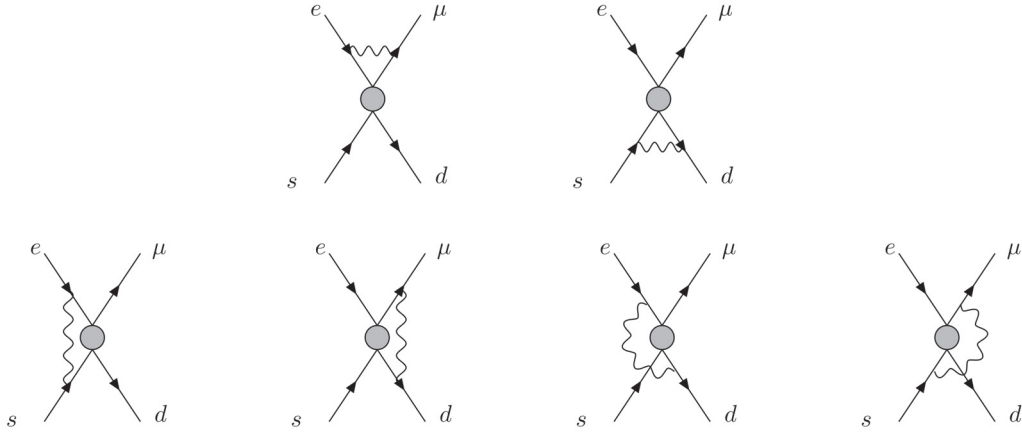


Figure 6.1: Examples of one-loop gauge vertex corrections to 4-fermion operators. The wavefunction renormalization diagrams are missing.

For the scalars and pseudoscalars, the wavefunction, first and second diagrams of figure 6.1 renormalize the coefficients, while the last four diagrams mix the tensors into the scalars and pseudoscalars:

$$(6.16) \quad \gamma_{SS}^{q,q} = \begin{array}{c|cc} & \epsilon_{S,L}^{qq} & \epsilon_{S,R}^{qq} \\ \hline \epsilon_{S,L}^{qq} & -6(1+Q_q^2) & 0 \\ \epsilon_{S,R}^{qq} & 0 & -6(1+Q_q^2) \end{array} \quad \gamma_{TS}^{q,q} = \begin{array}{c|cc} & \epsilon_{S,L}^{qq} & \epsilon_{S,R}^{qq} \\ \hline \epsilon_{T,L}^{qq} & 48Q_q & 0 \\ \epsilon_{T,R}^{qq} & 0 & 48Q_q \end{array}$$

$$(6.17) \quad \gamma_{PP}^{q,q} = \begin{array}{c|cc} & \epsilon_{P,L}^{qq} & \epsilon_{P,R}^{qq} \\ \hline \epsilon_{P,L}^{qq} & -6(1+Q_q^2) & 0 \\ \epsilon_{P,R}^{qq} & 0 & -6(1+Q_q^2) \end{array} \quad \gamma_{TP}^{q,q} = \begin{array}{c|cc} & \epsilon_{P,L}^{qq} & \epsilon_{P,R}^{qq} \\ \hline \epsilon_{T,L}^{qq} & -48Q_q & 0 \\ \epsilon_{T,R}^{qq} & 0 & 48Q_q \end{array} .$$

Similarly, the last four diagrams mix the (pseudo)scalars to the tensors. Only the wavefunction diagrams renormalize the tensors, because for the the first and second diagrams $\gamma^\mu \sigma \gamma_\mu = 0$. We obtain :

$$(6.18) \quad \gamma_{TT}^{q,q} = \begin{array}{c|cc} & \epsilon_{T,L}^{qq} & \epsilon_{T,R}^{qq} \\ \hline \epsilon_{T,L}^{qq} & 2(1+Q_q^2) & 0 \\ \epsilon_{T,R}^{qq} & 0 & 2(1+Q_q^2) \end{array} \quad \gamma_{S(P)T}^{q,q} = \begin{array}{c|cc} & \epsilon_{T,L}^{qq} & \epsilon_{T,R}^{qq} \\ \hline \epsilon_{S(P),L}^{qq} & (-)2Q_q & 0 \\ \epsilon_{S(P),R}^{qq} & 0 & 2Q_q \end{array}$$

Finally, for the vectors and axial vectors, there is no running, but the last four diagrams contribute to the mixing of vector and axial coefficients :

$$(6.19) \quad \gamma_{AV}^{q,q} = \begin{array}{c|cc} & \epsilon_{V,L}^{qq} & \epsilon_{V,R}^{qq} \\ \hline \epsilon_{A,L}^{qq} & 12Q_q & 0 \\ \epsilon_{A,R}^{qq} & 0 & -12Q_q \end{array} \quad \gamma_{VA}^{q,q} = \begin{array}{c|cc} & \epsilon_{A,L}^{qq} & \epsilon_{A,R}^{qq} \\ \hline \epsilon_{V,L}^{qq} & 12Q_q & 0 \\ \epsilon_{V,R}^{qq} & 0 & -12Q_q \end{array}$$

6.5.2 RGEs of operator coefficients

In this section we compute the evolution of the bounds from Λ_{exp} to Λ_W . In the previous section, we found a mixing between pseudoscalar and tensor coefficients, and between vector and axial coefficients. Thus, the coefficients that contributed only to the leptonic [semileptonic] decays at Λ_{exp} will also contribute to the semileptonic [leptonic] decays at Λ_W via the mixing.

The matrices describing the evolution of the coefficients from Λ_{exp} to Λ_W for all the decays were obtained with eqn. (6.13) and are given in appendix F.

6.5.3 Evolution of the bounds

In order to constrain the coefficients at Λ_W , the constraints needs to be expressed in terms of coefficients at Λ_W . However, the mixing of the pseudoscalar (axial) into the tensor (vector), and vice versa, implies that leptonic and semi-leptonic branching ratios can both depend on any of the ten coefficients, which we arrange in a vector as $\vec{\epsilon}^T = \left(\epsilon_{P,L}, \epsilon_{A,L}, \epsilon_{P,R}, \epsilon_{A,R}, \epsilon_{S,L}, \epsilon_{V,L}, \epsilon_{T,L}, \epsilon_{S,R}, \epsilon_{V,R}, \epsilon_{T,R} \right)_{\Lambda_W}$. The 10×10 matrix we need to invert to compute the bounds at Λ_W is now written :

$$(6.20) \quad (M')^{-1} = \mathcal{R}^T \begin{pmatrix} M_2^{-1} & 0_{4 \times 6} \\ 0_{6 \times 4} & M_3^{-1} \end{pmatrix} \mathcal{R}$$

where M_2^{-1} and M_3^{-1} are the 4×4 and 6×6 matrices defined in appendix G we inverted to obtain the bounds at Λ_{exp} (see section 6.4) and \mathcal{R} has the form of the matrices defined in eqn. (F.1), (F.2) and (F.3). Finally, eqn. (6.11) is written in the new basis as :

$$(6.21) \quad \vec{e}'^T (M')^{-1} \vec{e}' = 1$$

where \vec{e}' is the vector of coefficients at Λ_W , $(M')^{-1}$ the matrix in eqn. (6.20) and the superscript T means matrix transposition. All the covariance matrices at Λ_W can be found in appendix H. In table 6.2, 6.3 and 6.4 we summarize all the bounds on the coefficients at Λ_{exp} and Λ_W .

$\epsilon_{P,X}^{l_1 l_2 q_i q_j}$	Λ_{exp}	Λ_W	$S.O, \Lambda_{exp}$	$S.O, \Lambda_W$	$\epsilon_{S,X}^{l_1 l_2 q_i q_j}$	Λ_{exp}	Λ_W	$S.O, \Lambda_{exp}$	$S.O, \Lambda_W$
$\epsilon_{P,X}^{e\mu ds}$	2.32×10^{-7}	4.06×10^{-7}	1.28×10^{-8}	7.82×10^{-9}	$\epsilon_{S,X}^{e\mu ds}$	1.05×10^{-6}	5.68×10^{-7}	7.67×10^{-7}	4.68×10^{-7}
$\epsilon_{P,X}^{e\mu cu}$	1.75×10^{-3}	1.08×10^{-3}	7.92×10^{-5}	4.84×10^{-5}	$\epsilon_{S,X}^{e\mu cu}$	1.34×10^{-3}	8.25×10^{-4}	1.33×10^{-3}	8.1×10^{-4}
$\epsilon_{P,X}^{e\mu bd}$	2.35×10^{-4}	1.66×10^{-4}	5.13×10^{-6}	3.61×10^{-6}	$\epsilon_{S,X}^{e\mu bd}$	1.44×10^{-5}	1.01×10^{-5}	1.44×10^{-5}	1.01×10^{-5}
$\epsilon_{P,X}^{e\mu bs}$	1.75×10^{-4}	1.23×10^{-4}	8.27×10^{-6}	5.83×10^{-6}	$\epsilon_{S,X}^{e\mu bs}$	2.25×10^{-5}	1.59×10^{-5}	2.24×10^{-5}	1.58×10^{-5}

Table 6.2: Constraints on the dimensionless four-fermion coefficients $\epsilon_{P,X}^{l_1 l_2 q_i q_j}$ and $\epsilon_{S,X}^{l_1 l_2 q_i q_j}$ at the experimental (Λ_{exp} for K and D mesons decay and Λ_{m_b} for B meson decays) and weak (Λ_W) scale after the RGEs evolution. The last two columns are the sensitivities, or Single Operator (SO) at a time bounds, see subsection 6.5.4. All bounds apply under permutation of the lepton and/or quark indices.

$\epsilon_{A,X}^{l_1 l_2 q_i q_j}$	Λ_{exp}	Λ_W	$S.O, \Lambda_{exp}$	$S.O, \Lambda_W$	$\epsilon_{V,X}^{l_1 l_2 q_i q_j}$	Λ_{exp}	Λ_W	$S.O, \Lambda_{exp}$	$S.O, \Lambda_W$
$\epsilon_{A,X}^{e\mu ds}$	5.45×10^{-6}	5.45×10^{-6}	3.01×10^{-7}	3.01×10^{-7}	$\epsilon_{V,X}^{e\mu ds}$	4.94×10^{-6}	4.94×10^{-6}	2.93×10^{-6}	2.93×10^{-6}
$\epsilon_{A,X}^{e\mu cu}$	4.51×10^{-2}	4.52×10^{-2}	2.04×10^{-3}	2.04×10^{-3}	$\epsilon_{V,X}^{e\mu cu}$	1.45×10^{-3}	1.64×10^{-3}	1.39×10^{-3}	1.39×10^{-3}
$\epsilon_{A,X}^{e\mu bd}$	1.48×10^{-2}	1.48×10^{-2}	3.23×10^{-4}	3.23×10^{-4}	$\epsilon_{V,X}^{e\mu bd}$	1.49×10^{-5}	1.03×10^{-4}	1.48×10^{-5}	1.48×10^{-5}
$\epsilon_{A,X}^{e\mu bs}$	1.11×10^{-2}	1.11×10^{-2}	5.27×10^{-4}	5.27×10^{-4}	$\epsilon_{V,X}^{e\mu bs}$	2.56×10^{-5}	8.05×10^{-5}	2.54×10^{-5}	2.54×10^{-5}

Table 6.3: Constraints on the dimensionless four-fermion coefficients $\epsilon_{A,X}^{l_1 l_2 q_i q_j}$ and $\epsilon_{V,X}^{l_1 l_2 q_i q_j}$ at the experimental (Λ_{exp} for K and D mesons decay and Λ_{m_b} for B meson decays) and weak (Λ_W) scale after the RGEs evolution. The last two columns are the sensitivities, or Single Operator (SO) at a time bounds, see subsection 6.5.4. All bounds apply under permutation of the lepton and/or quark indices.

In the leptonic decays, the evolution of the bounds on the pseudoscalar coefficients between Λ_{exp} and Λ_W is the most important effect of the RGEs as shown in the first two columns

$\epsilon_{T_X}^{l_1 l_2 q_i q_j}$	Λ_{exp}	Λ_W	$S.O, \Lambda_{exp}$	$S.O, \Lambda_W$
$\epsilon_{T_X}^{e\mu ds}$	1.23×10^{-5}	1.45×10^{-5}	8.76×10^{-6}	1.03×10^{-5}
$\epsilon_{T_X}^{e\mu cu}$	2.01×10^{-3}	2.37×10^{-3}	1.93×10^{-3}	2.28×10^{-3}
$\epsilon_{T_X}^{e\mu bd}$	2.01×10^{-5}	2.26×10^{-5}	2×10^{-5}	2.25×10^{-5}
$\epsilon_{T_X}^{e\mu bs}$	3.89×10^{-5}	4.37×10^{-5}	3.87×10^{-5}	4.35×10^{-5}

Table 6.4: Constraints on the dimensionless four-fermion coefficients $\epsilon_{T_X}^{l_1 l_2 q_i q_j}$ at the experimental (Λ_{exp} for K and D mesons decay and Λ_{m_b} for B meson decays) and weak (Λ_W) scale after the RGEs evolution. The last two columns are the sensitivities, or Single Operator (SO) at a time bounds, see subsection 6.5.4. All bounds apply under permutation of the lepton and/or quark indices.

of the left panel of table 6.2. As can be seen in eqn. (F.1), (F.2) or (F.3), the running of the (pseudo)scalar coefficients is $\sim 1.6(1.4)$, which means that if we neglect the mixing of the tensor into (pseudo)scalar coefficients, the bounds on ϵ_S and ϵ_P will be better at Λ_W for all the decays we considered. However, the large mixing of the tensor coefficients into the (pseudo)scalar ones (see eqn. (6.16), (6.17) and eqn. (F.1) to (F.3)) weaken the bounds on pseudoscalar coefficients at Λ_W for the Kaon decay. This is due to the fact that the bounds on $\epsilon_T^{e\mu ds}$ (see the first two columns of table 6.4) are much weaker than the bounds on $\epsilon_P^{e\mu ds}$ at Λ_{exp} (see the first two columns of the left panel of table 6.2). Thus, the mixing of ϵ_T into ϵ_P will lead to weaker bounds on ϵ_P at Λ_W for the Kaon decay.

For the D, B and B_s meson decays, the bounds on ϵ_P are a bit closer to the bound on ϵ_T at Λ_{exp} . Even with the large mixing of the tensor into the pseudoscalar coefficients, the bounds on $\epsilon_P^{e\mu cu}$, $\epsilon_P^{e\mu bd}$ and $\epsilon_P^{e\mu bs}$ will be slightly better at Λ_W because the running will be larger than the mixing. In the semileptonic decays, there is also a mixing between scalar and tensor coefficients, but the bounds on scalar coefficients at Λ_W increases a bit because, similarly to $\epsilon_P^{e\mu cu}$, $\epsilon_P^{e\mu bd}$ and $\epsilon_P^{e\mu bs}$, the bounds on all the scalar coefficients (first two columns of the right panel of table 6.2) are close to the bounds on the tensor coefficients at Λ_{exp} . The running of the scalars will be stronger than the mixing of the tensors into the scalars, thus, the bounds on ϵ_S are better at Λ_W for all the decays.

For the axial and vector coefficients, there is no running and the mixing is small. The bounds on $\epsilon_A^{e\mu ds}$ and $\epsilon_V^{e\mu ds}$ at Λ_{exp} are very close (see table 6.3), this explains why there is no evolution of these bounds at Λ_W . However, for the D, B and B_s decays, the bounds on ϵ_A are much weaker than the bounds on ϵ_V at Λ_{exp} , especially for the B and B_s decay. Thus, the bounds on $\epsilon_A^{e\mu cu}$, $\epsilon_A^{e\mu bd}$ and $\epsilon_A^{e\mu bs}$ do not evolve significantly at Λ_W , but the mixing of the axial into vector coefficients will lead to weaker bounds on $\epsilon_V^{e\mu cu}$, $\epsilon_V^{e\mu bd}$ and $\epsilon_V^{e\mu bs}$ at Λ_W as shown in the first two columns of the two panels of table 6.3.

Finally, the running of tensor coefficients is tiny, and the mixing of the (pseudo)scalar coefficients into the tensor ones is small. Thus, the evolution of the bounds is small for the tensor coefficients (first two columns of table 6.4) as for the bounds on vector and axial coefficients in the Kaon decay (first two columns of table 6.3). Finally, the matching at Λ_W along with the evolution of the bounds between Λ_W and Λ_{NP} will be given in a future publication [288].

6.5.4 Single operator approximation

We also computed the sensitivities of the various decays to the coefficients at Λ_{exp} , and these are given in the third column of tables 6.2 to 6.4. The sensitivity is the value of the coefficient below which it could not have been observed, and is calculated as a ‘‘Single Operator’’ (SO) at a time bound, that is by allowing only one non-zero coefficient at a time in the branching ratio (see eqn (6.6) and (6.9)). This is different from setting bounds on coefficients (first two columns of table 6.2 to 6.4), which are obtained with all coefficients non-zero, and exclude the parameter space outside the allowed range. It is clear that the sensitivities are sometimes an excellent approximation to the bounds, and sometimes differ by orders of magnitude.

To compute the evolution of the sensitivities of the decays to the coefficients at Λ_W (given in the last column of table 6.2 to 6.4), we still kept only one non-zero coefficients at Λ_{exp} and considered only the running of the coefficients (the diagonal terms in eqn. (F.1) to (F.3)). For example, computing the sensitivity of the leptonic Kaon decay to a pseudoscalar coefficient at Λ_W in the SO approximation requires to multiply the first term in eqn. (G.3) by the first (or third) diagonal term squared in eqn. (F.1). Then, inverting the product and taking the square root will give the sensitivity of the decay to the coefficient at Λ_W .

6.5.5 Updating the bounds

In future years, the experimental data on LFV meson decays could improve, so in this section, we consider how to update our bounds, without inverting large matrices.

The bounds on coefficients at Λ_{exp} obtained in this work are of the form $|\epsilon| < \sqrt{BR^{exp}} \times \text{constant}$. Thus, all the bounds at Λ_{exp} given in tables 6.2 to 6.4 can be updated by rescaling by $\sqrt{(BR_{new}^{exp})/(BR_{old}^{exp})}$ when the data improves. However, in principle, the 10×10 matrix of eqn (6.20) must then be inverted to obtain the bounds at Λ_W . So we now describe approximations that allow to obtain the bounds at Λ_W with manageable matrices.

For the semileptonic decay, the bounds at Λ_{exp} can be obtained by neglecting all the interference terms between the scalar, vector and tensor coefficients of either chirality (see eqn. (6.9)). The 6×6 matrix in eqn. (G.2) then becomes diagonal and easy to invert. This approximation will give bounds at Λ_{exp} on $\epsilon_{S,X}$, $\epsilon_{V,X}$ and $\epsilon_{T,X}$ close to those obtained in the first column of tables

6.2 to 6.4 (which include the interference terms).

In the leptonic decay (eqn. (6.6)), a reasonable approximation for the bounds at Λ_{exp} is to keep the interference between axial and pseudoscalar coefficients of opposite chirality (with $m_2 = m_\mu$ in eqn. (6.6)). The other interference terms, proportional to $m_1 = m_e$, can be neglected. Thus, bounds on ϵ_A and ϵ_P at Λ_{exp} , which are a reasonable approximation to the first column of tables 6.2 and 6.3, can be obtained by inverting a 2×2 matrix in the basis $(\epsilon_{P,X}, \epsilon_{A,Y})$ where $X \in L, R$ and $Y \in R, L$, instead of the 4×4 matrix in eqn. (G.1).

To obtain bounds at Λ_W , it is necessary to keep the mixing between ϵ_S , ϵ_P , ϵ_T , and between ϵ_V and ϵ_A . Then, the bounds on ϵ_S , ϵ_P , ϵ_T , ϵ_V and ϵ_A at Λ_W can be obtained by considering M^{-1} in eqn. (6.20) as a product of 5×5 matrices in the basis $(\epsilon_{P,X}, \epsilon_{S,X}, \epsilon_{T,X}, \epsilon_{V,Y}, \epsilon_{A,Y})$ where X and Y are the chirality. However, ϵ_S , ϵ_P and ϵ_T must have the same chirality, but different from the chirality of ϵ_V and ϵ_A in order to take into account the mixing induced by the RGEs, that occurs only for coefficients of the same chirality (see eqn. (6.13), and (F.1) to (F.3)). This is due to the fact that it is necessary to keep the interference between axial and pseudoscalar coefficients of different chiralities to compute the bounds on $\epsilon_{P,X}$ and $\epsilon_{A,Y}$.

6.6 Conclusion

In this paper, we consider operators which simultaneously change lepton and quark flavour, and obtain constraints on the coefficients using available data on (semi)leptonic pseudoscalar meson decays. Section 6.2 lists the dimension six, two lepton two quark operators and their associated coefficients at the experimental scale Λ_{exp} . Scalar, pseudoscalar, vector, axial and tensor operators are included. The leptonic and semileptonic branching ratios of pseudoscalar mesons, as a function of the operator coefficients, are given in section 6.3. We find tensor operators do not contribute to the leptonic decays but only to the semileptonic decays, in which the interference between $\epsilon_{S,L}$ ($\epsilon_{S,R}$) and ϵ_{T_R} (ϵ_{T_L}) vanishes. The constraints on operator coefficients, evaluated at the experimental scale, are given in tables 6.2, 6.3 and 6.4 and discussed in section 6.4. The bounds are obtained via the appropriate covariance matrices, which allows to take into account the interferences among operators (see eqn. (6.6),(6.9),(G.1) and (G.2)). The matrices are given in appendix B. Section 6.5 gives the Renormalization Group evolution of the coefficients from the experimental to the weak scale Λ_W , and the formalism used to compute the covariances matrices at Λ_W . The weak-scale constraints on the coefficients are given in tables 6.2, 6.3 and 6.4. The large mixing of tensor coefficients into (pseudo)scalar coefficients has important consequences on the evolution of the bounds on scalar and pseudoscalar coefficients. Indeed, in the case of the kaon decay, the experimental-scale bounds on tensor coefficients are significantly weaker than those on

pseudoscalars. As a result, the pseudoscalar bounds are weaker at Λ_W , compared to the bounds at Λ_{exp} . The bounds on scalar coefficients at Λ_W are slightly stronger than at Λ_{exp} . There is no running for the vector and axial coefficients, due to the fact we consider quark-flavor changing operators, and the mixing is small, but the bounds on axial coefficients are much weaker than the bounds on vector coefficients for the D, B and B_s decays, this leads to much weaker bounds on vector coefficients at Λ_W . Similarly, the running and mixing of tensor coefficients are small. As a result, the bounds on the axial and tensor coefficients do not evolve significantly between the experimental and weak scales.

We conclude by noting the importance of including interferences among operators in computing the bounds on their coefficients. As shown in subsection 6.5.4, the sensitivities of the decays to ϵ_P and ϵ_A obtained at Λ_{exp} and to ϵ_P , ϵ_A and ϵ_V at Λ_W in the single operator approximation are better by several orders of magnitude compared to the bounds obtained by keeping the interferences among operators. We found that the Renormalization Group running between the experimental and weak scales has an important effect on the evolution of the bounds, especially the large mixing of the tensor (axial) into the pseudoscalar (vector), which lead to weaker bounds on pseudoscalar (vector) coefficients at Λ_W for the Kaon (D, B and B_s) decay.

CONCLUSIONS AND PROSPECTS

The Standard Model of particle physics proved to be a very successful theory, as most of its predictions have been confirmed by various experiments. However, despite of its success, the SM cannot be a complete theory as many unsolved issues remain. This is confirmed by many observations that cannot be explained in the frame of the SM, such as the matter-antimatter asymmetry in the Universe or the presence of dark matter and dark energy. Other issues, such as the hierarchy problem or the fact that gravity is not included in the SM are additional reasons to believe that the SM can be considered as an effective theory of a more fundamental theory. This has lead to the birth of BSM physics that aim at extending the SM in order to address the unsolved issues.

The discovery of neutrino oscillations proved that neutrinos are massive and was also another striking manifestation of BSM physics, as lepton flavour violation is not explained in the SM. Thus, flavour physics is a great place to search for BSM physics and could give insight on the way to construct a more fundamental theory. In particular, the observation of processes involving lepton flavour violation in the charged lepton sector would be a clear signal of BSM physics. Indeed, even in the SM extended with massive neutrinos, the rates of CLFV processes are strongly suppressed and cannot be observed by current or future experiments. Currently, various experiments are searching for CLFV processes and many others are under construction, and plan to improve the sensitivity to CLFV processes by several orders of magnitude.

In this thesis, we have presented the study of specific CLFV processes, and used an EFT approach to constrain new physics models. The motivation for this work is the huge potential of CLFV processes to constrain BSM models, in the context of the exceptional improvements in the

sensitivity expected for the future experiments.

In chapter 2, we made a review of the unsolved issues in the SM, and gave a short list of BSM models that aim at addressing these issues.

In chapter 3, we introduced the theoretical and experimental context for CLFV searches. We first discussed the state of the art in the muon channel, in which the sensitivity of the experiments to CLFV processes will greatly improve with the upcoming experiments. Then, we presented various searches in the tau channel, we saw that the sensitivity is lower than in the muon channel, but as for the muon channel, important improvements of the sensitivity in the tau channel are expected for the future experiments. We also discussed CLFV processes searches in the meson channel, which is also a very promising channel to constrain BSM models, due to the very large number of processes and the various experiments searching for these processes.

In chapter 4, we introduced the formalism of the EFT approach. We saw how the SM can be extended with the most general gauge invariant higher dimensional operators constructed from SM fields. In this approach, new physics effects can be described in terms of the effective operators and their associated coefficients. We also discussed the principles of renormalization and dimensional regularization, that are necessary to treat the divergences that appear in loop integrals. We presented the renormalization group equations, that govern the running and the mixing of coefficients with the energy scale. Finally, we presented two approaches in the EFT formalism : the top-down approach, and the bottom-up approach.

In chapter 5, we studied the conversion of a muon into an electron on nuclei in a top-down EFT. We considered operators that can mediate the conversion process and obtained constraints on the coefficients using available data. First, we listed the operators and their associated coefficients, that contribute to the conversion process. We gave details of our estimation of the spin dependent and independent rates and discussed the related uncertainties. Then, we considered three possible Leptoquarks scenarios, each containing an SU(2) singlet Leptoquark, with a mass at the TeV scale and with only one coupling to electrons and one to muons. We computed the running and the mixing from the new physics scale (the Leptoquark mass) down to the experimental scale via an approximate analytic solution to the one-loop RGEs of QED and QCD. With the spin dependent and independent branching ratios expressed as a function of the coefficients at the experimental scale, we used the current experimental upper limits on the $\mu \rightarrow e$ conversion process to constrain our coefficients, using a covariance matrix formalism. We then discussed the prospects for distinguishing the spin dependent and independent contributions. Finally, discussed the prospects for using different target nuclei in order to discriminate among the operators in the case where $\mu \rightarrow e$ conversion on nuclei is observed.

In chapter 6, we studied CLFV two and three body decays of pseudoscalar mesons in a bottom-up EFT. We considered operators that change lepton and quark flavour, and we obtained constraints on the coefficients using available data on (semi)leptonic pseudoscalar meson decays. We listed the operators and their associated coefficients at the experimental scale that contribute

to the CLFV (semi)leptonic pseudoscalar meson decays. Then we computed the leptonic and semileptonic branching ratios of CLFV pseudoscalar meson decays as a function of the coefficients at the experimental scale. Using again a covariance matrix formalism allows us to take into account the interferences between operators when computing bounds on the coefficients. We gave the constraints on the coefficients at the experimental scale and then we used the RGEs to evolve our coefficients to the weak scale, at which we computed the bounds again. Then, we computed the sensitivities of the decays to the operators in the single operator approximation. We studied the importance of including interferences among operators by comparing the sensitivities obtained in the single operator approximation to the bounds obtained by keeping the interferences. We concluded that it is critically important to keep the interferences among operators when computing bounds on coefficients, and that the running between the experimental and weak scales has an important effect on the evolution of the bounds.

With all the expected improvements in the experimental sensitivity to various CLFV processes in the coming years, we have very exciting times ahead of us. We will be able to test BSM models at an unprecedented level and we will have a beautiful opportunity to have a better understanding of the structure of quantum field theories, toward the final theory of everything.



$$G_O^{N,q}$$

When the quark Lagrangian of eqn (5.1) is matched onto the nucleon Lagrangian, the coefficients of the nucleon operators can be computed as $\tilde{C}_{O,Y}^{NN} = \sum_q G_O^{N,q} C_{O,Y}^{qq}$, for $O \in T, A, V, P$; for the scalar operator there is an additional gluon contribution as described in [206]. We take the $G_O^{N,q}$, defined at zero-momentum-transfer such that $\langle N(P) | \bar{q}(x) \Gamma_O q(x) | N(P) \rangle = G_O^{N,q} \bar{u}_N(P) \Gamma_O u_N(P)$, to be

$$\begin{aligned}
 \text{(A.1)} \quad & G_V^{p,u} = G_V^{n,d} = 2 \quad , \quad G_V^{p,d} = G_V^{n,u} = 1 \quad , \quad G_V^{p,s} = G_V^{n,s} = 0 \\
 \text{(A.2)} \quad & G_A^{p,u} = G_A^{n,d} = 0.84(1) \quad , \quad G_A^{p,d} = G_A^{n,u} = -0.43(1) \quad , \quad G_A^{p,s} = G_A^{n,s} = -.085(18) \\
 \text{(A.3)} \quad & G_S^{p,u} = \frac{m_p}{m_u} 0.021(2) = 9.0 \quad , \quad G_S^{p,d} = \frac{m_p}{m_d} 0.041(3) = 8.2 \quad , \quad G_S^{p,s} = \frac{m_N}{m_s} 0.043(11) = 0.42 \\
 \text{(A.4)} \quad & G_S^{n,u} = \frac{m_n}{m_u} 0.019(2) = 8.1 \quad , \quad G_S^{n,d} = \frac{m_n}{m_d} 0.045(3) = 9.0 \quad , \quad G_S^{n,s} = \frac{m_N}{m_s} 0.043(11) = 0.42 \\
 \text{(A.5)} \quad & G_P^{p,u} = 144 = G_P^{n,d} \quad , \quad G_P^{p,d} = -150 = G_P^{n,u} \quad , \quad G_P^{p,s} = -4.9 = G_P^{n,s} \\
 \text{(A.6)} \quad & G_T^{p,u} = G_T^{n,d} = 0.77(7) \quad , \quad G_T^{p,d} = G_T^{n,u} = -0.23(3) \quad , \quad G_T^{p,s} = G_T^{n,s} = .008(9) \quad .
 \end{aligned}$$

where the parenthese gives the uncertainty in the last figure(s). The axial G_A are the results inferred in Ref. [289] by using the HERMES measurements [290]. The scalar G_S induced by light quarks are from a dispersive determination [291], and an average of lattice results [292] is used for the strange quark; in all cases, the \overline{MS} quark masses at $\mu = 2$ GeV are taken as $m_u = 2.2$ MeV, $m_d = 4.7$ MeV, and $m_s = 96$ MeV [293]. The nucleon masses are $m_p = 938$ MeV and $m_n = 939.6$ MeV. The pseudoscalar results were calculated from data in the large- N_c approximation at $q^2 \approx 0$ [294], and here extrapolated to neutrons using isospin. The tensor results for the neutron are the lattice results of Cirigliano et al [295], which are here extrapolated to protons using isospin.

For comparison, the G_A have been obtained on the lattice; a recent determination [296] is

$$(A.7) \quad \begin{aligned} G_A^{p,u} = G_A^{n,d} &= 0.863(7)(14) \quad , \quad G_A^{p,d} = G_A^{n,u} = -0.345(6)(9) \\ G_A^{p,s} = G_A^{n,s} &= -0.0240(21)(11) \end{aligned}$$

The scalar $G_S^{N,q}$ have also recently been obtained on the lattice [297]:

$$(A.8) \quad G_S^{p,u} = \frac{m_p}{m_u} 0.0139(13)(12) = 5.9 \quad , \quad G_S^{p,d} = \frac{m_p}{m_d} 0.0253(28)(24) = 5.0$$

$$(A.9) \quad G_S^{n,u} = \frac{m_n}{m_u} 0.0116(13)(11) = 5.0 \quad , \quad G_S^{n,d} = \frac{m_n}{m_d} 0.0302(3) = 6.0$$

We observe that there is a 50% discrepancy with respect to the results of [291], obtained from pionic atoms and $\pi - N$ scattering [298]. Results similar to [291] were earlier obtained in [299], also using an effective theory.

THE TENSOR CONTRIBUTION TO THE SD AND SI RATES

We consider tensor operators

$$(B.1) \quad C_{T,L}^{uu} \mathcal{O}_{T,L}^{uu} + C_{T,L}^{dd} \mathcal{O}_{T,L}^{dd} + \{L \leftrightarrow R\}$$

at the experimental scale μ_N , which contribute at finite-momentum-transfer to the SI conversion process (see eqn (5.19)), and also to the SD processes:

$$(B.2) \quad \frac{\Gamma_{SI}}{\Gamma_{capt}} = 8B_0 \frac{m_\mu^2}{m_N^2} |Z(C_{T,L}^{uu} G_T^{p,u} + C_{T,L}^{dd} G_T^{p,d}) F_p(m_\mu) + (A-Z)(C_{T,L}^{uu} G_T^{n,u} + C_{T,L}^{dd} G_T^{n,d}) F_n(m_\mu)|^2 + \{L \leftrightarrow R\}$$

$$(B.3) \quad \frac{\Gamma_{SD}}{\Gamma_{capt}} = 32B_0 \frac{J_A + 1}{J_A} \left| S_p^A (C_{T,L}^{uu} G_T^{p,u} + C_{T,L}^{dd} G_T^{p,d}) + S_n^A (C_{T,L}^{uu} G_T^{n,u} + C_{T,L}^{dd} G_T^{n,d}) \right|^2 \frac{S_A(m_\mu)}{S_A(0)} + \{L \leftrightarrow R\} .$$

The ratio of these contributions, for a single operator, is

$$(B.4) \quad \frac{\Gamma_{SD}}{\Gamma_{SI}} \simeq 4 \frac{J_A + 1}{J_A} \frac{m_N^2}{m_\mu^2} \frac{|S_p^A G_T^{p,q} + S_n^A G_T^{n,q}|^2}{|Z G_T^{p,q} + (A-Z) G_T^{n,q}|^2} \sim \begin{cases} 0.7 & q = u \quad A = Al \\ 0.06 & q = d \quad A = Al \\ 0.03 & q = u \quad A = Ti \\ 0.01 & q = d \quad A = Ti \end{cases}$$

where we assumed that the form factors are comparable $\frac{S_A(m_\mu)}{S_A(0)} \simeq |F_p(m_\mu)|^2$ as is the case in Aluminium. Recall that $G_T^{n,u} \sim -\frac{1}{2}G_T^{p,u}$, so there is a partial cancellation in the SI amplitude, whereas the SD process arises mostly from an odd proton $S_p^A \gg S_n^A$, or mostly from an odd neutron $S_p^A \ll S_n^A$.

The estimates of eqn (B.4) assume that only one tensor coefficient is non-zero, so they neglect interferences, which can easily enhance the SI rate. For instance, RG running of the tensor operator from the New Physics scale to the experimental scale generically generates a scalar operator with comparable coefficient. The scalar-tensor interference contribution to the SI rate would be relatively enhanced, with respect to the tensor-squared, by $G_S^{N,q}/G_T^{N,q} \sim 10$, which would suppress the ratio in eqn (B.4) by another factor 1/10.



RG EVOLUTION

In this appendix, we review the Renormalisation Group evolution of operator coefficients from the leptoquark mass scale M (\sim TeV) down to the experimental scale Λ_{exp} (2 GeV), via the one-loop RGEs of QCD and QED [211, 212]. We consider the QED \times QCD invariant operator basis discussed in section 5.2. We neglect matching onto the SMEFT basis [182, 284] and running with the full SM RGEs [285, 300, 301], on the assumption that QED is a reasonable approximation if M is not much larger than m_W .

After including one-loop corrections in the \overline{MS} scheme, the operator coefficients will run with scale Λ according to [211]

$$(C.1) \quad \Lambda \frac{\partial}{\partial \Lambda} (C_I, \dots C_J, \dots) = \frac{\alpha_e}{4\pi} \vec{C} \Gamma^e + \frac{\alpha_s}{4\pi} \vec{C} \Gamma^s$$

where I, J represent the super- and subscripts which label operator coefficients, Γ^e and Γ^s are the QED and QCD anomalous dimension matrices and \vec{C} is a row vector that contains the QCD \times QED invariant operators coefficients listed in section 2 of chapter 5.

In this work, we use the approximate analytic solution [210] given in eqn (5.42):

$$C_I(\Lambda_{exp}) = C_J(M) \lambda^{a_J} \left(\delta_{JI} - \frac{\alpha_e \tilde{\Gamma}_{JI}^e}{4\pi} \log \frac{M}{\Lambda_{exp}} \right)$$

where the factors are given after eqn (5.42) and $\log \frac{M}{\Lambda_{exp}} \sim 6.21$.

Only QED loops contribute to operators mixing, while QCD loops only rescale scalar and tensor operators. In figure C.1, we present the QED diagrams required to compute the anomalous dimension γ of the four-fermion operators, where $f_1 \in \{e, \mu\}$ and $f_2 \in \{u, d, s, c, b, e, \mu, \tau\}$.

The operators coefficients below the scale M are organized in the vector \vec{C} as following :

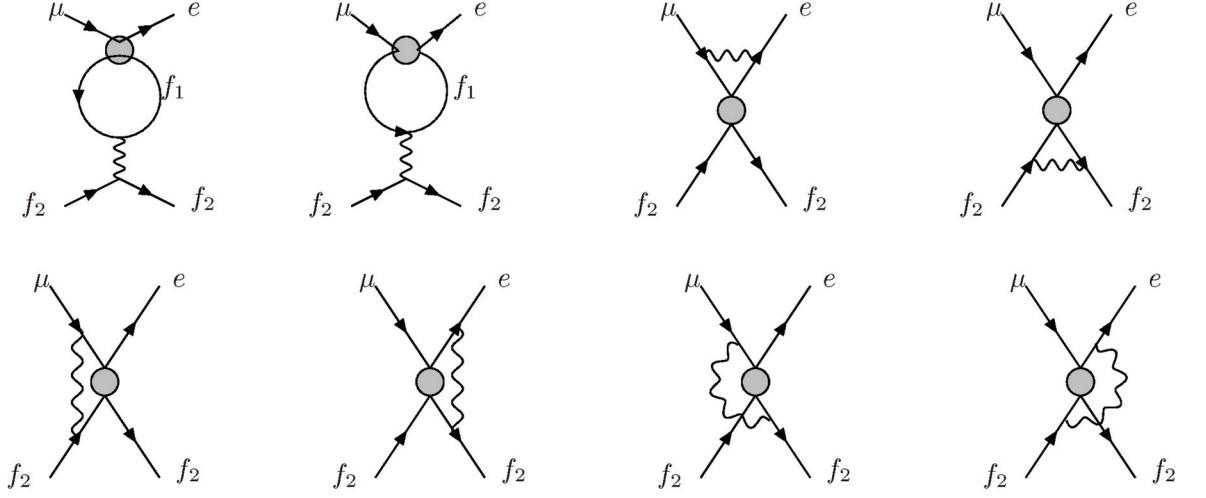


Figure C.1: Examples of one-loop gauge vertex corrections to 4-fermion operators. The first two diagrams are the penguins. The last six diagrams contribute to operator mixing and running, but can only change the Lorentz or gauge structure of the operators, not the flavour structure. Missing are the wave-function renormalisation diagrams; for $V \pm A$ Lorentz structure in the grey blob, this cancels diagrams 3 and 4.

$$(C.2) \quad \vec{C} = (\vec{C}_V^u, \vec{C}_V^d, \vec{C}_A^u, \vec{C}_A^d, \vec{C}_S^u, \vec{C}_S^d, \vec{C}_T^u, \vec{C}_T^d)$$

$$(C.3) \quad \vec{C}_V^f = (C_{VL}^{ff}, C_{VR}^{ff}) \quad \vec{C}_A^f = (C_{AL}^{ff}, C_{AR}^{ff})$$

$$(C.4) \quad \vec{C}_S^f = (C_{SL}^{ff}, C_{SR}^{ff}) \quad \vec{C}_T^f = (C_{TL}^{ff}, C_{TR}^{ff})$$

(C.5)

In the basis of \vec{C} , the QED anomalous dimension matrix can be written

$$\Gamma^e = \begin{bmatrix} \Gamma_{VA} & 0 \\ 0 & \Gamma_{ST} \end{bmatrix}$$

where

$$(C.6) \quad \Gamma_{ST} = \begin{bmatrix} \gamma_{S,S}^{u,u} & 0 & \gamma_{S,T}^{u,u} & 0 \\ 0 & \gamma_{S,S}^{d,d} & 0 & \gamma_{S,T}^{d,d} \\ \gamma_{T,S}^{u,u} & 0 & \gamma_{T,T}^{u,u} & 0 \\ 0 & \gamma_{T,S}^{d,d} & 0 & \gamma_{T,T}^{d,d} \end{bmatrix} \quad \text{and} \quad \Gamma_{VA} = \begin{bmatrix} 0 & 0 & \gamma_{V,A}^{u,u} & 0 \\ 0 & 0 & 0 & \gamma_{V,A}^{d,d} \\ \gamma_{A,V}^{u,u} & 0 & 0 & 0 \\ 0 & \gamma_{A,V}^{d,d} & 0 & 0 \end{bmatrix}$$

Vector and axial operators

The first penguin diagram and the last four give the following matrices :

$$(C.7) \quad \gamma_{V,A}^{f,f} = \frac{C_{A,L}^{ff} \quad C_{A,R}^{ff}}{C_{V,L}^{ff} \quad C_{V,R}^{ff}} \begin{vmatrix} C_{A,L}^{ff} & C_{A,R}^{ff} \\ -12Q_f & 0 \\ 0 & -12Q_f \end{vmatrix} \quad \gamma_{A,V}^{f,f} = \frac{C_{V,L}^{ff} \quad C_{V,R}^{ff}}{C_{A,L}^{ff} \quad C_{A,R}^{ff}} \begin{vmatrix} C_{V,L}^{ff} & C_{V,R}^{ff} \\ 12Q_f & 0 \\ 0 & 12Q_f \end{vmatrix}$$

Using these anomalous dimension matrices and the RGEs give :

$$(C.8) \quad C_{V,R}^{qq}(\Lambda_{exp}) = -3Q_q \frac{\alpha_e}{\pi} \log \frac{M}{\Lambda_{exp}} C_{A,L}^{qq}(M) + C_{V,R}^{qq}(M)$$

$$(C.9) \quad C_{A,R}^{qq}(\Lambda_{exp}) = 3Q_q \frac{\alpha_e}{\pi} \log \frac{M}{\Lambda_{exp}} C_{V,L}^{qq}(M) + C_{A,R}^{qq}(M)$$

where $q \in \{u, d\}$. We see that axial operators mix to vector operators and vice versa, but there is no rescaling for axial and vector operators.

Scalar operators

Combining the third and fourth diagrams of figure C.1 with the wavefunction diagrams renormalize the scalars while the last four diagrams mix the tensors to the scalars :

$$(C.10) \quad \gamma_{S,S}^{f,f} = \frac{C_{S,L}^{ff} \quad C_{S,R}^{ff}}{C_{S,L}^{ff} \quad C_{S,R}^{ff}} \begin{vmatrix} C_{S,L}^{ff} & C_{S,R}^{ff} \\ -6(1+Q_f^2) & 0 \\ 0 & -6(1+Q_f^2) \end{vmatrix} \quad \gamma_{T,S}^{f,f} = \frac{C_{S,L}^{ff} \quad C_{S,R}^{ff}}{C_{T,L}^{ff} \quad C_{T,R}^{ff}} \begin{vmatrix} C_{S,L}^{ff} & C_{S,R}^{ff} \\ +96Q_f & 0 \\ 0 & +96Q_f \end{vmatrix}$$

The scalars coefficients at the experimental scale read :

$$(C.11) \quad C_{S,L}^{qq}(\Lambda_{exp}) = -24\lambda^{aT} f_{TS} Q_q \frac{\alpha_e}{\pi} \log \frac{M}{\Lambda_{exp}} C_{T,L}^{qq}(M) + \lambda^{aS} \left[1 + \frac{3}{2} \frac{\alpha_e}{\pi} \log \frac{M}{\Lambda_{exp}} (1+Q_q^2) \right] C_{S,L}^{qq}(M)$$

Tensor operators

Similarly, the last four diagrams mix the scalars to the tensors. Only the wavefunction diagrams renormalize the tensors, because for the third and fourth diagrams $\gamma^\mu \sigma \gamma_\mu = 0$. We obtain the following matrices :

$$(C.12) \quad \gamma_{T,T}^{f,f} = \frac{C_{T,L}^{ff} \quad C_{T,R}^{ff}}{C_{T,L}^{ff} \quad C_{T,R}^{ff}} \begin{vmatrix} C_{T,L}^{ff} & C_{T,R}^{ff} \\ -2(1+Q_f^2) & 0 \\ 0 & -2(1+Q_f^2) \end{vmatrix} \quad \gamma_{S,T}^{f,f} = \frac{C_{T,L}^{ff} \quad C_{T,R}^{ff}}{C_{S,L}^{ff} \quad C_{S,R}^{ff}} \begin{vmatrix} C_{T,L}^{ff} & C_{T,R}^{ff} \\ 2Q_f & 0 \\ 0 & 2Q_f \end{vmatrix}$$

$$(C.13) \quad C_{T,L}^{qq}(\Lambda_{exp}) = -\lambda^{aS} f_{ST} Q_q \frac{\alpha_e}{2\pi} \log \frac{M}{\Lambda_{exp}} C_{S,L}^{qq}(M) + \lambda^{aT} \left[1 + \frac{\alpha_e}{2\pi} \log \frac{M}{\Lambda_{exp}} (1+Q_q^2) \right] C_{T,L}^{qq}(M)$$

Finally, the coefficients at the experimental scale Λ_{exp} are obtain via the matching condition :

$$(C.14) \quad \tilde{C}_{O,Y}^{NN}(\Lambda_{exp}) = \sum_{q=u,d,s} G_O^{N,q} C_{O,Y}^{qq}(\Lambda_{exp})$$



CONSTANTS

In this section, we give all the constants used in our calculations in chapter 6 :

P_1	K_L^0	K^+	D^0	D^+	D_S^+
$f_{P_1}(MeV)$	155.72 [302, 303]	155.6 [302, 303]	211.5 [302, 304]	212.6 [302, 304]	249.8 [304]
$f_+^{P_1\pi}(0)$	0.966 [303]	0.966 [303]	0.666 [303]	0.666 [303]	0.666 [303]
$f_+^{P_1K}(0)$	-	-	0.747 [303]	0.747 [303]	0.747 [303]
λ_+	2.82×10^{-2} [38]	2.97×10^{-2} [38]	-	-	-
λ_0	1.8×10^{-2} [38]	1.95×10^{-2} [38]	-	-	-

P_1	B^0	B_S^0	B^+
$f_{P_1}(MeV)$	190.9 [302]	230.7[304]	187.1 [302]
$f_+^{P_1\pi}(0)$	0.25 [305]	0.25 [305]	0.25 [305]
$f_+^{P_1K}(0)$	0.31 [305]	0.31 [305]	0.31 [305]
λ_+	-	-	-
λ_0	-	-	-

All the masses and lifetime can be found in [38].



KINEMATICS AND FORM FACTORS FOR SEMILEPTONIC DECAYS

In this section, we give the form factor and the detailed scalar product of eqn. (6.9).

The q^2 dependence of the form factors for the Kaon is given by [274] :

$$(E.1) \quad f_{+,0}^{K\pi}(q^2) = f_+^{K\pi}(0) \left(1 + \lambda_{+,0} \frac{q^2}{M_\pi^2} \right); \quad f_-^{K\pi}(q^2) = f_+^{K\pi}(0) (\lambda_0 - \lambda_+) \frac{M_{K^+}^2 - M_{\pi^+}^2}{M_{\pi^+}^2}$$

and for the D and B mesons, are given by [275, 276] :

$$(E.2) \quad f_+(q^2) = \frac{f_+(0)}{1 - q^2/m_{1-}^2}; \quad f_0(q^2) = \frac{f_0(0)}{1 - q^2/m_{0+}^2}; \quad f_-(q^2) = (f_0(q^2) - f_+(q^2)) \frac{M^2 - m_3^2}{q^2}$$

where $\lambda_{+,0}$ are constants, m_{JP} is the mass of the lightest resonance with the right quantum numbers to mediate the transition (D_s^+ and D_s^{*+} for example). We took $q^2 = q_{\max}^2 = (M - m_3)^2$ to compute the form factors f_+ , f_- and f_0 . All these values can be found in appendix D.

Finally, the scalar product in eqn. (6.9) can be written as functions of the two kinematical variables q^2 and $\cos\theta$ [38, 283] in the phase space integrals of eqn. (6.8).

$$(E.3) \quad p_1 \cdot p_2 = \frac{q^2 - m_1^2 - m_2^2}{2}, \quad p_1 \cdot q = \frac{q^2 + m_1^2 - m_2^2}{2}, \quad p_2 \cdot q = \frac{q^2 + m_2^2 - m_1^2}{2}$$

$$(E.4) \quad p_3 \cdot q = \frac{M^2 - m_3^2 - q^2}{2}, \quad p_1 \cdot p_3 = p_3 \cdot q - p_2 \cdot p_3$$

$$p_1 \cdot P = p_1 \cdot q + 2p_1 \cdot p_3, \quad p_2 \cdot P = p_2 \cdot q + 2p_2 \cdot p_3$$

$$(E.5) \quad p_2 \cdot p_3 = \frac{1}{4q^2}(M^2 - m_3^2 - q^2)(q^2 + m_2^2 - m_1^2) + \frac{1}{4q^2} \sqrt{\lambda(M^2, m_3^2, q^2)} \sqrt{\lambda(q^2, m_1^2, m_2^2)} \cos \theta$$

$$(E.6) \quad k \cdot p_3 = \frac{M^2 + m_3^2 - q^2}{2}, \quad P \cdot q = M^2 - m_3^2, \quad P^2 = 2M^2 + 2m_3^2 - q^2$$



RGEs

In this section, we give the 10×10 matrices obtained with eqn. (6.13) we used to obtain the bounds at Λ_W (with eqn. (6.20)).

For the decay of light quark (Kaon and D meson decays), the experimental scale is taken as 2 GeV because most of the time, it's the renormalization scale chosen to obtain the lattice form factors.

The evolution of the coefficients ($\epsilon^{e\mu ds}$) involved in the Kaon decays is given by :

$$\begin{aligned}
 & \text{(F.1)} \\
 & \left(\begin{array}{c} \epsilon_{P,L} \\ \epsilon_{A,L} \\ \epsilon_{P,R} \\ \epsilon_{A,R} \\ \epsilon_{S,L} \\ \epsilon_{V,L} \\ \epsilon_{T_L} \\ \epsilon_{S,R} \\ \epsilon_{V,R} \\ \epsilon_{T_R} \end{array} \right)_{\Lambda_{exp}} = \begin{pmatrix} 1.64 & 0 & 0 & 0 & 0 & 0 & -0.0429 & 0 & 0 & 0 \\ 0 & 1 & 0 & 0 & 0 & 0.00857 & 0 & 0 & 0 & 0 \\ 0 & 0 & 1.64 & 0 & 0 & 0 & 0 & 0 & 0 & 0.0429 \\ 0 & 0 & 0 & 1 & 0 & 0 & 0 & 0 & -0.00857 & 0 \\ 0 & 0 & 0 & 0 & 1.64 & 0 & 0.0429 & 0 & 0 & 0 \\ 0 & 0.00857 & 0 & 0 & 0 & 1 & 0 & 0 & 0 & 0 \\ -0.00162 & 0 & 0 & 0 & 0.00162 & 0 & 0.849 & 0 & 0 & 0 \\ 0 & 0 & 0 & 0 & 0 & 0 & 0 & 1.64 & 0 & 0.0429 \\ 0 & 0 & 0 & -0.00857 & 0 & 0 & 0 & 0 & 1 & 0 \\ 0 & 0 & 0.00162 & 0 & 0 & 0 & 0 & 0.00162 & 0 & 0.849 \end{pmatrix} \left(\begin{array}{c} \epsilon_{P,L} \\ \epsilon_{A,L} \\ \epsilon_{P,R} \\ \epsilon_{A,R} \\ \epsilon_{S,L} \\ \epsilon_{V,L} \\ \epsilon_{T_L} \\ \epsilon_{S,R} \\ \epsilon_{V,R} \\ \epsilon_{T_R} \end{array} \right)_{\Lambda_W}
 \end{aligned}$$

For the D meson decays, the evolution of the coefficients ($\epsilon^{e\mu cu}$) is given by :

$$\begin{aligned}
 & \text{(F.2)} \\
 & \left(\begin{array}{c} \epsilon_{P,L} \\ \epsilon_{A,L} \\ \epsilon_{P,R} \\ \epsilon_{A,R} \\ \epsilon_{S,L} \\ \epsilon_{V,L} \\ \epsilon_{T_L} \\ \epsilon_{S,R} \\ \epsilon_{V,R} \\ \epsilon_{T_R} \end{array} \right)_{\Lambda_{exp}} = \begin{pmatrix} 1.64 & 0 & 0 & 0 & 0 & 0 & 0.0857 & 0 & 0 & 0 \\ 0 & 1 & 0 & 0 & 0 & -0.0171 & 0 & 0 & 0 & 0 \\ 0 & 0 & 1.64 & 0 & 0 & 0 & 0 & 0 & 0 & -0.0857 \\ 0 & 0 & 0 & 1 & 0 & 0 & 0 & 0 & 0.0171 & 0 \\ 0 & 0 & 0 & 0 & 1.64 & 0 & -0.0857 & 0 & 0 & 0 \\ 0 & -0.0171 & 0 & 0 & 0 & 1 & 0 & 0 & 0 & 0 \\ 0.00325 & 0 & 0 & 0 & -0.00325 & 0 & 0.847 & 0 & 0 & 0 \\ 0 & 0 & 0 & 0 & 0 & 0 & 0 & 1.64 & 0 & -0.0857 \\ 0 & 0 & 0 & 0.0171 & 0 & 0 & 0 & 0 & 1 & 0 \\ 0 & 0 & -0.00325 & 0 & 0 & 0 & 0 & -0.00325 & 0 & 0.847 \end{pmatrix} \left(\begin{array}{c} \epsilon_{P,L} \\ \epsilon_{A,L} \\ \epsilon_{P,R} \\ \epsilon_{A,L} \\ \epsilon_{S,L} \\ \epsilon_{V,L} \\ \epsilon_{T_L} \\ \epsilon_{S,R} \\ \epsilon_{V,R} \\ \epsilon_{T_R} \end{array} \right)_{\Lambda_W}
 \end{aligned}$$

In the B and B_s meson decay, the reference scale is the b quark mass ($\Lambda_{m_b} \sim 4.18$ GeV). Thus, the evolution of the coefficients (ϵ^{eubd} and ϵ^{eubs}) is slightly smaller.

In fact, in eqn. (6.13), the part with the anomalous dimension that gives the matrix element in eqn. (F.1) is multiplied by a factor $\log(\frac{\Lambda_W}{\Lambda_{m_b}})/\log(\frac{\Lambda_W}{\Lambda_{exp}}) \sim 0.8$. Moreover, the strong coupling constant at Λ_{m_b} will also be smaller ($\alpha_s(\Lambda_{m_b}) \sim 0.23$ and $\alpha_s(\Lambda_{exp}) \sim 0.3$). Thus, for the B and B_s meson decays, the evolution of the coefficients (ϵ^{eubd} and ϵ^{eubs}) is given by :

$$\begin{aligned}
 & \text{(F.3)} \\
 & \left(\begin{array}{c} \epsilon_{P,L} \\ \epsilon_{A,L} \\ \epsilon_{P,R} \\ \epsilon_{A,R} \\ \epsilon_{S,L} \\ \epsilon_{V,L} \\ \epsilon_{T_L} \\ \epsilon_{S,R} \\ \epsilon_{V,R} \\ \epsilon_{T_R} \end{array} \right)_{\Lambda_{exp}} = \begin{pmatrix} 1.42 & 0 & 0 & 0 & 0 & 0 & -0.0317 & 0 & 0 & 0 \\ 0 & 1 & 0 & 0 & 0 & 0.00686 & 0 & 0 & 0 & 0 \\ 0 & 0 & 1.42 & 0 & 0 & 0 & 0 & 0 & 0 & 0.0317 \\ 0 & 0 & 0 & 1 & 0 & 0 & 0 & 0 & -0.00686 & 0 \\ 0 & 0 & 0 & 0 & 1.42 & 0 & 0.0317 & 0 & 0 & 0 \\ 0 & 0.00686 & 0 & 0 & 0 & 1 & 0 & 0 & 0 & 0 \\ -0.00126 & 0 & 0 & 0 & 0.00126 & 0 & 0.890 & 0 & 0 & 0 \\ 0 & 0 & 0 & 0 & 0 & 0 & 0 & 1.42 & 0 & 0.0317 \\ 0 & 0 & 0 & -0.00686 & 0 & 0 & 0 & 0 & 1 & 0 \\ 0 & 0 & 0.00126 & 0 & 0 & 0 & 0 & 0.00126 & 0 & 0.890 \end{pmatrix} \left(\begin{array}{c} \epsilon_{P,L} \\ \epsilon_{A,L} \\ \epsilon_{P,R} \\ \epsilon_{A,L} \\ \epsilon_{S,L} \\ \epsilon_{V,L} \\ \epsilon_{T_L} \\ \epsilon_{S,R} \\ \epsilon_{V,R} \\ \epsilon_{T_R} \end{array} \right)_{\Lambda_W}
 \end{aligned}$$



COVARIANCE MATRIX

In this section, we give details of the formalism introduced in section 6.4, eqn. (6.11). The matrices in the basis $(\epsilon_{P,L}, \epsilon_{A,L}, \epsilon_{P,R}, \epsilon_{A,R})$ and $(\epsilon_{S,L}, \epsilon_{V,L}, \epsilon_{T,L}, \epsilon_{S,R}, \epsilon_{V,R}, \epsilon_{T,R})$ are written :

$$(G.1) \quad M_2^{-1} = \frac{1}{BR_2^{exp}} \begin{bmatrix} SP'_+ & \frac{1}{2}SP_+VA'_+ & \frac{1}{2}SP_+SP'_- & \frac{1}{2}SP_+VA'_- \\ \frac{1}{2}SP_+VA'_+ & VA'_- & \frac{1}{2}SP_-VA'_+ & \frac{1}{2}VA_+VA'_- \\ \frac{1}{2}SP_+SP'_- & \frac{1}{2}SP_-VA'_+ & SP'_- & \frac{1}{2}SP_-VA'_- \\ \frac{1}{2}SP_+VA'_- & \frac{1}{2}VA_+VA'_- & \frac{1}{2}SP_-VA'_- & VA'_+ \end{bmatrix}$$

$$(G.2) \quad M_3^{-1} = \frac{1}{BR_3^{exp}} \begin{bmatrix} SP_+ & \frac{1}{2}SP_+VA_- & \frac{1}{2}SP_+T_+ & \frac{1}{2}SP_+SP_- & \frac{1}{2}SP_+VA_+ & \frac{1}{2}SP_+T_- \\ \frac{1}{2}SP_+VA_- & VA_- & \frac{1}{2}VA_-T_+ & \frac{1}{2}SP_-VA_- & \frac{1}{2}VA_+VA_- & \frac{1}{2}VA_-T_- \\ \frac{1}{2}SP_+T_+ & \frac{1}{2}VA_-T_+ & T_+ & \frac{1}{2}SP_-T_+ & \frac{1}{2}VA_+T_+ & \frac{1}{2}T_+T_- \\ \frac{1}{2}SP_+SP_- & \frac{1}{2}SP_-VA_- & \frac{1}{2}SP_-T_+ & SP_- & \frac{1}{2}SP_-VA_+ & \frac{1}{2}SP_-T_- \\ \frac{1}{2}SP_+VA_+ & \frac{1}{2}VA_+VA_- & \frac{1}{2}VA_+T_+ & \frac{1}{2}SP_-VA_+ & VA_+ & \frac{1}{2}VA_+T_- \\ \frac{1}{2}SP_+T_- & \frac{1}{2}VA_-T_- & \frac{1}{2}T_+T_- & \frac{1}{2}SP_-T_- & \frac{1}{2}VA_+T_- & T_- \end{bmatrix}$$

Inverting M_2^{-1} [M_3^{-1}] will give the bounds on the coefficients involved in the leptonic [semileptonic] decays. Finally, note that for semileptonic Kaon and D meson decays, the experimental upper limit are not the same for μ^+e^- and μ^-e^+ in the final state. In this case, we sum the M_3^{-1} for each bound and then invert it to obtain the covariance matrix of section 6.4. The matrix elements of eqn. (G.1) are written :

$$\begin{aligned}
 SP'_+ &= SP'_- = C_{2\text{body}} \tilde{P}'^2 (P_1^2 - m_i^2 - m_j^2) \\
 VA'_- &= VA'_+ = C_{2\text{body}} \tilde{A}'^2 [(P_1^2 - m_i^2 - m_j^2)(m_i^2 + m_j^2) + 4m_i^2 m_j^2] \\
 SP_+ VA'_- &= SP_- VA'_+ = -2C_{2\text{body}} \tilde{P}' \tilde{A}' m_j (P_1^2 + m_i^2 - m_j^2) \\
 SP_+ VA'_+ &= SP_- VA'_- = 2C_{2\text{body}} \tilde{P}' \tilde{A}' m_i (P_1^2 + m_j^2 - m_i^2) \\
 SP_+ SP'_- &= -4C_{2\text{body}} \tilde{P}'^2 m_j m_i \\
 VA_+ VA'_- &= -4C_{2\text{body}} \tilde{A}'^2 P_1^2 m_j m_i \\
 C_{2\text{body}} &= \frac{\tau_{P_1} r^* G_F^2}{\pi P_1^2}
 \end{aligned}
 \tag{G.3}$$

For simplicity we note $d\phi = \int_{(m_1+m_2)^2}^{(M-m_3)^2} dq^2 \int_{-1}^1 d\cos\theta \frac{\sqrt{\lambda(M^2, m_3^2, q^2)} \sqrt{\lambda(q^2, m_1^2, m_2^2)}}{q^2}$ and the matrix elements of eqn. (G.2) are written :

$$\begin{aligned}
 SP_+ &= SP_- = 2C_{3\text{body}} \tilde{S}^2 (p_1 \cdot p_2) d\phi \\
 VA_+ &= VA_- = \frac{1}{4} C_{3\text{body}} [f_+^2 (4(p_1 \cdot P)(p_2 \cdot P) - 2P^2(p_1 \cdot p_2)) + f_-^2 (4(p_1 \cdot q)(p_2 \cdot q) - 2q^2(p_1 \cdot p_2))] \\
 &\quad + 4f_+ f_- ((p_1 \cdot q)(p_2 \cdot P) + (p_1 \cdot P)(p_2 \cdot q) - (p_1 \cdot p_2)(P \cdot q)) d\phi \\
 T_+ &= T_- = 4C_{3\text{body}} \tilde{T}'^2 [4(p_1 \cdot q)(p_2 \cdot P)(P \cdot q) + 4(p_1 \cdot P)(p_2 \cdot q)(P \cdot q) - 2(p_1 \cdot p_2)(P \cdot q)^2 \\
 &\quad + 2P^2 q^2 (p_1 \cdot p_2) - 4P^2 (p_1 \cdot q)(p_2 \cdot q) - 4q^2 (p_1 \cdot P)(p_2 \cdot P)] d\phi \\
 SP_+ VA_- &= SP_- VA_+ = -2C_{3\text{body}} \tilde{S} m_2 [(f_+ (p_1 \cdot P) + f_- (p_1 \cdot q))] d\phi \\
 SP_+ VA_+ &= SP_- VA_- = 2C_{3\text{body}} \tilde{S} m_1 [(f_+ (p_2 \cdot P) + f_- (p_2 \cdot q))] d\phi \\
 SP_+ SP_- &= -4C_{3\text{body}} \tilde{S}^2 m_1 m_2 d\phi \\
 VA_+ VA_- &= -C_{3\text{body}} m_1 m_2 [f_-^2 q^2 + f_+^2 P^2 + 2f_+ f_- (P \cdot q)] d\phi \\
 T_+ T_- &= 16C_{3\text{body}} \tilde{T}'^2 m_1 m_2 [(P \cdot q)^2 - P^2 q^2] d\phi \\
 SP_+ T_+ &= SP_- T_- = 8C_{3\text{body}} \tilde{S} \tilde{T}' [(p_1 \cdot P)(p_2 \cdot q) - (p_1 \cdot q)(p_2 \cdot P)] d\phi \\
 SP_+ T_- &= SP_- T_+ = 0 \\
 VA_+ T_- &= VA_- T_+ = 4C_{3\text{body}} \tilde{T}' m_2 [f_+ ((p_1 \cdot q) p^2 - (P \cdot p_1)(P \cdot q)) + f_- ((p_1 \cdot q)(P \cdot q) - (p_1 \cdot P) q^2)] d\phi \\
 VA_+ T_+ &= VA_- T_- = 4C_{3\text{body}} \tilde{T}' m_1 [f_+ ((P^2)(p_2 \cdot q) - (p_2 \cdot P)(P \cdot q)) + f_- ((p_2 \cdot q)(P \cdot q) - (q^2)(p_2 \cdot P))] d\phi \\
 C_{3\text{body}} &= \frac{\tau_{P_1}}{\pi^3} \frac{8G_F^2}{512M^3}
 \end{aligned}
 \tag{G.4}$$



COVARIANCE MATRICES AT Λ_{exp} AND Λ_W

In this section, we give the covariance matrix at Λ_{exp} and at Λ_W , after the RGEs evolution.

Kaon decays

Using the upper limit of table 6.1, for the leptonic Kaon decay, we compute the associated covariance matrix in the basis $(\epsilon_{P,L}^{e\mu ds}, \epsilon_{A,L}^{e\mu ds}, \epsilon_{P,R}^{e\mu ds}, \epsilon_{A,R}^{e\mu ds})$:

$$\begin{pmatrix} 5.38 \times 10^{-14} & -2.33 \times 10^{-14} & -1.25 \times 10^{-15} & 1.26 \times 10^{-12} \\ -2.33 \times 10^{-14} & 2.97 \times 10^{-11} & 1.26 \times 10^{-12} & -4.03 \times 10^{-13} \\ -1.25 \times 10^{-15} & 1.26 \times 10^{-12} & 5.38 \times 10^{-14} & -2.33 \times 10^{-14} \\ 1.26 \times 10^{-12} & -4.03 \times 10^{-13} & -2.33 \times 10^{-14} & 2.97 \times 10^{-11} \end{pmatrix}$$

Then we use the bounds on semileptonic Kaon decay to compute the covariance matrix for the semileptonic decays in the basis $(\epsilon_{S,L}^{e\mu ds}, \epsilon_{V,L}^{e\mu ds}, \epsilon_{T,L}^{e\mu ds}, \epsilon_{S,R}^{e\mu ds}, \epsilon_{V,R}^{e\mu ds}, \epsilon_{T,R}^{e\mu ds})$:

$$\begin{pmatrix} 1.09 \times 10^{-12} & 3.51 \times 10^{-12} & 6.11 \times 10^{-12} & 1.39 \times 10^{-14} & 1.96 \times 10^{-13} & 7.49 \times 10^{-13} \\ 3.51 \times 10^{-12} & 2.44 \times 10^{-11} & 4.26 \times 10^{-11} & 1.96 \times 10^{-13} & 2.10 \times 10^{-12} & 6.50 \times 10^{-12} \\ 6.11 \times 10^{-12} & 4.26 \times 10^{-11} & 1.51 \times 10^{-10} & 7.49 \times 10^{-13} & 6.50 \times 10^{-12} & 1.58 \times 10^{-11} \\ 1.39 \times 10^{-14} & 1.96 \times 10^{-13} & 7.49 \times 10^{-13} & 1.09 \times 10^{-12} & 3.51 \times 10^{-12} & 6.11 \times 10^{-12} \\ 1.96 \times 10^{-13} & 2.10 \times 10^{-12} & 6.50 \times 10^{-12} & 3.51 \times 10^{-12} & 2.44 \times 10^{-11} & 4.26 \times 10^{-11} \\ 7.49 \times 10^{-13} & 6.50 \times 10^{-12} & 1.58 \times 10^{-11} & 6.11 \times 10^{-12} & 4.26 \times 10^{-11} & 1.51 \times 10^{-10} \end{pmatrix}$$

The diagonal elements give the bounds on $|\epsilon|^2$. The bounds on the coefficients are the square root of the diagonal elements. For instance, $\epsilon_{S,L}^{e\mu ds}$ is excluded above $\sqrt{1.09 \times 10^{-12}}$.

The covariance matrix in the basis $(\epsilon_{P,L}^{e\mu ds}, \epsilon_{A,L}^{e\mu ds}, \epsilon_{P,R}^{e\mu ds}, \epsilon_{A,R}^{e\mu ds}, \epsilon_{S,L}^{e\mu ds}, \epsilon_{V,L}^{e\mu ds}, \epsilon_{T_L}^{e\mu ds}, \epsilon_{S,R}^{e\mu ds}, \epsilon_{V,R}^{e\mu ds}, \epsilon_{T_R}^{e\mu ds})_{\Lambda_W}$ is :

$$\begin{pmatrix} 1.64 \times 10^{-13} & -2.55 \times 10^{-14} & -1.55 \times 10^{-14} & 7.73 \times 10^{-13} & -2.91 \times 10^{-14} & 1.31 \times 10^{-12} & 5.51 \times 10^{-12} & -9.15 \times 10^{-16} & 2.07 \times 10^{-13} & 5.75 \times 10^{-13} \\ -2.55 \times 10^{-14} & 2.97 \times 10^{-11} & 7.73 \times 10^{-13} & -4.03 \times 10^{-13} & -7.10 \times 10^{-15} & -4.64 \times 10^{-13} & -4.30 \times 10^{-13} & 7.35 \times 10^{-16} & -2.15 \times 10^{-14} & -6.72 \times 10^{-14} \\ -1.55 \times 10^{-14} & 7.73 \times 10^{-13} & 1.64 \times 10^{-13} & -2.55 \times 10^{-14} & 9.15 \times 10^{-16} & -2.07 \times 10^{-13} & -5.75 \times 10^{-13} & 2.91 \times 10^{-14} & -1.31 \times 10^{-12} & -5.51 \times 10^{-12} \\ 7.73 \times 10^{-13} & -4.03 \times 10^{-13} & -2.55 \times 10^{-14} & 2.97 \times 10^{-11} & -7.35 \times 10^{-16} & 2.15 \times 10^{-14} & 6.72 \times 10^{-14} & 7.10 \times 10^{-15} & 4.64 \times 10^{-13} & 4.30 \times 10^{-13} \\ -2.91 \times 10^{-14} & -7.10 \times 10^{-15} & 9.15 \times 10^{-16} & -7.35 \times 10^{-16} & 3.22 \times 10^{-13} & 8.29 \times 10^{-13} & -1.11 \times 10^{-12} & -8.03 \times 10^{-15} & -8.12 \times 10^{-14} & -3.49 \times 10^{-14} \\ 1.31 \times 10^{-12} & -4.64 \times 10^{-13} & -2.07 \times 10^{-13} & 2.15 \times 10^{-14} & 8.29 \times 10^{-13} & 2.44 \times 10^{-11} & 5.02 \times 10^{-11} & -8.12 \times 10^{-14} & 2.10 \times 10^{-12} & 7.66 \times 10^{-12} \\ 5.51 \times 10^{-12} & -4.30 \times 10^{-13} & -5.75 \times 10^{-13} & 6.72 \times 10^{-14} & -1.11 \times 10^{-12} & 5.02 \times 10^{-11} & 2.10 \times 10^{-10} & -3.49 \times 10^{-14} & 7.66 \times 10^{-12} & 2.19 \times 10^{-11} \\ -9.15 \times 10^{-16} & 7.35 \times 10^{-16} & 2.91 \times 10^{-14} & 7.10 \times 10^{-15} & -8.03 \times 10^{-15} & -8.12 \times 10^{-14} & -3.49 \times 10^{-14} & 3.22 \times 10^{-13} & 8.29 \times 10^{-13} & -1.11 \times 10^{-12} \\ 2.07 \times 10^{-13} & -2.15 \times 10^{-14} & -1.31 \times 10^{-12} & 4.64 \times 10^{-13} & -8.12 \times 10^{-14} & 2.10 \times 10^{-12} & 7.66 \times 10^{-12} & 8.29 \times 10^{-13} & 2.44 \times 10^{-11} & 5.02 \times 10^{-11} \\ 5.75 \times 10^{-13} & -6.72 \times 10^{-14} & -5.51 \times 10^{-12} & 4.30 \times 10^{-13} & -3.49 \times 10^{-14} & 7.66 \times 10^{-12} & 2.19 \times 10^{-11} & -1.11 \times 10^{-12} & 5.02 \times 10^{-11} & 2.10 \times 10^{-10} \end{pmatrix}$$

D meson meson decays

The bounds of table 6.1 on leptonic D meson decay give the following covariance matrix in the basis $(\epsilon_{P,L}^{e\mu cu}, \epsilon_{A,L}^{e\mu cu}, \epsilon_{P,R}^{e\mu cu}, \epsilon_{A,R}^{e\mu cu})$:

$$\begin{pmatrix} 3.07 \times 10^{-6} & -3.55 \times 10^{-7} & -2.86 \times 10^{-8} & 7.91 \times 10^{-5} \\ -3.55 \times 10^{-7} & 2.04 \times 10^{-3} & 7.91 \times 10^{-5} & 7.30 \times 10^{-7} \\ -2.86 \times 10^{-8} & 7.91 \times 10^{-5} & 3.07 \times 10^{-6} & -3.55 \times 10^{-7} \\ 7.91 \times 10^{-5} & 7.30 \times 10^{-7} & -3.55 \times 10^{-7} & 2.04 \times 10^{-3} \end{pmatrix}$$

Using bounds on the semileptonic decay of D and D_s meson give in the basis $(\epsilon_{S,L}^{e\mu cu}, \epsilon_{V,L}^{e\mu cu}, \epsilon_{T_L}^{e\mu cu}, \epsilon_{S,R}^{e\mu cu}, \epsilon_{V,R}^{e\mu cu}, \epsilon_{T_R}^{e\mu cu})$:

$$\begin{pmatrix} 1.80 \times 10^{-6} & 1.32 \times 10^{-7} & -3.19 \times 10^{-8} & -2.10 \times 10^{-8} & -1.61 \times 10^{-7} & 1.79 \times 10^{-8} \\ 1.32 \times 10^{-7} & 2.10 \times 10^{-6} & 3.65 \times 10^{-7} & -1.61 \times 10^{-7} & 9.7 \times 10^{-8} & 7.06 \times 10^{-7} \\ -3.19 \times 10^{-8} & 3.65 \times 10^{-7} & 4.03 \times 10^{-6} & 1.79 \times 10^{-8} & 7.06 \times 10^{-7} & 2.30 \times 10^{-7} \\ -2.10 \times 10^{-8} & -1.61 \times 10^{-7} & 1.79 \times 10^{-8} & 1.80 \times 10^{-6} & 1.32 \times 10^{-7} & -3.19 \times 10^{-8} \\ -1.61 \times 10^{-7} & 9.7 \times 10^{-8} & 7.06 \times 10^{-7} & 1.32 \times 10^{-7} & 2.10 \times 10^{-6} & 3.65 \times 10^{-7} \\ 1.79 \times 10^{-8} & 7.06 \times 10^{-7} & 2.30 \times 10^{-7} & -3.19 \times 10^{-8} & 3.65 \times 10^{-7} & 4.03 \times 10^{-6} \end{pmatrix}$$

The covariance matrix in the basis $(\epsilon_{P,L}^{e\mu cu}, \epsilon_{A,L}^{e\mu cu}, \epsilon_{P,R}^{e\mu cu}, \epsilon_{A,R}^{e\mu cu}, \epsilon_{S,L}^{e\mu cu}, \epsilon_{V,L}^{e\mu cu}, \epsilon_{T_L}^{e\mu cu}, \epsilon_{S,R}^{e\mu cu}, \epsilon_{V,R}^{e\mu cu}, \epsilon_{T_R}^{e\mu cu})_{\Lambda_W}$ is :

$$\begin{pmatrix} 1.15 \times 10^{-6} & -2.16 \times 10^{-7} & -1.15 \times 10^{-8} & 4.81 \times 10^{-5} & -1.45 \times 10^{-8} & -2.62 \times 10^{-8} & -2.97 \times 10^{-7} & -1.55 \times 10^{-9} & -8.69 \times 10^{-7} & -1.68 \times 10^{-8} \\ -2.16 \times 10^{-7} & 2.04 \times 10^{-3} & 4.81 \times 10^{-5} & 7.31 \times 10^{-7} & 1.81 \times 10^{-9} & 3.50 \times 10^{-5} & 8.22 \times 10^{-9} & 8.70 \times 10^{-9} & -1.09 \times 10^{-8} & 1.99 \times 10^{-7} \\ -1.15 \times 10^{-8} & 4.81 \times 10^{-5} & 1.15 \times 10^{-6} & -2.16 \times 10^{-7} & 1.55 \times 10^{-9} & 8.69 \times 10^{-7} & 1.68 \times 10^{-8} & 1.45 \times 10^{-8} & 2.62 \times 10^{-8} & 2.97 \times 10^{-7} \\ 4.81 \times 10^{-5} & 7.31 \times 10^{-7} & -2.16 \times 10^{-7} & 2.04 \times 10^{-3} & -8.70 \times 10^{-9} & 1.09 \times 10^{-8} & -1.99 \times 10^{-7} & -1.81 \times 10^{-9} & -3.50 \times 10^{-5} & -8.22 \times 10^{-9} \\ -1.45 \times 10^{-8} & 1.81 \times 10^{-9} & 1.55 \times 10^{-9} & -8.70 \times 10^{-9} & 6.80 \times 10^{-7} & 1.03 \times 10^{-7} & 2.73 \times 10^{-7} & -5.58 \times 10^{-9} & -5.42 \times 10^{-8} & 2.96 \times 10^{-8} \\ -2.62 \times 10^{-8} & 3.50 \times 10^{-5} & 8.69 \times 10^{-7} & 1.09 \times 10^{-8} & 1.03 \times 10^{-7} & 2.70 \times 10^{-6} & 4.31 \times 10^{-7} & -5.42 \times 10^{-8} & 9.66 \times 10^{-8} & 8.36 \times 10^{-7} \\ -2.97 \times 10^{-7} & 8.22 \times 10^{-9} & 1.68 \times 10^{-8} & -1.99 \times 10^{-7} & 2.73 \times 10^{-7} & 4.31 \times 10^{-7} & 5.62 \times 10^{-6} & 2.96 \times 10^{-8} & 8.36 \times 10^{-7} & 3.21 \times 10^{-7} \\ -1.55 \times 10^{-9} & 8.70 \times 10^{-9} & 1.45 \times 10^{-8} & -1.81 \times 10^{-9} & -5.58 \times 10^{-9} & -5.42 \times 10^{-8} & 2.96 \times 10^{-8} & 6.80 \times 10^{-7} & 1.03 \times 10^{-7} & 2.73 \times 10^{-7} \\ -8.69 \times 10^{-7} & -1.09 \times 10^{-8} & 2.62 \times 10^{-8} & -3.50 \times 10^{-5} & -5.42 \times 10^{-8} & 9.66 \times 10^{-8} & 8.36 \times 10^{-7} & 1.03 \times 10^{-7} & 2.70 \times 10^{-6} & 4.31 \times 10^{-7} \\ -1.68 \times 10^{-8} & 1.99 \times 10^{-7} & 2.97 \times 10^{-7} & -8.22 \times 10^{-9} & 2.96 \times 10^{-8} & 8.36 \times 10^{-7} & 3.21 \times 10^{-7} & 2.73 \times 10^{-7} & 4.31 \times 10^{-7} & 5.62 \times 10^{-6} \end{pmatrix}$$

B meson decays

The bound on the leptonic decay of the B meson (see table 6.1) gives the following covariance matrix in the basis $(\epsilon_{P,L}^{e\mu bd}, \epsilon_{A,L}^{e\mu bd}, \epsilon_{P,R}^{e\mu bd}, \epsilon_{A,R}^{e\mu bd})$:

$$\begin{pmatrix} 5.53 \times 10^{-8} & 9.23 \times 10^{-8} & 1.20 \times 10^{-9} & 3.48 \times 10^{-6} \\ 9.23 \times 10^{-8} & 2.20 \times 10^{-4} & 3.48 \times 10^{-6} & 6.89 \times 10^{-6} \\ 1.20 \times 10^{-9} & 3.48 \times 10^{-6} & 5.53 \times 10^{-8} & 9.23 \times 10^{-8} \\ 3.48 \times 10^{-6} & 6.89 \times 10^{-6} & 9.23 \times 10^{-8} & 2.20 \times 10^{-4} \end{pmatrix}$$

The covariance matrix in the basis $(\epsilon_{S,L}^{e\mu bd}, \epsilon_{V,L}^{e\mu bd}, \epsilon_{T_L}^{e\mu bd}, \epsilon_{S,R}^{e\mu bd}, \epsilon_{V,R}^{e\mu bd}, \epsilon_{T_R}^{e\mu bd})$ is:

$$\begin{pmatrix} 2.07 \times 10^{-10} & 1.21 \times 10^{-11} & 1.52 \times 10^{-12} & -3.90 \times 10^{-15} & -5.74 \times 10^{-14} & 5.18 \times 10^{-15} \\ 1.21 \times 10^{-11} & 2.23 \times 10^{-10} & 2.81 \times 10^{-11} & -5.74 \times 10^{-14} & 2.87 \times 10^{-14} & 2.32 \times 10^{-13} \\ 1.52 \times 10^{-12} & 2.81 \times 10^{-11} & 4.03 \times 10^{-10} & 5.18 \times 10^{-15} & 2.32 \times 10^{-13} & 3.50 \times 10^{-14} \\ -3.90 \times 10^{-15} & -5.74 \times 10^{-14} & 5.18 \times 10^{-15} & 2.07 \times 10^{-10} & 1.21 \times 10^{-11} & 1.52 \times 10^{-12} \\ -5.74 \times 10^{-14} & 2.87 \times 10^{-14} & 2.32 \times 10^{-13} & 1.21 \times 10^{-11} & 2.23 \times 10^{-10} & 2.81 \times 10^{-11} \\ 5.18 \times 10^{-15} & 2.32 \times 10^{-13} & 3.50 \times 10^{-14} & 1.52 \times 10^{-12} & 2.81 \times 10^{-11} & 4.03 \times 10^{-10} \end{pmatrix}$$

The covariance matrix in the basis $(\epsilon_{P,L}^{e\mu bd}, \epsilon_{A,L}^{e\mu bd}, \epsilon_{P,R}^{e\mu bd}, \epsilon_{A,R}^{e\mu bd}, \epsilon_{S,L}^{e\mu bd}, \epsilon_{V,L}^{e\mu bd}, \epsilon_{T_L}^{e\mu bd}, \epsilon_{S,R}^{e\mu bd}, \epsilon_{V,R}^{e\mu bd}, \epsilon_{T_R}^{e\mu bd})_{\Lambda_W}$ is:

$$\begin{pmatrix} 2.74 \times 10^{-8} & 6.51 \times 10^{-8} & 5.94 \times 10^{-10} & 2.45 \times 10^{-6} & -1.10 \times 10^{-12} & -4.46 \times 10^{-10} & 5.02 \times 10^{-11} & 1.89 \times 10^{-14} & 1.68 \times 10^{-8} & -8.41 \times 10^{-13} \\ 6.51 \times 10^{-8} & 2.20 \times 10^{-4} & 2.45 \times 10^{-6} & 6.89 \times 10^{-6} & -2.11 \times 10^{-12} & -1.51 \times 10^{-6} & 9.19 \times 10^{-11} & 7.76 \times 10^{-11} & 4.73 \times 10^{-8} & -3.47 \times 10^{-9} \\ 5.94 \times 10^{-10} & 2.45 \times 10^{-6} & 2.74 \times 10^{-8} & 6.51 \times 10^{-8} & -1.89 \times 10^{-14} & -1.68 \times 10^{-8} & 8.41 \times 10^{-13} & 1.10 \times 10^{-12} & 4.46 \times 10^{-10} & -5.02 \times 10^{-11} \\ 2.45 \times 10^{-6} & 6.89 \times 10^{-6} & 6.51 \times 10^{-8} & 2.20 \times 10^{-4} & -7.76 \times 10^{-11} & -4.73 \times 10^{-8} & 3.47 \times 10^{-9} & 2.11 \times 10^{-12} & 1.51 \times 10^{-6} & -9.19 \times 10^{-11} \\ -1.10 \times 10^{-12} & -2.11 \times 10^{-12} & -1.89 \times 10^{-14} & -7.76 \times 10^{-11} & 1.03 \times 10^{-10} & 7.83 \times 10^{-12} & -1.03 \times 10^{-11} & -2.10 \times 10^{-15} & -5.78 \times 10^{-13} & 3.15 \times 10^{-15} \\ -4.46 \times 10^{-10} & -1.51 \times 10^{-6} & -1.68 \times 10^{-8} & -4.73 \times 10^{-8} & 7.83 \times 10^{-12} & 1.06 \times 10^{-8} & 3.09 \times 10^{-11} & -5.78 \times 10^{-13} & -3.24 \times 10^{-10} & 2.41 \times 10^{-11} \\ 5.02 \times 10^{-11} & 9.19 \times 10^{-11} & 8.41 \times 10^{-13} & 3.47 \times 10^{-9} & -1.03 \times 10^{-11} & 3.09 \times 10^{-11} & 5.10 \times 10^{-10} & 3.15 \times 10^{-15} & 2.41 \times 10^{-11} & 4.30 \times 10^{-14} \\ 1.89 \times 10^{-14} & 7.76 \times 10^{-11} & 1.10 \times 10^{-12} & 2.11 \times 10^{-12} & -2.10 \times 10^{-15} & -5.78 \times 10^{-13} & 3.15 \times 10^{-15} & 1.03 \times 10^{-10} & 7.83 \times 10^{-12} & -1.03 \times 10^{-11} \\ 1.68 \times 10^{-8} & 4.73 \times 10^{-8} & 4.46 \times 10^{-10} & 1.51 \times 10^{-6} & -5.78 \times 10^{-13} & -3.24 \times 10^{-10} & 2.41 \times 10^{-11} & 7.83 \times 10^{-12} & 1.06 \times 10^{-8} & 3.09 \times 10^{-11} \\ -8.41 \times 10^{-13} & -3.47 \times 10^{-9} & -5.02 \times 10^{-11} & -9.19 \times 10^{-11} & 3.15 \times 10^{-15} & 2.41 \times 10^{-11} & 4.30 \times 10^{-14} & -1.03 \times 10^{-11} & 3.09 \times 10^{-11} & 5.10 \times 10^{-10} \end{pmatrix}$$

Bs meson

The bound on the leptonic decay of the B_s meson gives in the basis $(\epsilon_{P,L}^{e\mu bs}, \epsilon_{A,L}^{e\mu bs}, \epsilon_{P,R}^{e\mu bs}, \epsilon_{A,R}^{e\mu bs})$:

$$\begin{pmatrix} 3.06 \times 10^{-8} & -1.22 \times 10^{-8} & -3.40 \times 10^{-10} & 1.94 \times 10^{-6} \\ -1.22 \times 10^{-8} & 1.24 \times 10^{-4} & 1.94 \times 10^{-6} & -1.80 \times 10^{-7} \\ -3.40 \times 10^{-10} & 1.94 \times 10^{-6} & 3.06 \times 10^{-8} & -1.22 \times 10^{-8} \\ 1.94 \times 10^{-6} & -1.80 \times 10^{-7} & -1.22 \times 10^{-8} & 1.24 \times 10^{-4} \end{pmatrix}$$

The bound on the B_s meson decaying into Kaon (table 6.1) gives in the basis $(\epsilon_{S,L}^{e\mu bs}, \epsilon_{V,L}^{e\mu bs}, \epsilon_{T,L}^{e\mu bs}, \epsilon_{S,R}^{e\mu bs}, \epsilon_{V,R}^{e\mu bs}, \epsilon_{T,R}^{e\mu bs})$:

$$\begin{pmatrix} 5.05 \times 10^{-10} & 3.47 \times 10^{-11} & 5.07 \times 10^{-12} & -1.13 \times 10^{-14} & -1.65 \times 10^{-13} & 1.73 \times 10^{-14} \\ 3.47 \times 10^{-11} & 6.53 \times 10^{-10} & 9.54 \times 10^{-11} & -1.65 \times 10^{-13} & 8.78 \times 10^{-14} & 7.90 \times 10^{-13} \\ 5.07 \times 10^{-12} & 9.54 \times 10^{-11} & 1.51 \times 10^{-9} & 1.73 \times 10^{-14} & 7.90 \times 10^{-13} & 1.38 \times 10^{-13} \\ -1.13 \times 10^{-14} & -1.65 \times 10^{-13} & 1.73 \times 10^{-14} & 5.05 \times 10^{-10} & 3.47 \times 10^{-11} & 5.07 \times 10^{-12} \\ -1.65 \times 10^{-13} & 8.78 \times 10^{-14} & 7.90 \times 10^{-13} & 3.47 \times 10^{-11} & 6.53 \times 10^{-10} & 9.54 \times 10^{-11} \\ 1.73 \times 10^{-14} & 7.90 \times 10^{-13} & 1.38 \times 10^{-13} & 5.07 \times 10^{-12} & 9.54 \times 10^{-11} & 1.51 \times 10^{-9} \end{pmatrix}$$

The covariance matrix in the basis $(\epsilon_{P,L}^{e\mu bs}, \epsilon_{A,L}^{e\mu bs}, \epsilon_{P,R}^{e\mu bs}, \epsilon_{A,R}^{e\mu bs}, \epsilon_{S,L}^{e\mu bs}, \epsilon_{V,L}^{e\mu bs}, \epsilon_{T,L}^{e\mu bs}, \epsilon_{S,R}^{e\mu bs}, \epsilon_{V,R}^{e\mu bs}, \epsilon_{T,R}^{e\mu bs})_{\Lambda_W}$ is :

$$\begin{pmatrix} 1.52 \times 10^{-8} & -8.62 \times 10^{-9} & -1.69 \times 10^{-10} & 1.37 \times 10^{-6} & -1.35 \times 10^{-12} & 6.16 \times 10^{-11} & 6.41 \times 10^{-11} & -5.11 \times 10^{-15} & 9.39 \times 10^{-9} & 2.42 \times 10^{-13} \\ -8.62 \times 10^{-9} & 1.24 \times 10^{-4} & 1.37 \times 10^{-6} & -1.80 \times 10^{-7} & 1.21 \times 10^{-13} & -8.51 \times 10^{-7} & -1.29 \times 10^{-11} & 4.33 \times 10^{-11} & -1.24 \times 10^{-9} & -1.94 \times 10^{-9} \\ -1.69 \times 10^{-10} & 1.37 \times 10^{-6} & 1.52 \times 10^{-8} & -8.62 \times 10^{-9} & 5.11 \times 10^{-15} & -9.39 \times 10^{-9} & -2.42 \times 10^{-13} & 1.35 \times 10^{-12} & -6.16 \times 10^{-11} & -6.41 \times 10^{-11} \\ 1.37 \times 10^{-6} & -1.80 \times 10^{-7} & -8.62 \times 10^{-9} & 1.24 \times 10^{-4} & -4.33 \times 10^{-11} & 1.24 \times 10^{-9} & 1.94 \times 10^{-9} & -1.21 \times 10^{-13} & 8.51 \times 10^{-7} & 1.29 \times 10^{-11} \\ -1.35 \times 10^{-12} & 1.21 \times 10^{-13} & 5.11 \times 10^{-15} & -4.33 \times 10^{-11} & 2.51 \times 10^{-10} & 2.21 \times 10^{-11} & -3.90 \times 10^{-11} & -6.11 \times 10^{-15} & -4.33 \times 10^{-13} & 9.78 \times 10^{-15} \\ 6.16 \times 10^{-11} & -8.51 \times 10^{-7} & -9.39 \times 10^{-9} & 1.24 \times 10^{-9} & 2.21 \times 10^{-11} & 6.49 \times 10^{-9} & 1.07 \times 10^{-10} & -4.33 \times 10^{-13} & 8.57 \times 10^{-12} & 1.42 \times 10^{-11} \\ 6.41 \times 10^{-11} & -1.29 \times 10^{-11} & -2.42 \times 10^{-13} & 1.94 \times 10^{-9} & -3.90 \times 10^{-11} & 1.07 \times 10^{-10} & 1.91 \times 10^{-9} & 9.78 \times 10^{-15} & 1.42 \times 10^{-11} & 1.74 \times 10^{-13} \\ -5.11 \times 10^{-15} & 4.33 \times 10^{-11} & 1.35 \times 10^{-12} & -1.21 \times 10^{-13} & -6.11 \times 10^{-15} & -4.33 \times 10^{-13} & 9.78 \times 10^{-15} & 2.51 \times 10^{-10} & 2.21 \times 10^{-11} & -3.90 \times 10^{-11} \\ 9.39 \times 10^{-9} & -1.24 \times 10^{-9} & -6.16 \times 10^{-11} & 8.51 \times 10^{-7} & -4.33 \times 10^{-13} & 8.57 \times 10^{-12} & 1.42 \times 10^{-11} & 2.21 \times 10^{-11} & 6.49 \times 10^{-9} & 1.07 \times 10^{-10} \\ 2.42 \times 10^{-13} & -1.94 \times 10^{-9} & -6.41 \times 10^{-11} & 1.29 \times 10^{-11} & 9.78 \times 10^{-15} & 1.42 \times 10^{-11} & 1.74 \times 10^{-13} & -3.90 \times 10^{-11} & 1.07 \times 10^{-10} & 1.91 \times 10^{-9} \end{pmatrix}$$

BIBLIOGRAPHY

- [1] Sacha Davidson, Yoshitaka Kuno, and Albert Saporta.
Spin-dependent $\mu \rightarrow e$ conversion on light nuclei.
Eur. Phys. J., C78(2):109, 2018.
- [2] Sacha Davidson and Albert Saporta.
Constraints on $2\ell 2q$ operators from $\mu - e$ flavour-changing meson decays.
Phys. Rev., D99(1):015032, 2019.
- [3] S. L. Glashow.
Partial Symmetries of Weak Interactions.
Nucl. Phys., 22:579–588, 1961.
- [4] Steven Weinberg.
A Model of Leptons.
Phys. Rev. Lett., 19:1264–1266, 1967.
- [5] Abdus Salam.
Weak and Electromagnetic Interactions.
Conf. Proc., C680519:367–377, 1968.
- [6] Georges Aad et al.
Observation of a new particle in the search for the Standard Model Higgs boson with the ATLAS detector at the LHC.
Phys. Lett., B716:1–29, 2012.
- [7] Serguei Chatrchyan et al.
Observation of a new boson at a mass of 125 GeV with the CMS experiment at the LHC.
Phys. Lett., B716:30–61, 2012.
- [8] Yoshitaka Kuno and Yasuhiro Okada.
Muon decay and physics beyond the standard model.
Rev. Mod. Phys., 73:151–202, 2001.
- [9] Lorenzo Calibbi and Giovanni Signorelli.
Charged Lepton Flavour Violation: An Experimental and Theoretical Introduction.

- Riv. Nuovo Cim.*, 41(2):1, 2018.
- [10] A. M. Baldini et al.
Search for the lepton flavour violating decay $\mu^+ \rightarrow e^+ \gamma$ with the full dataset of the MEG experiment.
Eur. Phys. J., C76(8):434, 2016.
- [11] Wilhelm H. Bertl et al.
Search for the Decay $\mu^+ \rightarrow e^+ e^+ e^-$.
Nucl. Phys., B260:1–31, 1985.
- [12] Ann-Kathrin Perrevoort.
Status of the Mu3e Experiment at PSI.
EPJ Web Conf., 118:01028, 2016.
- [13] Wilhelm H. Bertl et al.
A Search for muon to electron conversion in muonic gold.
Eur. Phys. J., C47:337–346, 2006.
- [14] Yoshitaka Kuno.
A search for muon-to-electron conversion at J-PARC: The COMET experiment.
PTEP, 2013:022C01, 2013.
- [15] R. M. Carey et al.
Proposal to search for $\mu^- N \rightarrow e^- N$ with a single event sensitivity below 10^{-16} .
2008.
- [16] R. Appel et al.
Search for lepton flavor violation in K^+ decays.
Phys. Rev. Lett., 85:2877–2880, 2000.
- [17] Roel Aaij et al.
Search for the lepton-flavour violating decay $D^0 \rightarrow e^\pm \mu^\mp$.
Phys. Lett., B754:167–175, 2016.
- [18] J. P. Lees et al.
Searches for Rare or Forbidden Semileptonic Charm Decays.
Phys. Rev., D84:072006, 2011.
- [19] Bernard Aubert et al.
Search for the rare decay $B \rightarrow \pi l^+ l^-$.
Phys. Rev. Lett., 99:051801, 2007.

- [20] Gary Steigman.
Primordial Nucleosynthesis in the Precision Cosmology Era.
Ann. Rev. Nucl. Part. Sci., 57:463–491, 2007.
- [21] Richard H. Cyburt, Brian D. Fields, Keith A. Olive, and Evan Skillman.
New BBN limits on physics beyond the standard model from ${}^4\text{He}$.
Astropart. Phys., 23:313–323, 2005.
- [22] Gary Steigman.
Primordial nucleosynthesis: successes and challenges.
Int. J. Mod. Phys., E15:1–36, 2006.
- [23] G. Hinshaw et al.
Nine-Year Wilkinson Microwave Anisotropy Probe (WMAP) Observations: Cosmological
Parameter Results.
Astrophys. J. Suppl., 208:19, 2013.
- [24] P. A. R. Ade et al.
Planck 2015 results. XIII. Cosmological parameters.
Astron. Astrophys., 594:A13, 2016.
- [25] N. Aghanim et al.
Planck 2018 results. VI. Cosmological parameters.
2018.
- [26] Motohiko Yoshimura.
Unified Gauge Theories and the Baryon Number of the Universe.
Phys. Rev. Lett., 41:281–284, 1978.
[Erratum: *Phys. Rev. Lett.* 42,746(1979)].
- [27] Antonio Riotto and Mark Trodden.
Recent progress in baryogenesis.
Ann. Rev. Nucl. Part. Sci., 49:35–75, 1999.
- [28] Ian Affleck and Michael Dine.
A New Mechanism for Baryogenesis.
Nucl. Phys., B249:361–380, 1985.
- [29] A. Yu. Ignatiev, N. V. Krasnikov, V. A. Kuzmin, and A. N. Tavkhelidze.
Universal CP Noninvariant Superweak Interaction and Baryon Asymmetry of the Uni-
verse.
Phys. Lett., 76B:436–438, 1978.

BIBLIOGRAPHY

- [30] A. D. Sakharov.
Violation of CP Invariance, C asymmetry, and baryon asymmetry of the universe.
Pisma Zh. Eksp. Teor. Fiz., 5:32–35, 1967.
[Usp. Fiz. Nauk161,no.5,61(1991)].
- [31] J.H. Oort.
The force exerted by the stellar system in the direction perpendicular to the galactic plane
and some related problems.
Bull. Astron. Inst. Netherlands bf 6 ., page 249 33, 1932.
- [32] F. Zwicky.
Die Rotverschiebung von extragalaktischen Nebeln.
Helv. Phys. Acta, 6:110–127, 1933.
[Gen. Rel. Grav.41,207(2009)].
- [33] Yoshiaki Sofue and Vera Rubin.
Rotation curves of spiral galaxies.
Ann. Rev. Astron. Astrophys., 39:137–174, 2001.
- [34] Vera C. Rubin and W. Kent Ford, Jr.
Rotation of the Andromeda Nebula from a Spectroscopic Survey of Emission Regions.
Astrophys. J., 159:379–403, 1970.
- [35] K. G. Begeman, A. H. Broeils, and R. H. Sanders.
Extended rotation curves of spiral galaxies: Dark haloes and modified dynamics.
Mon. Not. Roy. Astron. Soc., 249:523, 1991.
- [36] Q. R. Ahmad et al.
Direct evidence for neutrino flavor transformation from neutral current interactions in the
Sudbury Neutrino Observatory.
Phys. Rev. Lett., 89:011301, 2002.
- [37] Y. Fukuda et al.
Evidence for oscillation of atmospheric neutrinos.
Phys. Rev. Lett., 81:1562–1567, 1998.
- [38] M. Tanabashi et al.
Review of Particle Physics.
Phys. Rev., D98(3):030001, 2018.
- [39] B. Pontecorvo.
Mesonium and anti-mesonium.
Sov. Phys. JETP, 6:429, 1957.

- [Zh. Eksp. Teor. Fiz.33,549(1957)].
- [40] Ziro Maki, Masami Nakagawa, and Shoichi Sakata.
Remarks on the unified model of elementary particles.
Prog. Theor. Phys., 28:870–880, 1962.
[,34(1962)].
- [41] B. Pontecorvo.
Inverse beta processes and nonconservation of lepton charge.
Sov. Phys. JETP, 7:172–173, 1958.
[Zh. Eksp. Teor. Fiz.34,247(1957)].
- [42] B. Pontecorvo.
Neutrino Experiments and the Problem of Conservation of Leptonic Charge.
Sov. Phys. JETP, 26:984–988, 1968.
[Zh. Eksp. Teor. Fiz.53,1717(1967)].
- [43] Samoil M. Bilenky, J. Hosek, and S. T. Petcov.
On Oscillations of Neutrinos with Dirac and Majorana Masses.
Phys. Lett., 94B:495–498, 1980.
- [44] J. Schechter and J. W. F. Valle.
Neutrino Masses in $SU(2) \times U(1)$ Theories.
Phys. Rev., D22:2227, 1980.
- [45] M. Doi, T. Kotani, H. Nishiura, K. Okuda, and E. Takasugi.
CP Violation in Majorana Neutrinos.
Phys. Lett., 102B:323–326, 1981.
- [46] Samoil M. Bilenky and S. T. Petcov.
Massive Neutrinos and Neutrino Oscillations.
Rev. Mod. Phys., 59:671, 1987.
[Erratum: *Rev. Mod. Phys.*60,575(1988)].
- [47] H. V. Klapdor-Kleingrothaus et al.
Latest results from the Heidelberg-Moscow double beta decay experiment.
Eur. Phys. J., A12:147–154, 2001.
- [48] Gregg B. Franklin.
The KATRIN Neutrino Mass Measurement: Experiment, Status, and Outlook.
In *13th Conference on the Intersections of Particle and Nuclear Physics (CIPANP 2018)*
Palm Springs, California, USA, May 29-June 3, 2018, 2018.

- [49] Roel Aaij et al.
Test of lepton universality using $B^+ \rightarrow K^+ \ell^+ \ell^-$ decays.
Phys. Rev. Lett., 113:151601, 2014.
- [50] R. Aaij et al.
Test of lepton universality with $B^0 \rightarrow K^{*0} \ell^+ \ell^-$ decays.
JHEP, 08:055, 2017.
- [51] Y. Amhis et al.
Averages of b -hadron, c -hadron, and τ -lepton properties as of summer 2016.
Eur. Phys. J., C77(12):895, 2017.
- [52] R. Aaij et al.
Measurement of the ratio of branching fractions $\mathcal{B}(B_c^+ \rightarrow J/\psi \tau^+ \nu_\tau)/\mathcal{B}(B_c^+ \rightarrow J/\psi \mu^+ \nu_\mu)$.
Phys. Rev. Lett., 120(12):121801, 2018.
- [53] J. P. Lees et al.
Evidence for an excess of $\bar{B} \rightarrow D^{(*)} \tau^- \bar{\nu}_\tau$ decays.
Phys. Rev. Lett., 109:101802, 2012.
- [54] M. Huschle et al.
Measurement of the branching ratio of $\bar{B} \rightarrow D^{(*)} \tau^- \bar{\nu}_\tau$ relative to $\bar{B} \rightarrow D^{(*)} \ell^- \bar{\nu}_\ell$ decays with hadronic tagging at Belle.
Phys. Rev., D92(7):072014, 2015.
- [55] Roel Aaij et al.
Measurement of the ratio of branching fractions $\mathcal{B}(\bar{B}^0 \rightarrow D^{*+} \tau^- \bar{\nu}_\tau)/\mathcal{B}(\bar{B}^0 \rightarrow D^{*+} \mu^- \bar{\nu}_\mu)$.
Phys. Rev. Lett., 115(11):111803, 2015.
[Erratum: *Phys. Rev. Lett.* 115, no. 15, 159901 (2015)].
- [56] Wolfgang Altmannshofer, Peter Stangl, and David M. Straub.
Interpreting Hints for Lepton Flavor Universality Violation.
Phys. Rev., D96(5):055008, 2017.
- [57] Guido D'Amico, Marco Nardecchia, Paolo Panci, Francesco Sannino, Alessandro Strumia, Riccardo Torre, and Alfredo Urbano.
Flavour anomalies after the R_{K^*} measurement.
JHEP, 09:010, 2017.
- [58] Gudrun Hiller and Ivan Nisandzic.
 R_K and R_{K^*} beyond the standard model.
Phys. Rev., D96(3):035003, 2017.

-
- [59] Li-Sheng Geng, Benjamín Grinstein, Sebastian Jäger, Jorge Martin Camalich, Xiu-Lei Ren, and Rui-Xiang Shi.
Towards the discovery of new physics with lepton-universality ratios of $b \rightarrow s\ell\ell$ decays.
Phys. Rev., D96(9):093006, 2017.
- [60] T. Hurth, F. Mahmoudi, D. Martinez Santos, and S. Neshatpour.
Lepton nonuniversality in exclusive $b \rightarrow s\ell\ell$ decays.
Phys. Rev., D96(9):095034, 2017.
- [61] Marco Ciuchini, Antonio M. Coutinho, Marco Fedele, Enrico Franco, Ayan Paul, Luca Silvestrini, and Mauro Valli.
On Flavourful Easter eggs for New Physics hunger and Lepton Flavour Universality violation.
Eur. Phys. J., C77(10):688, 2017.
- [62] D. V. Volkov and V. P. Akulov.
Is the Neutrino a Goldstone Particle?
Phys. Lett., 46B:109–110, 1973.
- [63] J. Wess and B. Zumino.
Supergauge Transformations in Four-Dimensions.
Nucl. Phys., B70:39–50, 1974.
[,24(1974)].
- [64] Yu. A. Golfand and E. P. Likhtman.
Extension of the Algebra of Poincare Group Generators and Violation of p Invariance.
JETP Lett., 13:323–326, 1971.
[Pisma Zh. Eksp. Teor. Fiz.13,452(1971)].
- [65] Jean-Loup Gervais and B. Sakita.
Field Theory Interpretation of Supergauges in Dual Models.
Nucl. Phys., B34:632–639, 1971.
[,154(1971)].
- [66] Glennys R. Farrar and Pierre Fayet.
Phenomenology of the Production, Decay, and Detection of New Hadronic States Associated with Supersymmetry.
Phys. Lett., 76B:575–579, 1978.
- [67] Peter Minkowski.
 $\mu \rightarrow e\gamma$ at a Rate of One Out of 10^9 Muon Decays?
Phys. Lett., 67B:421–428, 1977.

BIBLIOGRAPHY

- [68] Rabindra N. Mohapatra and Goran Senjanovic.
Neutrino Mass and Spontaneous Parity Nonconservation.
Phys. Rev. Lett., 44:912, 1980.
[,231(1979)].
- [69] Murray Gell-Mann, Pierre Ramond, and Richard Slansky.
Complex Spinors and Unified Theories.
Conf. Proc., C790927:315–321, 1979.
- [70] Tsutomu Yanagida.
Horizontal Symmetry and Masses of Neutrinos.
Prog. Theor. Phys., 64:1103, 1980.
- [71] Marco Drewes.
The Phenomenology of Right Handed Neutrinos.
Int. J. Mod. Phys., E22:1330019, 2013.
- [72] Thomas Appelquist, Hsin-Chia Cheng, and Bogdan A. Dobrescu.
Bounds on universal extra dimensions.
Phys. Rev., D64:035002, 2001.
- [73] Theodor Kaluza.
Zum Unitätsproblem der Physik.
Sitzungsber. Preuss. Akad. Wiss. Berlin (Math. Phys.), 1921:966–972, 1921.
- [74] Oskar Klein.
Quantentheorie und fünfdimensionale relativitätstheorie.
Zeitschrift für Physik A Hadrons and Nuclei, 37:895–906, 12 1926.
- [75] Geraldine Servant and Timothy M. P. Tait.
Is the lightest Kaluza-Klein particle a viable dark matter candidate?
Nucl. Phys., B650:391–419, 2003.
- [76] Juichi Saito.
Relics From the Early Kaluza-Klein Universe.
Prog. Theor. Phys., 77:322, 1987.
- [77] Edward W. Kolb and Richard Slansky.
Dimensional Reduction in the Early Universe: Where Have the Massive Particles Gone?
Phys. Lett., 135B:378, 1984.
- [78] JoAnne L. Hewett and Thomas G. Rizzo.
Much ado about leptoquarks: A Comprehensive analysis.
Phys. Rev., D56:5709–5724, 1997.

-
- [79] Jogesh C. Pati and Abdus Salam.
Lepton Number as the Fourth Color.
Phys. Rev., D10:275–289, 1974.
[Erratum: *Phys. Rev.*D11,703(1975)].
- [80] Jogesh C. Pati and Abdus Salam.
Is Baryon Number Conserved?
Phys. Rev. Lett., 31:661–664, 1973.
- [81] Jogesh C. Pati and Abdus Salam.
Unified Lepton-Hadron Symmetry and a Gauge Theory of the Basic Interactions.
Phys. Rev., D8:1240–1251, 1973.
- [82] Graham G. Ross.
GRAND UNIFIED THEORIES.
1985.
- [83] W. Buchmuller and D. Wyler.
Constraints on SU(5) Type Leptoquarks.
Phys. Lett., B177:377–382, 1986.
- [84] Goran Senjanovic and Aleksandar Sokorac.
Light Leptoquarks in SO(10).
Z. Phys., C20:255, 1983.
- [85] Paul H. Frampton and Bum-Hoon Lee.
SU(15) GRAND UNIFICATION.
Phys. Rev. Lett., 64:619, 1990.
- [86] Paul H. Frampton and Thomas W. Kephart.
Higgs sector and proton decay in su(15) grand unification.
Phys. Rev. D, 42:3892–3894, Dec 1990.
- [87] Paul H. Frampton.
Light leptoquarks as possible signature of strong electroweak unification.
Mod. Phys. Lett., A7:559–562, 1992.
- [88] H. Murayama and T. Yanagida.
A viable SU(5) GUT with light leptoquark bosons.
Mod. Phys. Lett., A7:147–152, 1992.
- [89] JoAnne L. Hewett and Thomas G. Rizzo.
Don't stop thinking about leptoquarks: Constructing new models.
Phys. Rev., D58:055005, 1998.

BIBLIOGRAPHY

- [90] S. S. Gershtein, A. A. Likhoded, and A. I. Onishchenko.
TeV-scale leptoquarks from GUTs/string/M-theory unification.
Phys. Rept., 320:159–173, 1999.
- [91] Ilja Dorsner and Pavel Fileviez Perez.
Unification without supersymmetry: Neutrino mass, proton decay and light leptoquarks.
Nucl. Phys., B723:53–76, 2005.
- [92] Edward Farhi and Leonard Susskind.
Technicolor.
Phys. Rept., 74:277, 1981.
- [93] E. Eichten, I. Hinchliffe, Kenneth D. Lane, and C. Quigg.
Super Collider Physics.
Rev. Mod. Phys., 56:579–707, 1984.
[Addendum: *Rev. Mod. Phys.* 58,1065(1986)].
- [94] Savas Dimopoulos and Leonard Susskind.
Mass Without Scalars.
Nucl. Phys., B155:237–252, 1979.
[2,930(1979)].
- [95] Savas Dimopoulos.
Technicolored Signatures.
Nucl. Phys., B168:69–92, 1980.
- [96] Howard Georgi and Sheldon L. Glashow.
Unextended hypercolor and unification.
Phys. Rev. Lett., 47:1511–1513, Nov 1981.
- [97] W. Buchmuller.
Composite Quarks and Leptons.
Acta Phys. Austriaca Suppl., 27:517–595, 1985.
- [98] Barbara Schrempp and Fridger Schrempp.
A Confining SU(2)-l X SU(2)-r Gauge Model of the Weak Interactions.
Nucl. Phys., B231:109–138, 1984.
- [99] L. F. Abbott and E. Farhi.
Are the Weak Interactions Strong?
Phys. Lett., 101B:69–72, 1981.
- [100] L. F. Abbott and E. Farhi.

- A Confining Model of the Weak Interactions.
Nucl. Phys., B189:547–556, 1981.
- [101] Jogesh C. Pati.
 A Model for a Unification of Scales: From $M(\text{planck})$ to $M(\nu)$.
Phys. Lett., B228:228–234, 1989.
- [102] Barbara Schrempp and Fridger Schrempp.
 LIGHT LEPTOQUARKS.
Phys. Lett., 153B:101–107, 1985.
- [103] José Wudka.
 Composite leptoquarks.
Physics Letters B, 167(3):337–342, feb 1986.
- [104] Damir Beirevi, Svjetlana Fajfer, Nejc Konik, and Olcyr Sumensari.
 Leptoquark model to explain the B -physics anomalies, R_K and R_D .
Phys. Rev., D94(11):115021, 2016.
- [105] Andreas Crivellin, Dario Müller, and Toshihiko Ota.
 Simultaneous explanation of $R(D^0)$ and bs^+ : the last scalar leptoquarks standing.
JHEP, 09:040, 2017.
- [106] Uma Mahanta.
 Implications of BNL measurement of $\delta a(\mu)$ on a class of scalar leptoquark interactions.
Eur. Phys. J., C21:171–173, 2001.
- [107] King-man Cheung.
 Muon anomalous magnetic moment and leptoquark solutions.
Phys. Rev., D64:033001, 2001.
- [108] Andreas Crivellin, Dario Müller, Adrian Signer, and Yannick Ulrich.
 Correlating lepton flavor universality violation in B decays with $\mu \rightarrow e\gamma$ using leptoquarks.
Phys. Rev., D97(1):015019, 2018.
- [109] Damir Beirevi and Olcyr Sumensari.
 A leptoquark model to accommodate $R_K^{\text{exp}} < R_K^{\text{SM}}$ and $R_{K^*}^{\text{exp}} < R_{K^*}^{\text{SM}}$.
JHEP, 08:104, 2017.
- [110] Damir Beirevi, Nejc Konik, Olcyr Sumensari, and Renata Zukanovich Funchal.
 Palatable Leptoquark Scenarios for Lepton Flavor Violation in Exclusive $b \rightarrow s\ell_1\ell_2$ modes.
JHEP, 11:035, 2016.

- [111] Ivo de Medeiros Varzielas and Gudrun Hiller.
Clues for flavor from rare lepton and quark decays.
JHEP, 06:072, 2015.
- [112] I. Dorner, S. Fajfer, A. Greljo, J. F. Kamenik, and N. Konik.
Physics of leptoquarks in precision experiments and at particle colliders.
Phys. Rept., 641:1–68, 2016.
- [113] S. T. Petcov.
The Processes $\mu \rightarrow e \gamma$, $\mu \rightarrow e e \text{ anti-}e$, Neutrino' \rightarrow Neutrino gamma in the
Weinberg-Salam Model with Neutrino Mixing.
Sov. J. Nucl. Phys., 25:340, 1977.
[Erratum: *Yad. Fiz.*25,1336(1977)].
- [114] Samoil M. Bilenky, S. T. Petcov, and B. Pontecorvo.
Lepton Mixing, $\mu \rightarrow e + \gamma$ Decay and Neutrino Oscillations.
Phys. Lett., 67B:309, 1977.
- [115] A. Abada, C. Biggio, F. Bonnet, M. B. Gavela, and T. Hambye.
Low energy effects of neutrino masses.
JHEP, 12:061, 2007.
- [116] S. Antusch, C. Biggio, E. Fernandez-Martinez, M. B. Gavela, and J. Lopez-Pavon.
Unitarity of the Leptonic Mixing Matrix.
JHEP, 10:084, 2006.
- [117] Robert H. Bernstein and Peter S. Cooper.
Charged Lepton Flavor Violation: An Experimenter's Guide.
Phys. Rept., 532:27–64, 2013.
- [118] P. Depommier et al.
New limit on the decay $\mu^+ \rightarrow e^+ \gamma$.
Phys. Rev. Lett., 39:1113–1116, Oct 1977.
- [119] A. van der Schaaf, R. Engfer, H.P. Povel, W. Dey, H.K. Walter, and C. Petitjean.
A search for the decay $\mu^+ \rightarrow e^+ \gamma$.
Nuclear Physics A, 340(2):249 – 270, 1980.
- [120] W. W. Kinnison et al.
A Search for $\mu^+ \rightarrow e^+ \gamma$.
Phys. Rev., D25:2846, 1982.
- [121] R. D. Bolton et al.

- Search for rare muon decays with the crystal box detector.
Phys. Rev. D, 38:2077–2101, Oct 1988.
- [122] M. L. Brooks et al.
New limit for the family number nonconserving decay $\mu^+ \rightarrow e^+ \gamma$.
Phys. Rev. Lett., 83:1521–1524, 1999.
- [123] A. M. Baldini et al.
Search for the lepton flavour violating decay $\mu^+ \rightarrow e^+ \gamma$ with the full dataset of the MEG experiment.
Eur. Phys. J., C76(8):434, 2016.
- [124] A. M. Baldini et al.
MEG Upgrade Proposal.
2013.
- [125] A. M. Baldini et al.
The design of the MEG II experiment.
Eur. Phys. J., C78(5):380, 2018.
- [126] S. M. Korenchenko, B. F. Kostin, Guenakh Mitselmakher, K. G. Nekrasov, and V. S. Smirnov.
Search for $\mu^+ \rightarrow e^+ e^+ e^-$ Decay.
Sov. Phys. JETP, 43:1, 1976.
[Zh. Eksp. Teor. Fiz.70,3(1976)].
- [127] R. D. Bolton et al.
Search for the muon-number-nonconserving decay $\mu \rightarrow e^+ e^+ e^-$.
Phys. Rev. Lett., 53:1415–1418, Oct 1984.
- [128] W. Bertl et al.
A new upper limit for the decay $\mu^+ \rightarrow e^+ e^+ e^-$.
Physics Letters B, 140(5):299 – 303, 1984.
- [129] U. Bellgardt et al.
Search for the decay $\mu^+ \rightarrow e^+ e^+ e^-$.
Nuclear Physics B, 299(1):1 – 6, 1988.
- [130] V. A. Baranov et al.
Search for $\mu^+ \rightarrow e^+ e^+ e^-$ decay.
Sov. J. Nucl. Phys., 53:802–807, 1991.
[Yad. Fiz.53,1302(1991)].
- [131] A. Blondel et al.

- Research Proposal for an Experiment to Search for the Decay $\mu \rightarrow eee$.
2013.
- [132] D. A. Bryman, M. Blecher, K. Gotow, and R. J. Powers.
Search for the reaction $\mu^- \rightarrow e^+ \nu_e$.
Phys. Rev. Lett., 28:1469–1471, 1972.
- [133] A. Badertscher et al.
Upper limit for muon-electron conversion in sulfur.
Phys. Rev. Lett., 39:1385–1387, Nov 1977.
- [134] A. Badertscher et al.
A search for muon-electron and muon-positron conversion in sulfur.
Nuclear Physics A, 377(2):406 – 440, 1982.
- [135] S. Ahmad et al.
Search for muon-electron and muon-positron conversion.
Phys. Rev. D, 38:2102–2120, Oct 1988.
- [136] C. Dohmen et al.
Test of lepton-flavour conservation in $\mu \rightarrow e$ conversion on titanium.
Physics Letters B, 317(4):631 – 636, 1993.
- [137] W. Honecker et al.
Improved limit on the branching ratio of $\mu \rightarrow e$ conversion on lead.
Phys. Rev. Lett., 76:200–203, Jan 1996.
- [138] Y. Kuno et al.
An Experimental Search for a $\mu - N \rightarrow e - N$ Conversion at Sensitivity of the Order of 10^{-18}
with a Highly Intense Muon Source: PRISM.
2006.
- [139] Truong Minh Nguyen.
Search for $\mu \rightarrow e$ conversion with DeeMe experiment at J-PARC MLF.
PoS, FPCP2015:060, 2015.
- [140] A. Badertscher et al.
Search for $\mu^- \rightarrow e^+$ conversion on sulfur.
Physics Letters B, 79(4):371 – 375, 1978.
- [141] A. and others Badertscher.
New upper limits for muon-electron conversion in sulfur.
Lettere al Nuovo Cimento (1971-1985), 28(12):401–408, Jul 1980.

- [142] J. Kaulard et al.
Improved limit on the branching ratio of $\mu^- \rightarrow e^+$ conversion on titanium.
Physics Letters B, 422(1):334 – 338, 1998.
- [143] J. Schechter and J. W. F. Valle.
Neutrinoless Double beta Decay in SU(2) x U(1) Theories.
Phys. Rev., D25:2951, 1982.
- [144] S. Ahmed et al.
Update of the search for the neutrinoless decay $\bar{\tau} \mu \gamma$.
Phys. Rev. D, 61:071101, Mar 2000.
- [145] Bernard Aubert et al.
The BaBar detector.
Nucl. Instrum. Meth., A479:1–116, 2002.
- [146] A. Abashian et al.
The Belle Detector.
Nucl. Instrum. Meth., A479:117–232, 2002.
- [147] Roel Aaij et al.
Search for the lepton flavour violating decay $\tau^- \rightarrow \mu^- \mu^+ \mu^-$.
JHEP, 02:121, 2015.
- [148] R Aaij et al.
Searches for violation of lepton flavour and baryon number in tau lepton decays at LHCb.
Phys. Lett., B724:36–45, 2013.
- [149] Georges Aad et al.
Probing lepton flavour violation via neutrinoless $\tau \rightarrow 3\mu$ decays with the ATLAS detector.
Eur. Phys. J., C76(5):232, 2016.
- [150] Bernard Aubert et al.
Searches for Lepton Flavor Violation in the Decays $\tau_{+-} \rightarrow e_{+-} \gamma$ and $\tau_{+-} \rightarrow \mu_{+-} \gamma$.
Phys. Rev. Lett., 104:021802, 2010.
- [151] K. Hayasaka et al.
Search for Lepton Flavor Violating Tau Decays into Three Leptons with 719 Million Produced Tau+Tau- Pairs.
Phys. Lett., B687:139–143, 2010.
- [152] K. Hayasaka et al.

BIBLIOGRAPHY

- New Search for $\tau \rightarrow \mu \gamma$ and $\tau \rightarrow e \gamma$ Decays at Belle.
Phys. Lett., B666:16–22, 2008.
- [153] J. P. Lees et al.
Limits on tau Lepton-Flavor Violating Decays in three charged leptons.
Phys. Rev., D81:111101, 2010.
- [154] Y. Miyazaki et al.
Search for lepton flavor violating tau- decays into l- eta, l- eta-prime and l- pi0.
Phys. Lett., B648:341–350, 2007.
- [155] Bernard Aubert et al.
Search for Lepton Flavor Violating Decays $\tau^\pm \rightarrow \ell^\pm \pi^0, \ell^\pm \eta, \ell^\pm \eta'$.
Phys. Rev. Lett., 98:061803, 2007.
- [156] Y. Miyazaki et al.
Search for Lepton Flavor Violating tau- Decays into l-K0s and l-K0sK0s.
Phys. Lett., B692:4–9, 2010.
- [157] Y. Miyazaki et al.
Search for Lepton-Flavor-Violating tau Decays into a Lepton and a Vector Meson.
Phys. Lett., B699:251–257, 2011.
- [158] Y. Nishio et al.
Search for lepton-flavor-violating tau \rightarrow l V0 decays at Belle.
Phys. Lett., B664:35–40, 2008.
- [159] Bernard Aubert et al.
Search for Lepton Flavor Violating Decays tau \rightarrow l- K0(s) with the BABAR Experiment.
Phys. Rev., D79:012004, 2009.
- [160] Bernard Aubert et al.
Improved limits on lepton flavor violating tau decays to l phi, l rho, l K* and l anti-K*.
Phys. Rev. Lett., 103:021801, 2009.
- [161] T. Aushev et al.
Physics at Super B Factory.
2010.
- [162] J. Bennett.
Belle II Physics Prospects, Status and Schedule.
J. Phys. Conf. Ser., 770(1):012044, 2016.

- [163] J. Z. Bai et al.
The BES detector.
Nucl. Instrum. Meth., A344:319–334, 1994.
- [164] J. Z. Bai et al.
The BES upgrade.
Nucl. Instrum. Meth., A458:627–637, 2001.
- [165] M. Ablikim et al.
Design and Construction of the BESIII Detector.
Nucl. Instrum. Meth., A614:345–399, 2010.
- [166] M. N. Achasov et al.
Spherical neutral detector for VEPP-2M collider.
Nucl. Instrum. Meth., A449:125–139, 2000.
- [167] G. Viehhauser.
CLEO III operation.
Nucl. Instrum. Meth., A462:146–151, 2001.
- [168] K. Lang et al.
A Straw drift chamber spectrometer for studies of rare kaon decays.
Nucl. Instrum. Meth., A522:274–293, 2004.
- [169] A. Augusto Alves, Jr. et al.
The LHCb Detector at the LHC.
JINST, 3:S08005, 2008.
- [170] M. N. Achasov et al.
Search for Lepton Flavor Violation Process $e^+e^- \rightarrow e\mu$ in the Energy Region $\sqrt{s} = 984 - 1060$ MeV and $\phi \rightarrow e\mu$ Decay.
Phys. Rev., D81:057102, 2010.
- [171] M. Ablikim et al.
Search for the lepton flavor violation process $J/\psi \rightarrow e\mu$ at BESIII.
Phys. Rev., D87:112007, 2013.
- [172] M. Ablikim et al.
Search for the lepton flavor violation processes $J/\psi \rightarrow \mu\tau$ and $e\tau$.
Phys. Lett., B598:172–177, 2004.
- [173] W. Love et al.
Search for Lepton Flavor Violation in Upsilon Decays.
Phys. Rev. Lett., 101:201601, 2008.

- [174] D. Ambrose et al, BNL E871 Collaboration.
New Limit on Muon and Electron Lepton Number Violation from $K_L^0 \rightarrow \mu^\pm e^\mp$ Decay.
Phys. Rev. Lett., 81:5734–5737, Dec 1998.
- [175] R.Aaij, LHCb Collaboration.
Search for the lepton-flavor-violating decays $B_s^0 \rightarrow e^\pm \mu^\mp$ and $B^0 \rightarrow e^\pm \mu^\mp$.
Phys. Rev. Lett., 111:141801, Sep 2013.
- [176] Bernard Aubert et al.
Searches for the decays $B^0 \rightarrow l^\pm \tau^\mp$ and $B^+ \rightarrow l^+ \nu$ ($l=e, \mu$) using hadronic tag reconstruction.
Phys. Rev., D77:091104, 2008.
- [177] Bernard Aubert et al.
Measurements of branching fractions, rate asymmetries, and angular distributions in the rare decays $B \rightarrow K \ell^+ \ell^-$ and $B \rightarrow K^* \ell^+ \ell^-$.
Phys. Rev., D73:092001, 2006.
- [178] J. P. Lees et al.
A search for the decay modes $B^{+-} \rightarrow h^{+-} \tau^{+-} l$.
Phys. Rev., D86:012004, 2012.
- [179] P. Abreu et al.
Search for lepton flavor number violating Z0 decays.
Z. Phys., C73:243–251, 1997.
- [180] Shankha Banerjee, Biplob Bhattacharjee, Manimala Mitra, and Michael Spannowsky.
The Lepton Flavour Violating Higgs Decays at the HL-LHC and the ILC.
JHEP, 07:059, 2016.
- [181] Steven Weinberg.
Phenomenological lagrangians.
Physica A: Statistical Mechanics and its Applications, 96(1):327 – 340, 1979.
- [182] W. Buchmuller and D. Wyler.
Effective Lagrangian Analysis of New Interactions and Flavor Conservation.
Nucl. Phys., B268:621–653, 1986.
- [183] Chung Ngoc Leung, S. T. Love, and S. Rao.
Low-Energy Manifestations of a New Interaction Scale: Operator Analysis.
Z. Phys., C31:433, 1986.
- [184] Thomas Appelquist and J. Carazzone.
Infrared Singularities and Massive Fields.
Phys. Rev., D11:2856, 1975.

-
- [185] Murray Gell-Mann and F. E. Low.
Quantum electrodynamics at small distances.
Phys. Rev., 95:1300–1312, 1954.
- [186] L. V. Ovsyannikov.
General solution to the renormalization group equations.
Dokl. Akad. Nauk Ser. Fiz., 109:1112–1114, 1956.
[76(1956)].
- [187] K. Symanzik.
Small distance behavior in field theory and power counting.
Commun. Math. Phys., 18:227–246, 1970.
- [188] Curtis G. Callan, Jr.
Broken scale invariance in scalar field theory.
Phys. Rev., D2:1541–1547, 1970.
- [189] Gerard 't Hooft.
Dimensional regularization and the renormalization group.
Nucl. Phys., B61:455–468, 1973.
- [190] Steven Weinberg.
New approach to the renormalization group.
Phys. Rev., D8:3497–3509, 1973.
- [191] Andreas Petermann.
La normalisation des constantes dans la théorie des quanta
Normalization of constants in
the quanta theory.
Helv. Phys. Acta, 26:499–520, 1953.
- [192] J. F. Ashmore.
A Method of Gauge Invariant Regularization.
Lett. Nuovo Cim., 4:289–290, 1972.
- [193] G. M. Cicuta and E. Montaldi.
Analytic renormalization via continuous space dimension.
Lett. Nuovo Cim., 4:329–332, 1972.
- [194] C. G. Bollini and J. J. Giambiagi.
Lowest order divergent graphs in n -dimensional space.
Phys. Lett., 40B:566–568, 1972.
- [195] C. G. Bollini and J. J. Giambiagi.

- Dimensional Renormalization: The Number of Dimensions as a Regularizing Parameter.
Nuovo Cim., B12:20–26, 1972.
- [196] Gerard 't Hooft and M. J. G. Veltman.
Regularization and Renormalization of Gauge Fields.
Nucl. Phys., B44:189–213, 1972.
- [197] Gerard 't Hooft and M. J. G. Veltman.
Combinatorics of gauge fields.
Nucl. Phys., B50:318–353, 1972.
- [198] William A. Bardeen, A. J. Buras, D. W. Duke, and T. Muta.
Deep Inelastic Scattering Beyond the Leading Order in Asymptotically Free Gauge Theories.
Phys. Rev., D18:3998, 1978.
- [199] T. Kinoshita.
Mass singularities of Feynman amplitudes.
J. Math. Phys., 3:650–677, 1962.
- [200] T. D. Lee and M. Nauenberg.
Degenerate Systems and Mass Singularities.
Phys. Rev., 133:B1549–B1562, 1964.
[,25(1964)].
- [201] D. J. Gross.
Applications of the Renormalization Group to High-Energy Physics.
Conf. Proc., C7507281:141–250, 1975.
- [202] C. Dohmen et al.
Test of lepton flavor conservation in $\mu \rightarrow e$ conversion on titanium.
Phys. Lett., B317:631–636, 1993.
- [203] S. Weinberg and G. Feinberg.
Electromagnetic Transitions Between μ Meson and Electron.
Phys. Rev. Lett., 3:111–114, 1959.
- [204] Oruganti U. Shanker.
 Z Dependence of Coherent μe Conversion Rate in Anomalous Neutrinoless Muon Capture.
Phys. Rev., D20:1608, 1979.
- [205] Andrzej Czarnecki, William J. Marciano, and Kirill Melnikov.
Coherent muon electron conversion in muonic atoms.
AIP Conf. Proc., 435(1):409–418, 1998.

-
- [206] Vincenzo Cirigliano, Ryuichiro Kitano, Yasuhiro Okada, and Paula Tuzon.
On the model discriminating power of $\mu \rightarrow e$ conversion in nuclei.
Phys. Rev., D80:013002, 2009.
- [207] Ryuichiro Kitano, Masafumi Koike, and Yasuhiro Okada.
Detailed calculation of lepton flavor violating muon electron conversion rate for various nuclei.
Phys. Rev., D66:096002, 2002.
[Erratum: *Phys. Rev.*D76,059902(2007)].
- [208] T. S. Kosmas, G. K. Leontaris, and J. D. Vergados.
Lepton flavor nonconservation.
Prog. Part. Nucl. Phys., 33:397–448, 1994.
- [209] H. C. Chiang, E. Oset, T. S. Kosmas, A. Faessler, and J. D. Vergados.
Coherent and incoherent (μ -, e -) conversion in nuclei.
Nucl. Phys., A559:526–542, 1993.
- [210] Vincenzo Cirigliano, Sacha Davidson, and Yoshitaka Kuno.
Spin-dependent $\mu \rightarrow e$ conversion.
Phys. Lett., B771:242–246, 2017.
- [211] Sacha Davidson.
 $\mu \rightarrow e\gamma$ and matching at m_W .
Eur. Phys. J., C76(7):370, 2016.
- [212] Andreas Crivellin, Sacha Davidson, Giovanni Marco Pruna, and Adrian Signer.
Renormalisation-group improved analysis of $\mu \rightarrow e$ processes in a systematic effective-field-theory approach.
JHEP, 05:117, 2017.
- [213] Andreas Crivellin, Francesco D’Eramo, and Massimiliano Procura.
New Constraints on Dark Matter Effective Theories from Standard Model Loops.
Phys. Rev. Lett., 112:191304, 2014.
- [214] Ulrich Haisch and Felix Kahlhoefer.
On the importance of loop-induced spin-independent interactions for dark matter direct detection.
JCAP, 1304:050, 2013.
- [215] Antonio Pich.
Effective field theory: Course.

- In *Probing the standard model of particle interactions. Proceedings, Summer School in Theoretical Physics, NATO Advanced Study Institute, 68th session, Les Houches, France, July 28-September 5, 1997. Pt. 1, 2*, pages 949–1049, 1998.
- [216] R. Machleidt and D. R. Entem.
Chiral effective field theory and nuclear forces.
Phys. Rept., 503:1–75, 2011.
- [217] P. Klos, J. Menéndez, D. Gazit, and A. Schwenk.
Large-scale nuclear structure calculations for spin-dependent WIMP scattering with chiral effective field theory currents.
Phys. Rev., D88(8):083516, 2013.
[Erratum: *Phys. Rev.*D89,no.2,029901(2014)].
- [218] Vincenzo Cirigliano, Michael L. Graesser, and Grigory Ovanessian.
WIMP-nucleus scattering in chiral effective theory.
JHEP, 10:025, 2012.
- [219] Martin Hoferichter, Philipp Klos, and Achim Schwenk.
Chiral power counting of one- and two-body currents in direct detection of dark matter.
Phys. Lett., B746:410–416, 2015.
- [220] Andreas Crivellin, Martin Hoferichter, and Massimiliano Procura.
Accurate evaluation of hadronic uncertainties in spin-independent WIMP-nucleon scattering: Disentangling two- and three-flavor effects.
Phys. Rev., D89:054021, 2014.
- [221] Vincenzo Cirigliano, Wouter Dekens, Emanuele Mereghetti, and André Walker-Loud.
Neutrinoless double- decay in effective field theory: The light-Majorana neutrino-exchange mechanism.
Phys. Rev., C97(6):065501, 2018.
- [222] Anthony Bartolotta and Michael J. Ramsey-Musolf.
Coherent $\mu - e$ conversion at next-to-leading order.
Phys. Rev., C98(1):015208, 2018.
- [223] J. Engel, S. Pittel, and P. Vogel.
Nuclear physics of dark matter detection.
Int. J. Mod. Phys., E1:1–37, 1992.
- [224] A. Liam Fitzpatrick, Wick Haxton, Emanuel Katz, Nicholas Lubbers, and Yiming Xu.
The Effective Field Theory of Dark Matter Direct Detection.
JCAP, 1302:004, 2013.

- [225] J. Engel, M. T. Ressel, I. S. Towner, and W. E. Ormand.
Response of mica to weakly interacting massive particles.
Phys. Rev., C52:2216–2221, 1995.
- [226] Michael E. Peskin and Daniel V. Schroeder.
An Introduction to quantum field theory.
Addison-Wesley, Reading, USA, 1995.
- [227] James D. Bjorken and Sidney D. Drell.
Relativistic quantum fields.
1965.
- [228] M. E. Rose.
Relativistic electron theory.
American Journal of Physics, 29(12):866–866, 1961.
- [229] C. Itzykson and J. B. Zuber.
Quantum Field Theory.
International Series In Pure and Applied Physics. McGraw-Hill, New York, 1980.
- [230] H. De Vries, C. W. De Jager, and C. De Vries.
Nuclear charge and magnetization density distribution parameters from elastic electron scattering.
Atom. Data Nucl. Data Tabl., 36:495–536, 1987.
- [231] Marco Cirelli, Eugenio Del Nobile, and Paolo Panci.
Tools for model-independent bounds in direct dark matter searches.
JCAP, 1310:019, 2013.
- [232] T. Suzuki, David F. Measday, and J. P. Roalsvig.
Total Nuclear Capture Rates for Negative Muons.
Phys. Rev., C35:2212, 1987.
- [233] V. A. Bednyakov and F. Simkovic.
Nuclear spin structure in dark matter search: The Zero momentum transfer limit.
Phys. Part. Nucl., 36:131–152, 2005.
[Fiz. Elem. Chast. Atom. Yadra36,257(2005)].
- [234] V. A. Bednyakov and F. Simkovic.
Nuclear spin structure in dark matter search: The Finite momentum transfer limit.
Phys. Part. Nucl., 37:S106–S128, 2006.
- [235] K.J.R. Rosman.
Pure Appl.Chem., 71,1593-1607, 1999.

- [236] J. Engel and P. Vogel.
Phys. Rev. D **40**:3132–3135, 1989.
- [237] Gary Prezeau, Andriy Kurylov, Marc Kamionkowski, and Petr Vogel.
New contribution to wimp-nucleus scattering.
Phys. Rev. Lett., **91**:231301, 2003.
- [238] C. Körber, A. Nogga, and J. de Vries.
First-principle calculations of Dark Matter scattering off light nuclei.
Phys. Rev., **C96**(3):035805, 2017.
- [239] Francesco Romeo.
Search for leptoquark-like signatures with the ATLAS and CMS detectors.
Nucl. Part. Phys. Proc., **273-275**:638–643, 2016.
- [240] Vardan Khachatryan et al.
Search for pair production of first and second generation leptoquarks in proton-proton collisions at $\sqrt{s} = 8\text{TeV}$.
Phys. Rev., **D93**(3):032004, 2016.
- [241] Georges Aad et al.
Searches for scalar leptoquarks in pp collisions at $\sqrt{s} = 8\text{ TeV}$ with the ATLAS detector.
Eur. Phys. J., **C76**(1):5, 2016.
- [242] S. Bellucci, Maurizio Lusignoli, and L. Maiani.
Leading Logarithmic Corrections to the Weak Leptonic and Semileptonic Low-energy Hamiltonian.
Nucl. Phys., **B189**:329–346, 1981.
- [243] Gerhard Buchalla, Andrzej J. Buras, and Michaela K. Harlander.
The Anatomy of Epsilon-prime / Epsilon in the Standard Model.
Nucl. Phys., **B337**:313–362, 1990.
- [244] Vardan Khachatryan et al.
Search for heavy Majorana neutrinos in $e^\pm e^\pm + \text{jets}$ and $e^\pm \mu^\pm + \text{jets}$ events in proton-proton collisions at $\sqrt{s} = 8\text{ TeV}$.
JHEP, **04**:169, 2016.
- [245] Georges Aad et al.
Search for heavy Majorana neutrinos with the ATLAS detector in pp collisions at $\sqrt{s} = 8\text{ TeV}$.
JHEP, **07**:162, 2015.

-
- [246] Ernesto Arganda, Ana M. Curiel, Maria J. Herrero, and David Temes.
Lepton flavor violating Higgs boson decays from massive seesaw neutrinos.
Phys. Rev., D71:035011, 2005.
- [247] M. Raidal et al.
Flavour physics of leptons and dipole moments.
Eur. Phys. J., C57:13–182, 2008.
- [248] Yoshitaka Kuno.
A search for muon-to-electron conversion at J-PARC: The COMET experiment.
PTEP, 2013:022C01, 2013.
- [249] R. M. Carey et al.
Proposal to search for $\mu^- N \rightarrow e^- N$ with a single event sensitivity below 10^{-16} .
2008.
- [250] Roel Aaij et al.
Search for the lepton-flavour violating decay $D^0 \rightarrow e^\pm \mu^\mp$.
Phys. Lett., B754:167–175, 2016.
- [251] R. Appel et al.
Search for lepton flavor violation in K^+ decays.
Phys. Rev. Lett., 85:2877–2880, 2000.
- [252] J. P. Lees et al.
Searches for Rare or Forbidden Semileptonic Charm Decays.
Phys. Rev., D84:072006, 2011.
- [253] H. Georgi.
Effective field theory.
Ann. Rev. Nucl. Part. Sci. 43 (1993) 209-252.
- [254] Aneesh V. Manohar.
Introduction to Effective Field Theories.
In *Les Houches summer school: EFT in Particle Physics and Cosmology Les Houches, Chamonix Valley, France, July 3-28, 2017*, 2018.
- [255] Antonio Pich.
Effective Field Theory with Nambu-Goldstone Modes.
In *Les Houches summer school: EFT in Particle Physics and Cosmology Les Houches, Chamonix Valley, France, July 3-28, 2017*, 2018.
- [256] Sacha Davidson, David C. Bailey, and Bruce A. Campbell.

- Model independent constraints on leptoquarks from rare processes.
Z. Phys., C61:613–644, 1994.
- [257] Deirdre Black, Tao Han, Hong-Jian He, and Marc Sher.
tau - mu flavor violation as a probe of the scale of new physics.
Phys. Rev., D66:053002, 2002.
- [258] Michael Carpentier and Sacha Davidson.
Constraints on two-lepton, two quark operators.
Eur. Phys. J., C70:1071–1090, 2010.
- [259] Yi Cai and Michael A. Schmidt.
A Case Study of the Sensitivity to LFV Operators with Precision Measurements and the LHC.
JHEP, 02:176, 2016.
- [260] Derek E. Hazard and Alexey A. Petrov.
Lepton flavor violating quarkonium decays.
Phys. Rev., D94(7):074023, 2016.
- [261] Derek E. Hazard and Alexey A. Petrov.
Radiative lepton flavor violating B, D, and K decays.
2017.
- [262] Gerhard Buchalla, Andrzej J. Buras, and Markus E. Lautenbacher.
Weak decays beyond leading logarithms.
Rev. Mod. Phys., 68:1125–1144, 1996.
- [263] Y. Sato et al.
Measurement of the branching ratio of $\bar{B}^0 \rightarrow D^{*+} \tau^- \bar{\nu}_\tau$ relative to $\bar{B}^0 \rightarrow D^{*+} \ell^- \bar{\nu}_\ell$ decays with a semileptonic tagging method.
Phys. Rev., D94(7):072007, 2016.
- [264] J. P. Lees et al.
Measurement of an Excess of $\bar{B} \rightarrow D^{(*)} \tau^- \bar{\nu}_\tau$ Decays and Implications for Charged Higgs Bosons.
Phys. Rev., D88(7):072012, 2013.
- [265] Sébastien Descotes-Genon, Lars Hofer, Joaquim Matias, and Javier Virto.
Global analysis of $b \rightarrow s \ell \ell$ anomalies.
JHEP, 06:092, 2016.

- [266] Marco Ciuchini, Marco Fedele, Enrico Franco, Satoshi Mishima, Ayan Paul, Luca Silvestrini, and Mauro Valli.
 $B \rightarrow K^* \ell^+ \ell^-$ decays at large recoil in the Standard Model: a theoretical reappraisal.
JHEP, 06:116, 2016.
- [267] Sebastian Jäger and Jorge Martin Camalich.
Reassessing the discovery potential of the $B \rightarrow K^* \ell^+ \ell^-$ decays in the large-recoil region: SM challenges and BSM opportunities.
Phys. Rev., D93(1):014028, 2016.
- [268] Gudrun Hiller and Martin Schmaltz.
 R_K and future $b \rightarrow s \ell \ell$ physics beyond the standard model opportunities.
Phys. Rev., D90:054014, 2014.
- [269] Christoph Bobeth, Gudrun Hiller, and Danny van Dyk.
General analysis of $\bar{B} \rightarrow \bar{K}^{(*)} \ell^+ \ell^-$ decays at low recoil.
Phys. Rev., D87(3):034016, 2013.
[Phys. Rev.D87,034016(2013)].
- [270] Wolfgang Altmannshofer, Paride Paradisi, and David M. Straub.
Model-Independent Constraints on New Physics in $b \rightarrow s$ Transitions.
JHEP, 04:008, 2012.
- [271] Sacha Davidson, Michelangelo L. Mangano, Stephane Perries, and Viola Sordini.
Lepton Flavour Violating top decays at the LHC.
Eur. Phys. J., C75(9):450, 2015.
- [272] O.Shanker.
Flavour violation, scalar particles and leptoquarks.
*Nucl. Phys. B*206 (1982) 253 DOI:10.1016/0550-3213(82)90534-X.
- [273] Margarete Herz.
Bounds on leptoquark and supersymmetric, R parity violating interactions from meson decays.
2002.
- [274] J. Bijnens, G. Colangelo, G. Ecker, and J. Gasser.
Semileptonic kaon decays.
pages 315–389, 1994.
- [275] Rajan Gupta.
Calculations of hadronic matrix elements using lattice QCD.
1993.

- [276] Daping Du, A. X. El-Khadra, Steven Gottlieb, A. S. Kronfeld, J. Laiho, E. Lunghi, R. S. Van de Water, and Ran Zhou.
Phenomenology of semileptonic B-meson decays with form factors from lattice QCD.
Phys. Rev., D93(3):034005, 2016.
- [277] Jon A. Bailey et al.
 $|V_{ub}|$ from $B \rightarrow \pi \ell \nu$ decays and (2+1)-flavor lattice QCD.
Phys. Rev., D92(1):014024, 2015.
- [278] Jon A. Bailey et al.
 $B \rightarrow Kl^+l^-$ Decay Form Factors from Three-Flavor Lattice QCD.
Phys. Rev., D93(2):025026, 2016.
- [279] Patricia Ball and Roman Zwicky.
New results on $B \rightarrow \pi, K, \eta$ decay formfactors from light-cone sum rules.
Phys. Rev., D71:014015, 2005.
- [280] Xing-Dao Guo, Xi-Qing Hao, Hong-Wei Ke, Ming-Gang Zhao, and Xue-Qian Li.
Looking for New Physics via Semi-leptonic and Leptonic rare decays of D and D_s .
Chin. Phys., C41(9):093107, 2017.
- [281] Andreas Crivellin, Lars Hofer, Joaquim Matias, Ulrich Nierste, Stefan Pokorski, and Janusz Rosiek.
Lepton-flavour violating B decays in generic Z' models.
Phys. Rev., D92(5):054013, 2015.
- [282] Andreas Crivellin, Giancarlo D'Ambrosio, Martin Hoferichter, and Lewis C. Tunstall.
Violation of lepton flavor and lepton flavor universality in rare kaon decays.
Phys. Rev., D93(7):074038, 2016.
- [283] V. Ilisie.
Concepts in Quantum Field Theory.
Springer, 2016, 978-3-319-22966-9.
- [284] B. Grzadkowski, M. Iskrzynski, M. Misiak, and J. Rosiek.
Dimension-Six Terms in the Standard Model Lagrangian.
JHEP, 10:085, 2010.
- [285] Rodrigo Alonso, Elizabeth E. Jenkins, Aneesh V. Manohar, and Michael Trott.
Renormalization Group Evolution of the Standard Model Dimension Six Operators III:
Gauge Coupling Dependence and Phenomenology.
JHEP, 04:159, 2014.

- [286] S. Bellucci, M. Lusignoli and L. Maiani, Nucl. Phys. B 189 (1981) 329. .
DOI:10.1016/0550-3213(81)90384-9.
- [287] G. Buchalla, A. J. Buras and M. K. Harlander, Nucl. Phys. B 337 (1990) 313.
DOI:10.1016/0550-3213(90)90275-I.
- [288] S. Davidson and A. Saporta.
work in progress.
- [289] G. Belanger, F. Boudjema, A. Pukhov, and A. Semenov.
Dark matter direct detection rate in a generic model with micrOMEGAs 2.2.
Comput. Phys. Commun., 180:747–767, 2009.
- [290] A. Airapetian et al.
Precise determination of the spin structure function $g(1)$ of the proton, deuteron and neutron.
Phys. Rev., D75:012007, 2007.
- [291] Martin Hoferichter, J. Ruiz de Elvira, Bastian Kubis, and Ulf-G. Meißner.
High-Precision Determination of the Pion-Nucleon Term from Roy-Steiner Equations.
Phys. Rev. Lett., 115:092301, 2015.
- [292] Parikshit Junnarkar and Andre Walker-Loud.
Scalar strange content of the nucleon from lattice QCD.
Phys. Rev., D87:114510, 2013.
- [293] K. A. Olive et al.
Review of Particle Physics.
Chin. Phys., C38:090001, 2014.
- [294] Hai-Yang Cheng.
Low-energy Interactions of Scalar and Pseudoscalar Higgs Bosons With Baryons.
Phys. Lett., B219:347–353, 1989.
- [295] Tanmoy Bhattacharya, Vincenzo Cirigliano, Rajan Gupta, Huey-Wen Lin, and Boram Yoon.
Neutron Electric Dipole Moment and Tensor Charges from Lattice QCD.
Phys. Rev. Lett., 115(21):212002, 2015.
- [296] Jeremy Green et al.
Up, down, and strange nucleon axial form factors from lattice QCD.
Phys. Rev., D95(11):114502, 2017.
- [297] S. Durr et al.
Lattice computation of the nucleon scalar quark contents at the physical point.

- Phys. Rev. Lett.*, 116(17):172001, 2016.
- [298] Jacobo Ruiz de Elvira, Martin Hoferichter, Bastian Kubis, and Ulf-G. Meißner.
Extracting the σ -term from low-energy pion-nucleon scattering.
J. Phys., G45(2):024001, 2018.
- [299] J. M. Alarcon, J. Martin Camalich, and J. A. Oller.
The chiral representation of the πN scattering amplitude and the pion-nucleon sigma term.
Phys. Rev., D85:051503, 2012.
- [300] Giovanni Marco Pruna and Adrian Signer.
The $\mu \rightarrow e\gamma$ decay in a systematic effective field theory approach with dimension 6 operators.
JHEP, 10:014, 2014.
- [301] Elizabeth E. Jenkins, Aneesh V. Manohar, and Michael Trott.
Renormalization Group Evolution of the Standard Model Dimension Six Operators II:
Yukawa Dependence.
JHEP, 01:035, 2014.
- [302] Jonathan L. Rosner, Sheldon Stone, and Ruth S. Van de Water.
Leptonic Decays of Charged Pseudoscalar Mesons - 2015.
Submitted to: Particle Data Book, 2015.
- [303] S. Aoki et al.
Review of lattice results concerning low-energy particle physics.
Eur. Phys. J., C77(2):112, 2017.
- [304] A. Bazavov et al.
 B - and D -meson leptonic decay constants from four-flavor lattice QCD.
Phys. Rev., D98(7):074512, 2018.
- [305] Alexander Khodjamirian, Thomas Mannel, and Nils Offen.
Form-factors from light-cone sum rules with B -meson distribution amplitudes.
Phys. Rev., D75:054013, 2007.